A Comparison of Vascular Development, Hydraulic Properties and Resistance to Embolism in Early First-Year Seedlings of Three Inland Pacific Northwest Conifer Species

A Thesis
Presented in Partial Fulfillment of the Requirements for the
Degree of Master of Science
with a
Major in Natural Resources
in the
College of Graduate Studies
University of Idaho
by

Megan L. Riley

Major Professor: Daniel Johnson, Ph.D.
Committee Members: Blair McLaughlin, Ph.D.; David Tank, Ph.D.
Department Administrator: Randall Brooks, Ph.D.

December 2016

Authorization to Submit Thesis

This thesis of Megan L. Riley, submitted for the degree of Master of Science with a Major in Natural Resources and titled, "A Comparison of Vascular Development, Hydraulic Properties and Resistance to Embolism in Early First-Year Seedlings of Three Inland Pacific Northwest Conifer Species," has been reviewed in final form. Permission, as indicated by the signatures and dates below, is now granted to submit final copies to the College of Graduate Studies for approval.

Major Professor: _____ Date: _____
Daniel Johnson, Ph.D.

Committee Members: _____ Date: _____
Blair McLaughlin, Ph.D.

_____ Date: _____
David Tank, Ph.D.

Department
Administrator: _____ Date: _____
Randall Brooks, Ph.D.

Abstract

The first-year seedling stage is vital in terms of determining species distributions and migration under a changing climate, yet conifers experience the highest rates of mortality during their first year and it is the tree life stage least studied. In this study, we compared anatomical and theoretical functional traits of *Pseudotsuga menziesii, Larix occidentalis,* and *Pinus ponderosa* to *in vitro* measurements and *in vivo* visualization of vulnerability to embolism. Theoretical measurements suggest that vulnerability to embolism varies greatly for each species over the first 10 weeks of growth and so the timing of drought onset is critical in regards to potential resistance to hydraulic dysfunction in seedlings. Additionally, i*n vivo* imaging of embolism during desiccation indicated that *in planta* resistance to hydraulic dysfunction cannot necessarily be inferred from results based on standard *in vitro* laboratory methodologies.

Acknowledgements

I would like to acknowledge funding support from NSF grant # IOS-1146746 and express my appreciation to the Stillinger Administrative Committee for continued support through the C.R. Stillinger Forest Science Research Fellowship. I would like to thank Ann Norton, director of the Ibest Optical Imaging Core, for her time, patience, enthusiasm and incredible wealth of knowledge she was willing to share in pursuit of beautiful confocal microscopy images. A special thank you to those that made the imaging at the Advanced Light Source (ALS) beamline (Beamline 8.3.2) in Berkeley, CA possible: Craig Brodersen, Adam Roddy and Andrew McElrone and Dula Parkinson (the beamline master). The Advanced Light Source is supported by the Director, Office of Science, Office of Basic Energy Sciences, of the U.S. Department of Energy under Contract No. DE-AC02-05CH11231. An extended thank you to Adam Roddy for psychrometry water potential measurements.

The greenhouse upkeep of seedlings could not have been done without the help of our Tree Phys lab soldiers: Forrest Sherman, Eric Larson, Molly Rard, Ryan Spaniel, Laura Young, Laurie Bell, and Dario Paiva, who kept my seedlings well fed and well-watered during the growing season. Lastly, a whole-hearted thank you to Jason Schlafmann, who put his attention to detail and excellent work ethic to use in prepping stems for confocal imaging as well as leaf area measurements, of which there were many.

Finally, I would like to acknowledge my lab mate Kathryn for her excellent editing skills and moral support, my advisor Dr. Dan Johnson with his continuous support and who was always ready with a solution to a problem I couldn't see my way around, and to my committee members, Drs. David Tank and Blair McLoughlin, who understand what it is to do science and for being flexible with the multitude of changes along the way.

Table of Contents

Authorization to Submit ii
Abstract iii
Acknowledgements iv
Table of Contents v
List of Figures vii
List of Tables ix
Abbreviations x

Chapter 1: The first 10 weeks: A comparison of vascular development, anatomy and functional traits of very young *L. occidentalis*, *P. menziesii* and *P. ponderosa* seedlings 1
1.1 Introduction 1
1.1.1 Hypotheses and Objectives 3
1.2 Materials and Methods 4
1.2.1 Plant Materials and Growing Conditions 4
1.2.2 Confocal Laser Scanning Microscopy (CLSM) 5
1.2.3 Anatomical Measurements 6
1.2.4 Functional Properties 7
1.2.5 Leaf Area Measurements 8
1.2.6 Common Garden Experiment 8
1.2.7 Statistical Analyses 8
1.3 Results 10
1.3.1 Confocal Assisted Identification of Anatomy 10
1.3.2 Development over the First 10 Weeks of Growth 11
1.3.3 Anatomical and Functional Characteristics 11
1.3.4 Common Garden Experiment 16
1.4 Discussion 16
1.5 Conclusion 22
1.6 References 23

Chapter 2: A comparison of P_{50} estimates, anatomical characteristics, and functional traits to *in planta* embolism in very young conifer stems using X-ray computed microtomography 29
2.1 Introduction 29
2.1.1 Hypotheses and Objectives 32
2.2 Materials and Methods 32
2.2.1 Plant Materials and Growing Conditions 32
2.2.2 Confocal Laser Scanning Microscopy (CLSM) 33
2.2.3 X-ray Computed Micro-tomography (microCT) 33
2.2.4 Vulnerability Curves 34
2.2.5 Anatomical and Trait Characteristic Comparisons 35
2.2.6 Statistical Analyses 36
2.3 Results 37
2.3.1 Anatomical and Trait Comparisons 37
2.3.2 Vulnerability Curves 38
2.3.3 MicroCT Imaging 38
2.4 Discussion 39
2.5 Conclusion 44
2.6 References 46
Figures 53
Appendix: Mean Values for Anatomical and Functional Traits 76

List of Figures

Figure 1.1: Composite Confocal Microscopy Image of *P. menziesii* 53

Figure 1.2: Differentiating Xylem 54

Figure 1.3: Example of Stem and Xylem Area Measurements 54

Figure 1.4: Tracheid and Pit Measurements 55

Figure 1.5: Vascular Tissue of 3-week-old *P. menziesii* 55

Figure 1.6: Vascular Development over 10 Weeks 56

Figure 1.7: Correlations Between Seedling Area Measurements 57

Figure 1.8: Relationships between Stem Cross-Sectional Area and Calculated Total Functional Xylem Area 58

Figure 1.9: Total Functional Xylem Area and Functional Tracheid Lumen Fraction 59

Figure 1.10: Leaf Area to Functional Xylem Area Ratio Comparisons 60

Figure 1.11: Leaf Area vs. Total Functional Xylem Area 61

Figure 1.12: Lumen Area Distributions 62

Figure 1.13: Tracheid Characteristics: Tracheid Diameter, Cell Wall Thickness, and Thickness-to-span Ratio 63

Figure 1.14: Thickness-to-span Ratios at Weeks 2 and 10 64

Figure 1.15: Correlations of the Four Measured Pit Features 64

Figure 1.16: Correlation Between Torus Diameter and Torus Width 65

Figure 1.17: Torus Width Comparisons 65

Figure 1.18: Torus-to-Pit Aperture Overlap Comparisons 66

Figure 1.19: Stem Conductance at Week 10 for all Species 66

Figure 1.20: $K_{s(t)}$, $K_{L(t)}$ and Leaf Area over Time per Species 67

Figure 1.21: $K_{s(t)}$ and $K_{L(t)}$ for Each Week 68

Figure 1.22: Comparison of $K_{s(t)}$ and $K_{L(t)}$ at Weeks 2 and 10 per Species 69

Figure 2.1: Vulnerability Curves.....70

Figure 2.2: MicroCT Image of Vascular Tissue 71

Figure 2.3: Comparison of MicroCT and CLSM Microscopy Images 71

Figure 2.4: MicroCT Images of Embolism in *L. occidentalis, P. menziesii* and *P. ponderosa* during Desiccation 72

List of Tables

Table 1.1: Study species 4
Table 1.2: Summary of Statistical Analyses for Variables of Interest 10
Table 2.1: Anatomical and Functional Traits of Interest 37
Table A.1: Stem, Xylem and Leaf Area Measurements 76
Table A.2: Anatomical Measurements 77
Table A.3: Functional Traits 78

Abbreviations

Abbreviations	Explanation	Units
Anatomical Features		
Tw	Tracheid double wall thickness	μm
D_{pa}	Pit aperture diameter	μm
D_m	Margo membrane diameter	μm
D_{tor}	Torus diameter	μm
W_t	Torus width	μm
D_t	Span; tracheid lumen diameter	μm
A_t	Tracheid lumen area	μm^2
T_{den}	Tracheid density	# mm^{-2}
A_L	Leaf Area	m^2
A_s or D_s	Cross-sectional stem area or diameter	mm^2/mm
A_x or D_x	Cross-sectional xylem area or diameter (includes pith)	mm^2/mm
A_{tx}	Actual measured total xylem area	mm^2
A_{sx}	Xylem sampled area	mm^2
A_{sfx}	Functional xylem area within A_{sx}	mm^2
A_{tfx}	Calculated total functional xylem area	mm^2
Functional Traits		
$K_{s(t)}$	Theoretical xylem specific conductivity	Kg m^{-1} s^{-1} MPa^{-1}
$K_{h(t)}$	Theoretical hydraulic conductance	Kg m s^{-1} MPa^{-1}
$K_{L(t)}$	Theoretical leaf specific conductivity	Kg m^{-1} s^{-1} MPa^{-1}
K_s	Measured xylem specific conductivity	Kg m^{-1} s^{-1} MPa^{-1}
K_h	Measured hydraulic conductance	Kg m s^{-1} MPa^{-1}
TPO	Torus-to-pit aperture overlap	-
Tw Dt^{-1}	Thickness-to-span ratio	-
A_L:A_{tfx}	Leaf area to functional area	-
A_{tfx}:A_x	Functional tracheid lumen fraction	-
P_{50}	Water potential at which 50% of maximum hydraulic conductivity is lost	MPa
PLC	Percent Loss Conductivity	%
F_m	Bordered pit margo flexibility	-
V_{ef}	Valve effect of the bordered pit membrane	-

Chapter 1

The first 10 weeks: A comparison of vascular development, anatomy and functional traits of very young *L. occidentalis*, *P. menziesii* and *P. ponderosa* seedlings

INTRODUCTION

"Wood is a marvelous tissue; it never ceases to fascinate… be it as a construction material for buildings, ships, fine musical instruments, or as the delicate structure one sees in the microscope" (Zimmermann 1983). Martin Zimmermann's *Xylem Structure and the Ascent of Sap* (1983) remains a seminal resource for tree physiologists nearly 35 years after its first publication, yet the first wood cellular structures were described centuries ago (Mazzarello 1999). Wood anatomy has since been a topic of research (see Schweingruber 2007 and references therein), first made possible by the advent of the compound microscope (Preston 1964) and necessitated by the immense scope of wood and fiber products produced and used globally (Dickison 2000). Extensive research has definitively illustrated how wood anatomy governs the physical (grain, texture, color, specific gravity, density) and thus biomechanical (strength, hardness, flexibility, permeability, shrinkage and deformation), properties of wood (Dickison 2000).

An expansion of this research began in the early 20th century (Real and Brown 1991) and continues today, facilitated by continual advances in technological and analytic tools and fueled by changes in the understanding of our natural environment, research now encompasses all aspects of plant functional anatomy and ecophysiology. Vast amounts of literature explore plant development, growth, and physiology including cellular ontogeny (Esau 1977), physical and chemical tissue composition (Noves et al. 2010), chemical and hormone signaling (e.g. Hedden and Thomas 2006), primary vascular development (See review by Lucas et al. 2013), water and solute transport systems (Hacke and Sperry 2001; Tyree and Zimmerman 2002; Woodruff 2014) and numerous physiological processes such as photosynthesis and transpiration, water potential gradients, water use efficiency, sapflow, and wound and stress responses (e.g. Lambers et al. 1998; Pallardy 2008). Additionally, with a

changing climate there is significant interest in predicting mortality on individual and stand level scales (Martinez-Vilalta et al. 2002; Cheaib et al. 2012; McDowell et al. 2013).

We now understand that, just as wood anatomy dictates the biomechanical properties of wood products, it also plays a primary role in plant physiological processes such as water transport (Zimmerman 1983) and resistance to hydraulic dysfunction (Sperry et al. 1994; Sperry et al. 2006; Dalla-Salda et al. 2011). Despite the voluminous amounts of research, a black box remains in the woody plant life-history story; there remains a paucity of research on first-year species-specific development, functional anatomy, and hydraulic properties as compared to other life stages (see Chapter 2 Discussion). Large compilations (e.g. Esau 1977 and Hacke 2015) typically describe general anatomy or properties that encompass broad groups of plants rather than focus on species-specific traits. For vascular development in general, such as cellular ontogeny and xylogenesis, research is often performed on model species, such as Arabidopsis (Chaffey et al. 2002; Zhang et al. 2011; Lehmann and Hardtke 2016), *Zinnia* species (Chaffey 1999), and *Populus* species (Mellerowicz et al. 2001; Chang 2014). Yet, only *Populus* has true wood, and conifers lack many of the cellular components that comprise a large portion of these species' xylem tissue, such as vessels and fibers.

There are numerous aspects of species-specific early first-year seedling anatomical and functional properties that are unknown such as: (1) contributions of primary xylem to seedling hydraulic properties and resistance to hydraulic dysfunction, (2) the timing and characteristics of the transition from primary to secondary xylem development and how this changes seedling hydraulic capacities and resistance to hydraulic dysfunction, (3) secondary xylem expansion and how this early developmental period determines potential hydraulic functional properties and potential mechanisms for mitigating drought induced hydraulic dysfunction. The first year of life is a perilous stage in tree life history as first-year seedlings experience the highest rates of mortality (e.g. Burns and Honkala 1990), yet seedling survival is critical for maintaining natural forest regeneration and facilitating species migrations, especially in light of current climate change predictions.

Currently, it is unknown if the mechanisms for mediating drought-induced mortality and hydraulic dysfunction are similar between seedling, sapling, and mature stages of life (Anderegg and Anderegg 2013; Clark et al. 2016); young seedlings may not have the necessary anatomical structures to resist cavitation nor the carbohydrate and water stores to

survive long term stomatal closure during prolonged drought episodes (Johnson et al. 2011). Additionally, seedlings likely lack potential external mitigation factors such as differences in leaf cuticle thickness, stomatal closure (i.e. "leaky" stomata), rooting depths, sapwood area, capacitance, and mycorrhizal associations; thus, seedlings may be more heavily reliant on anatomical morphologies for basic hydraulic function and embolism resistance.

Previous research on saplings and mature trees have illustrated that numerous anatomical characteristics correlate with various hydraulic parameters. One of the most commonly reported parameters is the water potential at which 50% hydraulic conductivity is lost (P_{50}) (see Gleason et al. 2016). This value is often used as a proxy for drought tolerance whereby a more negative P_{50} means more embolism resistant and thus greater drought tolerance. Several of those correlated characteristics include tracheid lumen diameter (D_t), tracheid density (T_{den}, # mm^{-2}), thickness-to-span ratio (Tw Dt^{-1}), and torus-to-pit aperture overlap (TPO) (Sterck et al. 2012; Ogasa et al. 2013; Bouche et al. 2014). In addition to these characteristics, there are additional functional traits (see Functional Properties section) that shed light on hydraulic properties and carbon investment strategies.

In order to help clarify basic anatomical development and hydraulic function in very young seedlings, we analyzed vascular development, xylem anatomical characteristics and functional traits at 2, 3, 4, 6 and 10 weeks after planting in three native inland Pacific Northwest conifers: *Pinus ponderosa* Dougl. ex Laws, *Pseudotsuga menziesii* (Mirb.) Franco, and *Larix occidentalis* Nutt. (Table 1.1). We also compared anatomical characteristics from the 10 week-old seedlings to actual mortality in a common garden experiment. Quantifying and analyzing these anatomical and functional traits will elucidate potential maximum hydraulic capabilities, carbon investment priorities, water transport strategies, and resistance to drought-induced hydraulic dysfunction as these seedlings transition from primary to secondary growth.

Hypothesis and Objectives

(1) Objective: document stem anatomy and development in these three species.

(2) Hypothesis: Drought resistance of seedlings will necessarily rely primarily on xylem resistance to cavitation, therefore anatomical characteristics of *P. ponderosa, P. menziesii,* and *L. occidentalis* will indicate a decreasing spectrum of drought tolerant characteristics respectively based on estimates of drought tolerance.

(3) Hypothesis: Mortality in the common garden experiment will be correlated to the seedlings with xylem that is least resistant to embolism, as interpreted by anatomical analyses.

MATERIALS AND METHODS

Plant Materials and Growing Conditions

Table 1.1. Study Species.

Species	**Relative Drought Tolerance***
Larix occidentalis	Least
Pseudotsuga menziesii var. *glauca,*	Mid
Pinus ponderosa var. *ponderosa*	Most

* Determined from a review conducted by Piñol and Sala (2000)

Seeds from all species were germinated in April 2015 at the University of Idaho's Franklin H. Pitkin Forest Nursery located in Moscow, ID, USA (46°43'N, 116°59'W). Seeds were sourced from the local region to minimize geographical differences in intra-species characteristics. Seeds were sown in trays of 96 – 3.8 x 21.0 cm "conetainers" (SC10R, Stuewe & Sons, Tangent, OR, USA) containing a commercial potting mix (Metro-Mix Custom Blend, Sun Gro Horticulture, Agawam, MA, USA) consisting of 40-50% Sphagnum peat moss, vermiculite, and aged fine bark.

All trays were watered according to procedures discussed by Landis (1989) and were fertilized weekly using a locally procured MiracleGro Fertilizer (NPK 24:8:16) targeted at a Nitrogen application of 100ppm. Additional phosphoric acid (H_3PO_4) was used to further acidify the water or aqueous fertilizer. Trays were randomized weekly within the greenhouse benches in order to minimize microclimate variations and edge effects. The greenhouse bay was computer-automated climate controlled with 15-minute monitoring intervals of temperature and relative humidity. Supplemental lighting extended the photoperiod to 14 hours a day.

Confocal Laser Scanning Microscopy (CLSM)

Confocal Laser Scanning Microcopy (CLSM) utilizes laser beams of differing wavelengths and a pinhole light aperture to optically image specimens in an X, Y and Z direction, creating an optical 3-D image. It has been well established for analyzing plant cellular and anatomical characteristics (for a review, see Hepler and Grunning 1998). During growth, a minimum of five seedlings were randomly collected from each species at each time period. They were collected from the greenhouse whole, wrapped in wet paper towels, bagged and immediately transported to the lab where they were placed in FAA (95% ethanol: acetic acid: 37% formaldehyde: water; 50:5:10:35 v/v) (Ruzin 1999), degassed under a partial vacuum overnight, and retained in FAA until commencement of the imaging. For the very young, delicate samples, the entire seedling (root, stem, crown) was placed into the fixative. In older or larger samples, the seedlings were severed either slightly below the root collar or at the crown (or both) just prior to fixation. In this case, roots and crowns were retained and stored separately in FAA.

Prior to imaging, the fixed specimens were rinsed 3 times in DI water at 15 minutes per rinse. If not previously excised, the root and crown were removed from the main stem, which was then transected at approximately the mid-stem point, 0.09 ± 0.02cm (SE), 1.4 ± 0.06cm, and 2.1 ± 0.03cm *for L. occidentalis, P. menziesii* and *P. ponderosa* respectively and the crowns were retained for leaf area measurements (see below). The upper stem segments were processed according to Kitin et al. (2003) and the lower halves were retained in FAA for future analyses. The upper half of the stem segments were placed in 0.01% or 0.06% Safranin O under vacuum for 30 minutes, rinsed in DI water to remove excess stain, dehydrated then rehydrated in stepped acetone concentrations (DI, 25%, 50%, 75%, 100%) at 15 minutes per interval. The specimens were finally cleared in stepped glycerol concentrations (25%, 50%, 75%, and 100%) and stored in 100% glycerol. Immediately before imaging, the stem segments were hand sectioned from the mid-stem end using a double-edged razor blade and mounted in glycerol on a microscope slide with a cover slip; average section widths measured 80 ± 4μm (SD).

Sections were optically scanned using Olympus Fluoview Confocal Microscope with excitation of three laser lines 405, 488, and 559 nm and three emission filters (SDM490, SDM560 and BF respectively). The ranges of these emission filters were 425-475nm, 500-

545nm, and 575-675nm respectively, but each range could be further restricted in order to better distinguish specific anatomical characteristics of interest (Bond et al. 2007, Sant'Anna et al. 2013). Narrowing the range of SDM560 and BF filters to 520-540nm and 575-520nm respectively often reduced background cellular noise, making the cell walls easier to view. Overlaying the three different images, each produced from a single excitation laser (Fig. 1.1 A-C), into a composite image (Fig. 1.1D) at three different magnifications (10x, 20x and 60x) provided details for distinguishing anatomical characteristics and facilitated anatomical measurements.

Anatomical Measurements

Four to seven seedlings per species per time period were measured for anatomical properties for a total of 79 measured seedlings. Week 10 was chosen as the end point of anatomical analyses as we assumed from this point forward there will be no additional major anatomical development besides the expansion of secondary xylem and development of the cork tissue (which is outside the scope of this study).

All tracheid anatomical features were measured on mature primary and secondary xylem, where mature tracheids were defined by the lack of live cell contents as viewed with confocal microscopy (Fig. 1.2). All mature tracheids were assumed participatory in stem water transport. Stem cross-sectional diameters (D_s), xylem cross-sectional diameters (D_x) and total xylem areas (A_{tx}) per stem were measured utilizing the 10x and 20x CLSM images. The xylem cross-sectional diameter consisted of the average of two to five linear measurements from xylem edge to xylem edge, whereas the total xylem area was measured directly to include differentiating xylem but to exclude the pith (Fig. 1.3). A sample area (A_{sx}) was randomly delineated per stem, approximately wedge-shaped, that included entire radial files of xylem from the pith to cambium. Functional xylem area (A_{sfx}) was measured directly (60x magnification) within this sample area and extrapolated to estimate total stem functional xylem area (A_{tfx}):

$$A_{tfx} = \left(\frac{A_{sfx}}{A_{sx}}\right) A_{tx}$$

When the sample area size exceeded that of the 60x field of view (211.97 x 211.97μm), several scans were taken encompassing the entire sample and subsequently stitched together using ImageJ "Pairwise Stitching" plugin (Preibisch et al. 2009). Lumen area for all mature

tracheids within the sample area were measured and converted into circle equivalent diameters (D_t) (i.e. span; tracheid lumen diameter) (Fig. 1.4). A randomized subset of an average of 31 ± 12.05 (SD) tracheids within the sample area were selected for wall thickness (Tw) measurements, which consisted of the double wall thickness between the selected tracheid and at least two adjacent functional tracheids (Sperry et al. 2006; Bouche 2014) (Fig. 1.4). Bordered pit anatomical characteristics including pit aperture diameter (D_{pa}), margo membrane diameter (D_m) (assumed to be the inner diameter of the pit), torus diameter (D_{tor}) and torus width (W_t), were measured (Fig. 1.4) in primary and secondary xylem within the 60x field of view or within the total xylem area if xylem area was smaller than the field of view. Bordered pits characteristics were only measured when the adjoining two tracheids were mature and there was no evidence of cell plasma (Esau 1977) within the pit space. All anatomical measurements were performed utilizing Fiji/ImageJ (Schindelin et al. 2012; Rasband, W.S. ImageJ, U.S. National Institutes of Health, Bethesda, Maryland, USA, imagej.nih.gov/ij/, 1997-2014).

Functional Properties

Theoretical values for hydraulic conductance ($K_{h(t)}$), xylem specific hydraulic conductivity ($K_{s(t)}$) and leaf specific conductivity ($K_{L(t)}$) illustrate the maximum theoretical conductivity per species, allowing for a comparison of conducting efficiency between each species at each time period. Theoretical xylem specific conductivity ($K_{s(t)}$) per stem is based on average tracheid lumen diameter and calculated from the Hagen-Poiseuille equation (Santiago et al. 2004; Tyree and Ewers 1991) as:

$$K_{s(t)} = \frac{\pi\rho}{128\eta A_{tfx}} \sum_{i=1}^{n} D_{t\,i}^{4}$$

where

$$\sum_{i=1}^{n} D_{t\,i}^{4} = \text{sampled} \sum_{i=1}^{n} D_{t\,i}^{4} \left(\frac{A_{tfx}}{A_{fx}}\right)$$

$K_{s(t)}$ is the xylem specific conductivity (kg m^{-1} MPa^{-1} s^{-1}), ρ is the density of water (kg m^{-1}) and η is the dynamic viscosity of water (MPa) at 20°C, and other symbols were described previously. Stem conductance ($K_{h(t)}$) was estimated by multiplying $K_{s(t)}$ by A_{tfx} (Tyree and Ewers 1991) and theoretical leaf specific conductivity ($K_{L(t)}$) was estimated by dividing $K_{h(t)}$

by the leaf area (A_L) measured distal to stem measurement (Tyree and Zimmermann 2002); in this case, leaf area measurements were entire seedling crowns. Thickness-to-span ratios (Tw Dt^{-1}) were calculated for all tracheids in which Tw was measured. Torus-to-pit aperture diameter overlap [$TPO = (D_{tor}-D_{pa})/D_{tor}$] was calculated for all pits where both a torus diameter and at least one pit aperture diameter were measured.

Functional tracheid lumen fraction (A_{tfx}:A_x) were necessarily calculated for each stem as many of the lignified cells within the primary xylem area were live parenchyma and thus non-conductive; theoretical measurements based on total xylem area (A_x or A_{tx}) would overestimate actual conductivity. A_{tfx}:A_s was also calculated to determine if there was a relationship between stem area and total functional xylem.

Leaf Area Measurements

Leaf area measurements were performed on a random subset of 5 ± 1.2 (SD) crowns per species per time period. Cotyledons were included in leaf area if they were still attached to the crown stem. All leaves were removed, placed under clear Plexiglass to flatten needles and photographed with a ruler for scale. Area measurements were performed using Fiji/ImageJ.

Common Garden Experiment

An equivalent of at least one full tray per species (n>96) was randomly selected for a qualitative common garden experiment, in which all trays were watered simultaneously and percent mortality was estimated during dry down to 100% mortality. Morality was assumed when (1) needles were brown or (2) needles were desiccated and brittle to the touch. Seedling mortality experiment commenced on September 11, 2015 and concluded October 14, 2015 for a total of 34 days. Well-watered seedlings from each species were retained as controls on physical appearance.

Statistical Analyses

For each trait, assumptions of normality and residual homogeneity were analyzed and variables were transformed if necessary. "Boxcox" from the "MASS" package (Venables and Ripley 2002) was used to determine transformations when the standard natural log or square root was insufficient at correcting heterogeneity of residuals. Mixed-effects models were used to account for the non-independence of repeated measures of tracheids within individual trees and pit aperture measurements (random factors). All statistical analyses were performed in R Studio (RStudio Team 2015). Mixed-effects models were fitted with "lmer" from the

"lmerTest:lmer" package (Kuznetsova et al. 2016); "lm" was used for fixed-effects models. Model comparisons that contained at least one random factor were analyzed using likelihood ratio tests (Zuur et al. 2009; Hector 2015). Fixed-effects models were analyzed with either likelihood ratio tests or analysis of variance (ANOVA) type II or III as all analyses were assumed to be unbalanced. The exception was torus width (W_t), in which the best model was selected to eliminate collinearity between interaction effects. Post-hoc pairwise Tukey tests were performed with "lsmeans" package (Lenth 2016) for all models, which takes into account random factors and ANOVA types II and III. Results were considered statistically significant at $\alpha < 0.05$.

Table 1.2. Summary of Statistical Analyses for Variables of Interest

Variable	**Transformation**	**Final Models** ┼	**Evaluation Method**
$K_{s(t)}$	Natural log	$Log(K_{s(t)})$~species*week	ANOVA type III
$K_{h(t)}$	Natural log	$Log(K_{h(t)})$~species*week	ANOVA type III
$K_{L(t)}$	None	$K_{L(t)}$~species+week	ANOVA type II
A_t	Square root	$Sqrt(A_t)$~species*week+(1|tree)	Likelihood Ratio
D_t	Square root	$Sqrt(D_t)$~species*week+(1|tree)	Likelihood Ratio
Tw	Root	$Tw^{0.26}$~species*week	Likelihood Ratio
Tw Dt^{-1}	Natural log	$Log(Tw\ Dt^{-1})$~ species*week+(1|tree)	Likelihood Ratio
D_m	None	Not analyzed independently	N/A
D_{pa}	None	Not analyzed independently	N/A
D_{tor}	None	Not analyzed independently	N/A
W_t	Natural log	$Log(W_t)$~species+week+type+ type:species	Likelihood Ratio
TPO	Power	TPO^2 ~ species*type	ANOVA type III
A_L	Root	$A_L{}^{0.06}$~species*week	ANOVA type III
A_s	Natural log	$Log(A_s)$~species*week	ANOVA type III
A_x	Natural log	$Log(A_x)$~species*week	ANOVA type III
A_{tx}	Natural log	$Log(A_{tx})$~species*week	ANOVA type III
A_{tfx}	Natural log	$Log(A_{tfx})$~species*week	ANOVA type III
A_L:A_{tfx}	Root	$(A_L/A_{tfx})^{-0.6}$~species*week	ANOVA type III
T_{den}	Root	$T_{den}{}^{-0.6}$ ~ species*week	ANOVA type III

┼ R formatting language; "type" either primary xylem or secondary xylem; "log" refers to natural log transformation in R.

RESULTS

Confocal Assisted Identification of Anatomy

A combination of 10x, 20x and 60x images were used to facilitate identification of anatomical components and subsequent analyses. The 60x magnification provided sufficient resolution to distinguish a number of anatomical characteristics including mature (i.e. dead)

xylem, differentiating xylem, vascular cambium, cell membranes, bordered pits with associated tori, phloem (Fig. 1.5) and cell wall S1 – S3 layers (not shown).

Development over the First 10 Weeks of Growth

Initial primary growth (i.e. elongation of the hypocotyl) included 2 – 4 proto xylem clusters for *P. menziesii* and *L. occidentalis* and 4 – 6 clusters for *P. ponderosa* (Fig 1.6 A, F, K). Differentiation of primary xylem continued adjacent to the pith and then centrifugally, transitioning to secondary xylem differentiation via vascular cambium between 2 and 3 weeks for *P. menziesii* and *P. ponderosa* (Fig. 1.6 B, L). with the exception of *L. occidentalis*, in which differentiation and lignification of cells moved inward into the pith before vascular secondary cambium growth began (Fig.1.6 G). Vascular cambium can be visualized by the 2nd week for all species and secondary phloem is visible by the 3rd week. Surprisingly, within the primary xylem, a substantial portion of cells appear to be lignified parenchyma. A Casparian strip or suberized endodermis is present in all species from week 2 (best visualized in *P. ponderosa* Fig. 1.6 K-O); by week 10, it expanded beyond the initial stem diameter, splitting the primary epidermis and initiating stem diameter growth. Four to six initial primary resin ducts were visible in *P. ponderosa* by the second week (Fig. 1.6 K) and some irregularly spaced ducts were visualized in *L. occidentalis* by week 10 (Fig. 1.6 J), but no resin ducts are visible in *P. menziesii* at any time period. Variations in color between weeks and between species are due to differing Safranin O concentrations (0.01% or 0.06%), tissue age, tissue composition, and distance of image section from stained stem end during stem processing as well as post-processing image analysis modifications to enhance tissues and areas of interest.

Anatomical and Functional Characteristics

All statistical analyses were performed on transformed variables and therefore all significant results are in terms of transformed scales while some graphs and all tables of values are reported on original scales. See Appendix Tables A.1, A.2 and A.3 for untransformed means ± SE for areas, anatomy, and functional traits respectively. Unless otherwise noted, statistical significance for comparisons between weeks were only reported for adjacent weeks. Refer to in-text Table 1.2 for statistical models for each variable.

Correlations were analyzed between the four different area measurements (Fig. 1.7) in order to see if an easily measured variable, such as stem area, could be used as a predictor for functional xylem area, which is much more time consuming to analyze. There was a very

strong correlation between measured total xylem area (A_{tx}) and estimated total functional xylem area as A_{tfx}, which fundamentally depends on A_{tx} [$R^2 = 0.98$, $P < 0.0001$]. However, it is not a 1:1 line, which indicates that extrapolating actual total functional xylem, as opposed to simple xylem cross sectional area, is important for young seedlings. However, once the relationship is known, Atfx can be very accurately predicted from A_{tx} for all three species. The correlation between A_s and A_{tfx} is relatively poor, indicating that that predictions of functional xylem area cannot be accurately modeled as a function of stem cross-sectional area [$R^2 = 0.38$, and $P < 0.0001$]. Intra-species relationships (Fig. 1.8) illustrate a better relationship for *L. occidentalis* but weaker for *P. menziesii* and *P. ponderosa*. Untransformed means ± standard error per species per week for all four area variables are available in Appendix Table A.1.

L. occidentalis and *P. menziesii* exhibited similar total functional xylem areas (A_{tfx}) for weeks 2 through 6 while *P. ponderosa* was significantly higher for all time periods (Fig. 1.9, dotted lines). All species experienced a large increase in functional xylem area between weeks 6 and 10. At week 10, differences between species were significant with *P. ponderosa*, *L. occidentalis*, and *P. menziesii* represent the descending order of total functional xylem area. The functional tracheid lumen fraction (A_{tfx}:A_x) per species per week (Fig. 1.9, solid lines) illustrate that though *L. occidentalis* had the lowest total functional xylem area for 4 of the 5 time periods, it had the greatest ratio of functional xylem to cross-sectional xylem area while *P. ponderosa* has the lowest ratio for all time periods except week 10.

Leaf area to sapwood area (A_L:A_s) is an oft reported trait that has numerous implications for dry climate adaptation (e.g. Tyree and Zimmermann 2002; Maherali et al. 2002). In our case, we used total functional xylem area (A_{tfx}) as our sapwood area, as this is the area of the xylem assumed to be functional in transporting water to the crown. Trends over time (Fig. 1.10 A) for all species showed a decreasing A_L:A_{tfx} ratio between weeks 3 to 6 followed by a subsequent increase between week 6 and 10; averaged over all species, there were no significant differences comparing weeks 2 and 10, likely due to the larger variance in the youngest seedlings. At weeks 2 and 10, *L. occidentalis* had the smallest A_L:A_{tfx} ratio as compared to the other two species (Fig. 1.10 B, C). By week 10, the intra-species variation was considerably smaller and *P. menziesii* seemed to exhibit the greatest A_L:A_{tfx} compared to the other two species, though it was not significantly different from *P. ponderosa* (Fig. 1.10

C). An alternate way of visualizing the change in A_L to A_{tfx} over time was to plot A_L as a function of A_{tfx} (Fig. 1.11), where the slope of the line between any two adjacent time points represents the ratio of crown to xylem area (i.e. A_L:A_s). The steepest slope occurred from weeks 6 to 10 for *P. menziesii*, which is consistent with *P. menziesii* exhibiting the largest A_L:A_{tfx} ratio by the latter time period. The larger A_L:A_{tfx} indicates that a smaller xylem area supplies a given crown area, which indicates *P. menziesii* would exhibit the most negative water potentials for a given transpiration rate and that dysfunction within a given xylem area may have a greater impact on crown water availability compared to the other two species.

Within the functional xylem areas, histograms of lumen area showed skewed distributions of tracheid sizes with shifting means per time period per species (Fig. 1.12 A-C). *P. ponderosa* seedlings contained the largest tracheids as well as the largest mean tracheid areas at each time period as compared to the other two species. This was consistent with *P. ponderosa* exhibiting the lowest tracheid density when averaged over all time periods (now shown). However, at week 10 there was no significant difference between tracheid density among the three species, which is indicative that the largest tracheids are contained within the primary xylem and confirmed by the increase and subsequent decrease in mean tracheid diameters over time. *P. menziesii* appeared to have the highest tracheid density (not shown); however, this result was not significant, likely due to a larger variance combined with a small sample size (not shown). This result was consistent with the tracheid diameter distribution for *P. menziesii*, which exhibited the smallest average tracheid diameters and the narrowest distributions. See Appendix Table A.2 for average tracheid diameters.

Across all species, mean tracheid diameters increased between weeks 2 to 3 and decrease between weeks 4 to 6 (Fig. 1.13 A) while cell wall thickness increased between each time period from weeks 2 to 10 (Fig. 1.13 B). D_t and Tw were almost completely independent of one another, but did exhibit a very slight negative correlation [slope: -0.01, adjusted R^2 = 0.004, P = 0.002]. The thickness-to-span ratios (Tw Dt^{-1}) increased from week to week with significant increases between weeks 3 to 4 and 4 to 6 (Fig. 1.13 C). This indicated that tracheid wall thickness as opposed to tracheid diameter governed changing thickness-to-span ratios in growing seedlings. While Bouche et al. (2014) also found that tracheid wall thickness controlled Tw Dt^{-1}, others have found that Tw remains relatively constant and Dt controls Tw Dt^{-1} (Pittermann et al. 2006b; Sperry et al. 2006). Initially, *P. ponderosa* exhibited the larger

thickness-to-span ratio, but by week 10, *P. menziesii* had significantly higher thickness-to-span ratios than other two species (Fig. 1.14 A, B). Comparing only weeks 2 and 10, *L. occidentalis* and *P. menziesii* both experienced overall significant increases in thickness-to-span ratios, while *P. ponderosa* seedlings showed no significant change.

Overall, four pit features were measured directly. There were relatively good positive correlations between margo diameter (D_m) and torus diameter (D_{tor}) [$R^2 = 0.59$; $P < 0.0001$], and marginal correlations between D_m and pit aperture (D_{pa}) [$R^2 = 0.44$, $P<0.0001$] as well as D_{tor} to D_{pa} [$R^2 = 0.32$, $P<0.0001$] (Fig. 1.15). Torus width (W_t), our primary pit feature of interest, appeared to be nearly uncorrelated with every other pit feature, although there was a very slight positive correlation with torus diameter [$R^2 = 0.009$; $P = 0.03$]. Categorizing W_t between primary and secondary xylem illustrated that tori within the primary xylem are significantly wider across all species (Fig. 1.16 A) compared to tori within the secondary xylem, though intra-species analyses show that differences between primary and secondary xylem W_t were not significant in *P. menziesii*. Over time, W_t decreased, indicating a transition in the seedlings from primary to secondary xylem (Fig. 1.16 B). Comparing all three species across xylem type and time, *L. occidentalis* exhibits the largest W_t while *P. menziesii* and *P. ponderosa* were not significantly different from one another (Fig. 1.17).

Torus-to-pit aperture overlap (TPO) was the primary pit functional trait of interest, as a large overlap coincides with better ability to seal embolized tracheids. Model fitting for TPO indicated that xylem type (i.e. primary or secondary xylem) was not a significant factor but it was retained due to interaction effects between species and xylem type. TPO between primary and secondary xylem were significantly different in *P. menziesii* and *P. ponderosa* but not in *L. occidentalis*, with primary xylem containing smaller TPOs in general, and in many cases negative values (Fig. 1.18 A, open circles below 0.0), indicating that the torus diameter is actually smaller than the pit aperture and likely not effective in preventing air seeding (expansion of air from one tracheid into an adjacent water-filled tracheid). In terms of secondary xylem, *L. occidentalis* had the smallest overlap when averaged over all time periods, while *P. ponderosa* and *P. menziesii* were not significantly different (Fig. 1.18 B).

Theoretical stem conductance ($K_{h(t)}$) per week, averaged across all species, significantly increased over time (Fig. 1.19 A) and by week 10, all species were significantly different from one another with *P. ponderosa* exhibiting the largest conductance and *P.*

menziesii being substantially lower as compared to the other two species (Fig. 1.19 B). When normalized by functional xylem area (i.e. theoretical xylem specific conductivity; $K_{s(t)}$), conductivity significantly decreased between weeks 4 to 6 and 6 to 10 (Fig. 1.20 A). When normalized by leaf area (i.e. theoretical leaf specific conductivity; $K_{L(t)}$), conductivity increased from weeks 2 through 6 followed by a statistically significant decrease from weeks 6 to 10 (Fig. 1.20 B). Although increases between adjacent weeks from 2 to 6 were not significant, the difference between weeks 2 and 4 was significant.

Intra – species analyses over time demonstrated different trends in $K_{s(t)}$ and $K_{L(t)}$ per species (Fig. 1.21 A, B). Week was not a statistically significant factor for $K_{s(t)}$ ($P=0.06$), but it was retained due to a significant interaction effect between time period and species. $K_{s(t)}$ for all species trended downwards toward lower specific conductivities, but changes for *L. occidentalis* were not significantly different (Fig. 1.21 A). Although variations were not statistically significant between adjacent time periods for *P. ponderosa*, there were significant decreases between weeks 3 to 6 and weeks 4 to 10. $K_{s(t)}$ for *P. menziesii* significantly decreased between weeks 4 to 6 and weeks 6 to 10, which mimicked the trend over time averaged over all species (Fig. 1.20 A). In week 2, *P. menziesii* $K_{s(t)}$ was significantly lower than *P. ponderosa*, but not significantly different from *L. occidentalis* (Fig. 1.22 A), while in week 10, *P. menziesii* was significantly lower compared to both species (Fig. 1.22 B). For both time periods, *L. occidentalis* and *P. ponderosa* were not significantly different. The differences for *L. occidentalis* and *P. ponderosa* at week 2 are not significantly different from week 10.

$K_{L(t)}$ exhibited clear fluctuations from weeks 2 to 10 (Fig. 1.21 B, solid lines) for *L. occidentalis* and *P. ponderosa*. The drop in $K_{L(t)}$ at week 2 for *L. occidentalis* was likely biased low by $n = 2$ measurements for this time period. Despite fluctuations, $K_{L(t)}$ dropped significantly for all species between weeks 6 and 10. Conversely, leaf area for all three species exhibited a rapid expansion between weeks 6 and 10 similar to functional xylem area expansion; *P. ponderosa* exhibited the greatest leaf area development (Fig. 21 B; dotted lines). The decrease in $K_{L(t)}$ with an increasing leaf area indicates that crown expansion exceeded the xylem area expansion for the same time period, thus changes in leaf area as opposed to changes in xylem area govern changes in $K_{L(t)}$. At weeks 2 and 10, *P. menziesii* was significantly lower than *L. occidentalis* and *P. ponderosa*, which were not significantly

different from one another (Fig. 1.22 C, D). Although $K_{L(t)}$ fluctuated over time, there were ultimately no differences for all species between the first and last time periods, although variability for two of the three species was much smaller at the latter time period.

Common Garden Experiment

L. occidentalis seedlings were the first and most responsive to drought with extensive yellowing, moderate wilting and some observed mortality by day 12 of the drought experiment, while *P. ponderosa* seedlings showed some yellowing of basal needles and cotyledons and *P. menziesii* seedlings displayed no discernable effects. *L. occidentalis* seedlings reached near 100% mortality by day 18, indicating that it was the most susceptible to drought induced hydraulic dysfunction. By day 24, *P. ponderosa* exhibited greater than 50% seedling mortality while *P. menziesii* exhibited only 3 individual cases of mortality but an obvious change to the majority of seedlings' leaf appearance, looking less vibrantly green compared to well-watered seedlings. By day 30, *P. ponderosa* seedlings experienced ca. 90% mortality while approximately 50% of the *P. menziesii* were still green but severely desiccated to the touch. By day 34, only three *P. menziesii* seedlings appeared alive, though they were severely stunted.

DISCUSSION

Overall, seedlings within the first 2 to 3 weeks of life were much more hydraulically conductive as compared to their older seedling counterparts, with larger tracheids, wider pits (D_m), and larger theoretical xylem specific conductivities, which facilitate maximum water transport to the crown per a given xylem area. However, from an anatomical perspective, they seem less able to mitigate hydraulic dysfunction with smaller thickness-to-span ratios (driven by smaller tracheid cell wall thicknesses), and smaller torus-to-pit aperture overlaps, which are less resistant to tracheid implosion and air seeding respectively.

Interestingly, observations of tori in week 2 seedlings were surprisingly infrequent (Fig. 1.17 B), even though the torus widths tended to be thicker in primary xylem and thus should have been easier to visualize using CLSM. One possible explanation is that the margo structures are more delicate and more susceptible to damage and subsequent torus displacement during transection; however, this should be a non-issue with CLSM, which is capable of scanning into the tissue beyond the mechanically damaged transected edge of the

sample. As week 2 is comprised entirely of protoxylem and the initial xylem clusters for all species (Fig. 1.16 A, F, K), this begs the question as to whether or not many of the bordered pits present within the initial xylem clusters have torus-margo membranes. It is plausible that these conduits may have simple pit membranes, which are not detectable at the maximum magnification used with CLSM in this experiment.

All species transitioned to production of secondary xylem via vascular cambium by week 3, although *L. occidentalis* was the only species to exhibit fully lignified xylem and axial parenchyma within the pith area. Between weeks 3 and 10, the seedlings underwent substantive xylem expansion and anatomical development. Week 10 functional characteristics effectively represented traits reflective of secondary xylem with smaller tracheid diameters, thicker cell walls, thinner tori and larger torus-to-aperture overlaps.

Surprisingly, for many of the functional traits, *L. occidentalis* and *P. ponderosa* were not significantly different at week 10 including $K_{s(t)}$, $K_{L(t)}$, Tw Dt^{-1}, and T_{den}, though *P. ponderosa* exhibited the highest A_L, A_{tfx}, and $K_{h(t)}$, indicating that *P. ponderosa* seedlings may be capable of transporting larger quantities of water, which increase the potential for photosynthesis and growth. A growing body of recent literature has linked pit properties and conductance; the wider pits in *P. ponderosa* likely contribute to higher conductivity compared to the other two species (Schulte et al. 2015).

By week 10, *L. occidentalis* exhibited the lowest A_L:A_{tfx} ratio and the highest tracheid lumen fraction but the lowest torus-to-pit aperture overlap and largest torus width. The low TPO (Table A.3) is most likely indicative of *L. occidentalis* being the least resistant to hydraulic dysfunction via air seedling; this conclusion is corroborated by the common garden experiment in which larch seedlings were the quickest to reach 100% mortality. The high tracheid lumen fraction of *L. occidentalis* illustrated that, in terms of carbon investment strategies, *L. occidentalis* may be more efficient in carbon allocation for xylem construction, whereby a greater proportion of xylem built is functional in water transport in the young seedlings. As illustrated in Figs. 14 and 26, *L. occidentalis* did not require the additional mechanical support of secondary xylem until after week 6, when the seedlings experienced substantial stem, xylem and crown growth, though lignification of the pith no doubt contributed to mechanical stability at younger stages.

This strategy can be contrasted against *P. ponderosa*, whose crown and xylem growth increased across all time periods and thus necessitated greater mechanical stability; though, why a greater portion of xylem were not functional is intriguing. One plausible explanation relates to the stomata-like openings found in the epidermis of *P. ponderosa* (MLR in prep). If the seedlings were actively photosynthesizing in the stem with adjacent pores available for gas exchange, the seedlings do not necessarily require water transport all the way to the crown and can instead route water radially to the chlorophyll in the stem.

By week 10. *P. menziesii* seedlings exhibited the highest A_L:A_{tfx} ratio, the largest thickness-to-span ratios, the lowest stem conductance, the lowest total functional xylem area, the lowest theoretical xylem and leaf specific conductivities, and tied with *P. ponderosa* for the lowest tracheid lumen fraction (A_{tfx}:A_x) and largest torus-to-pit aperture overlap. Combined with the results from the common garden experiment, this presents a very strong argument for the safety versus efficiency trade-off (Zimmermann 1983; Pitterman et al. 2006a; but see Gleason et al. 2016) in very young seedlings, in which the xylem of *P. menziesii* is more resistant to embolism, air seeding, and tension-induced implosion, but at the cost of hydraulic efficiency. The large A_L:A_{tfx} for *P. menziesii* indicates that for a given crown area (i.e. demand), the supply (i.e. functional xylem area) is much smaller, which would lead to overall more negative water potentials for a given transpiration flux as compared to the other two species. This would necessitate more embolism resistant xylem. What this doesn't take into account are other physiological and morphological responses, such as water use efficiency and rooting depth, which may make *P. ponderosa* more competitive in xeric conditions.

Another interesting anatomical implication for geographic distributions and potential recovery from drought induced stress relates to the lumen diameter distributions (Fig. 1.12). *P. ponderosa* distributions are skewed much farther right than the other two species, meaning it has greater numbers of very large tracheids. This implies not only a greater capacity to transport water but the potential to maintain a much greater proportion of functional tracheids during desiccation. In terms of P_{50} values, *P. ponderosa* my reach a water potential corresponding to 50% loss of conductivity, but if the loss corresponds to the largest of the tracheids (theoretically), then the *P. ponderosa* seedlings may still be capable of transporting

a significant amount of water should it become available again, meaning *P. ponderosa* seedlings may have a significant advantage in survivability after re-watering.

Conversely, *L. occidentalis* is drought deciduous, which is a unique attribute for a conifer species. It is therefore not surprising that it can functionally compete with *P. ponderosa* in terms of $K_{s(t)}$ and $K_{L(t)}$. *L. occidentalis* in the Pacific Northwest have been observed as having high transpiration rates and stomata that are not particularly sensitive to ambient humidity (Baker, unpublished), which appear to be capable of maximized water transport facilitating transpiration during the growing season. It then follows that this species would have to lowest A_L:A_{tfx} ratio, which means that for a given transpiration rate, this species is capable of maintaining the overall least negative water potentials. *Larix* spp. are also capable of allometric adjustments, such as dropping needles, to reduce the potential for embolism. Alternatively, the species may simply embolize over the growing season and produce new, conductive wood in the spring or refill prior to next year's budbreak, although definitive conclusions regarding refilling of embolized tracheids in conifer wood remain elusive (see review by Brodersen and McElrone 2013).

The current mechanistic paradigm for embolism refilling attributes the actual refilling process to axial parenchyma, which is supported both by circumstantial evidence and through direct visualization; water droplet formation on the lumen walls of embolized vessels have been shown to occur adjacent to axial parenchyma (Brodersen et al. 2010). These three species have prodigious amount of lignified, vasicentric axial parenchyma; if the current paradigm holds true, embolism refilling may represent a plausible drought mitigation strategy for these young seedlings. Refilling of the pith and primary xylem during initial stages of growth would result in a myriad of benefits by increasing overall hydraulic conductance and replenishing capacitive reserves. *P. ponderosa*, which had the smallest functional tracheid lumen fraction and conversely may have the greatest parenchyma area (within the xylem area, in additional to tracheids, there are axial parenchyma, lignified parenchyma walls, resin ducts [*P. ponderosa* and *L. occidentalis*] and radial parenchyma [rays]), which may give *P. ponderosa* seedlings a competitive advantage in xeric conditions where water availability fluctuates. One additional fascinating discovery was the presence of stomata-like pores and within the epidermis of *P. ponderosa*, which to the authors' knowledge, has never been reported in conifer seedlings, though they have been reported in *Arabidopsis* flower stalks

(see Nadeau and Sack 2002 and references therein). This implies a potential for large photosynthetic rates with associated production of carbohydrates within the seedlings stems, which would be in closer proximity to the axial parenchyma to facilitate quicker osmotic adjustments to ease xylem tension or facilitate rapid refilling.

One significant limitation to our study was the artificially induced drought in our common garden experiment, which was not representative of drought in field conditions. Often, precipitation tapers over the season rather than abruptly ceases, and melting snow packs during the spring provide additional plant accessible water. Additionally, *P. ponderosa* is known to root deep and fast during establishment, which allows it access to water resources not necessarily accessible to other, shallower rooted species. Combined with larger tracheids, greater tracheal area distributions and larger conductivities, *P. ponderosa* may be capable of outcompeting *P. menziesii* and *L. occidentalis* in xeric conditions with minimal water availability.

We would also be amiss if we did not further discuss the mechanisms for air seedling and potential influences of TPO, W_t and other pit membrane characteristics not measured. In conifers, there are several hypotheses in regards air seeding mechanisms: torus displacement when pressures exceed the torus' ability to remain flush against the inside of the bordered pit (Domec et al. 2006; Mayr et al. 2014), seal capillary seeding (Delzon et al. 2010), torus capillary seeding (Jansen et al. 2012), and torus prolapse (Zelinka et al. 2015). With a smaller TPO, the membrane is not as effective sealing off the embolized conduit, which would facilitate seal capillary seeding or torus displacement. Several studies have concluded that, due to the correlation between TPO and cavitation, the most likely mechanisms for air seeding occur at the torus-pit aperture interface (Delzon et al. 2010; Bouche et al. 2014), though there is some additional support for torus pore air seeding in Pinaceae (Jansen et al. 2012; Bouche et al. 2014).

Other research has shown no correlation between margo porosity and cavitation resistance (Pittermann et al. 2010) and little to no correlation between pit conductivity and pressure required to induce air seeding (Hacke et al. 2004; Pitterman et al. 2006b). Margo flexibility has been both positively and negatively correlated with embolism resistance (Hacke et al. 2004; Domec et al 2006; Delzon et al. 2010), but Bouche et al. (2014) found little

difference in margo flexibility between 115 different species, which is a strong indication that the margo may play a somewhat insignificant role in embolism resistance.

Additionally, torus width remains an understudied but potentially critical anatomical component (Schulte et al. 2015). Mechanical-displacement experiments performed by Zelinka et al. (2015) showed the torus itself to be surprisingly flexible. We hypothesize here that thicker tori may be less flexible and reduce sealing capacity when aspirated and thus would be more prone to seal capillary seeding; this would be further exacerbated by a small TPO; however, a thicker torus may reduce torus capillary seeding and the potential for torus prolapse. To our surprise, our results indicate that torus width is either uncorrelated or only very slightly correlated to any other pit anatomical or functional characteristic, including TPO ($P = 0.08$). W_t is likely to be related to embolism resistance in the sense that the widest tori are observed both in primary xylem and in *L. occidentalis*, which we hypothesize to be the most embolism prone tissue type and species, yet its independence from other traits indicates that it may be co-evolved feature that inherently plays a causative role in embolism resistance, though teasing apart the influences between TPO and W_t will be necessary in future research. Regardless, anatomical knowledge and predictions on seedling hydraulic properties would be enhanced by further research on the torus-margo structures in seedling bordered pits, especially as further research continues to refine the role of pits in hydraulic conductivity and embolism resistance.

A last caveat to this study is that, due to time and funding limitations, SEM imaging and subsequent analyses were not performed on seedling pits. As discussed earlier, evidence put forth in a growing body of recent literature supports the hypothesis that xylem conductivity in conifers is dependent upon pits in general, and specifically, the largest of the margo pores sizes and total margo pore area (Schulte et al. 2015 and references therein). However, in terms of air seeding resistance, the margo plays a somewhat controversial role. While several different mechanisms are hypothesized, there is evidence for multiple potential mechanisms at play simultaneously within Pinaceae (Bouche et al. 2014, Mayr et al. 2014; Schulte et al. 2015). Schulte et al. (2015) posit that a margo with larger pores and finer "spokes" are more prone to cavitation fatigue and thus more likely to lead to hydraulic dysfunction. However, as *in planta* embolism refilling is controversial, it is unknown how cavitation fatigue figures into actual plant embolism resistance.

CONCLUSION

Based on anatomical measurements, we expect that protoxylem, metaxylem, then secondary xylem would be the order of increasing resistance to embolism and air seeding. While tracheid implosion is not frequently observed *in situ* (implosion pressure is generally more negative than embolism pressure), this may not hold true with protoxylem, in which the cell walls are only helically thickened (not shown). Contrary to our hypothesis, by week 10, xylem of *P. menziesii* appeared to be the most embolism resistant, followed by *P. ponderosa* and then *L. occidentalis*, based on torus-to-pit aperture overlap, thickness-to-span ratio, tracheid density, and torus width. Our common garden experiment supports this conclusion, where embolism resistance and therefore resistance to hydraulic dysfunction in absence of any source of water is dependent upon anatomy where external mitigating factors are excluded.

However, considerable changes in anatomy over the initial 10-week growth period are indicative of potentially drastic changes in embolism resistance depending on the developmental stage and the species. Seedling age at the onset of limited water availability is likely to have a significant influence on survivability for all species, especially due to lack of external mitigating factors, such as rooting depth and thick needle cuticles. With such substantial differences in key morphological and functional traits, we would expect *in situ* vulnerability curves generated at any given time period to be different from any other week.

Our comparisons here suggest that in terms of geographical locations *P. ponderosa* is capable of out-competing both *P. menziesii* and *L. occidentalis* in xeric habitats, yet extreme, long-term drought events may have the greatest impact on *P. ponderosa* if the drought conditions exceed *P. ponderosa*'s ability to recover after re-watering, which may be inherently linked to tracheid size distributions and potential embolism refilling capabilities. Further research defining this mortality threshold in these species at the seedling stage as well as determining the capacity for embolism refilling will further enhance prediction of distribution changes and potential mortality events.

REFERENCES

Anderegg, W.R.L., Anderegg, L.D.L. 2013. Hydraulic and carbohydrate changes in experimental drought-induced mortality of saplings in two conifer species. Tree Physiology 33:252-260.

Bond, J., Donaldson, L., Hitchcock, K. 2008. Safranin fluorescent staining of wood cell walls. Biotechnic & Histochemistry 83(3-4):161-171.

Bouche, P.S., Larter, M., Domec, J.-C., Burlett, R., Gasson, P., Jansen, S., Delzon, S. 2014. A broad survey of hydraulic and mechanical safety in the xylem of conifers. Journal of Experimental Botany 65(15):4419-4431.

Burns, Russell M., Honkala, B.H. (tech. coords.) 1990. Silvics of North America: 1. Conifers; 2. Hardwoods. Agriculture Handbook 654. U.S. Department of Agriculture, Forest Service, Washington, DC.

Chaffey, N. 1999. Wood formation in forest trees: from Arabidopsis to Zinnia. Trends in Plant Science 4(6):203-204.

Chaffey, N., Cholewa, E., Regan, S., Sundberg, B. 2002. Secondary xylem development in *Arabidopsis*: a model for wood formation. Physiologia Plantarium 114:594-600.

Chang, S.-S., Quignard, F., Almeras, T., Clair, B. 2014. Mesoporosity changes from cambium to mature tension wood: a new step toward the understanding of maturation stress generation in trees. New Phytologist 205:1277-1287.

Cheaib, A., Badeau, V., Boe, J., Chuine, I., Delire, C., Dufrêne, E., François, C., Gritti, E.S., Legay, M., Pagé, C. and Thuiller, W. 2012. Climate change impacts on tree ranges: model intercomparison facilitates understanding and quantification of uncertainty. Ecology letters, 15(6):533-544.

Clark, J.S., Iverson, L., Woodall, C.W., Allen, C.D., Bell, D.M., Bragg, D.C…Zimmerman, N.E. 2016. The impacts of increasing drought on forest dynamics, structure and biodiversity in the United States. Global Change Biology 22:2329-2352.

Dalla-Salda, G., Martinez-Meier, A., Cochard, H., Rozenberg, P. 2011. Genetic variation of xylem hydraulic properties shows that wood density is involved in adaptation to drought in Douglas-fir (*Pseudotsuga menziesii* (Mirb.)). Annals of Forest Science 68:747-757.

Delzon S., Douthe, C., Sala, A., Cochard, H. 2010. Mechanism of water-stress induced cavitation in conifers: bordered pit structure and function support the hypothesis of seal capillary-seeding. Plant, Cell and Environment 33:2101–2111.

Dickison, W.C. 2000. Integrative Plant Anatomy. Academic Press, San Diego

Domec, J.-C., Lackenbruch, B., Meinzer, F. 2006. Bordered pit structure and function determine spatial patterns of air-seeding thresholds in xylem of Douglas-fir (Pseudotsuga menzeisii; Pinaceae) trees. American Journal of Botany 93(11): 1588-1600.

Esau, K. 1977. Anatomy of Seed Plants. 2nd Ed. John Wiley & Sons Toronto, Canada.

Gleason, S.M., Westoby, M., Jansen, S., Choat, B., Hacke, U.G., Pratt, R.B., Bhaskar, R….Zanné, A.E. 2016. Weak tradeoff between xylem safety and xylem-specific hydraulic efficiency across the world's woody plant species. New Phytologist 209:123-136.

Hacke, U.H. [ed.]. 2015. Functional and Ecological Xylem Anatomy. Springer International Publishing, Switzerland.

Hacke, U.G., Sperry, J.S. 2001. Functional and ecological xylem anatomy. Perspectives in Plant Ecology, Evolution and Systematics 4(2):97-115.

Hacke, U.G., Sperry, J.S., Pittermann, J. 2004. Analysis of circular bordered pit function II. Gymnosperm tracheids with torus-margo pit membranes. American Journal of Botany 9(3):386-400.

Hector, A.R. 2015. The New Statistics with R: An Introduction for Biologists. Oxford University Press, New York.

Hedden, P., Thomas, S.G. (eds). 2006. Frontmatter, in Annual Plant Reviews Volume 24: Plant Hormone Signaling. Blackwell Publishing, Oxford, UK.

Hepler, P.K., Gunning, B.E.S. 1998. Confocal fluorescence microscopy of plant cells. Protoplasm 201:121-157.

Jansen, S., Lamy, J.B., Burlett, R., Cochard, H., Gasson, P., Delzon, S. 2012. Plasmodesmatal pores in the torus of bordered pit membranes affect cavitation resistance of conifer xylem. Plant, Cell and Environment 35:1109–1120.

Johnson, D.M., McCulloh, K.A., Reinhardt, K. 2011. The earliest stages of tree growth: development, physiology and impacts of microclimate. In: Meinzer, F.C., Lackenbruch, B., Dawson, T.E. (eds). Size- and Age-Related Changes in Tree Structure and Function: 65-87. Springer, Netherlands.

Kitin, P., Sano, Y., Funada, R. 2003. Three-dimensional imaging and analysis of differentiating secondary xylem by confocal microscopy. IAWA Journal 24(3):211-222.

Kuznetsova, A., Brockhoff, P.B., Christensen, H.B. 2016. lmerTest: Tests in Linear Mixed Effects Models. R package version 2.0-32. https://CRAN.R-project.org/package=lmerTest.

Lambers, H., Chapin, F.S., Pons, T.L. 1998. Plant Physiological Ecology. Springer, New York.

Lehmann, F., Hardtke, C.S. 2016. Secondary growth of the *Arabidopsis* hypocotyl – vascular development in 4 dimensions. ScienceDirect 29:9-15.

Lenth, R.V. 2016. Least-Squares Means: The R Package lsmeans. Journal of Statistical Software 69(1):1-32.

Logan, M. 2010. Biostatistical Design and Analysis Using R: A Practical Guide. Wiley-Blackwell, West Sussex, UK.

Lucas, W.J., Groover, A., Lichtenberger, R., Furuta, K., Yadav, S.-R., Helariutta, Y., He, X.-Q….Kachroo, P. 2013. The Plant Vascular System: Evolution, Development and Functions. Journal of Integrative Plant biology 55(4):294-388.

Maherali, H., Williams, B.L., Paige, K.N., DeLucia, E.H. 2002. Hydraulic differentiation of ponderosa pine populations along a climate gradient is not associated with ecotypic divergence. Functional Ecology 16:510-521.

Martinez-Vilalta, J., Piñol, J., Beaven K. 2002. A hydraulic model to predict drought-induced mortality in woody plants: an application to climate change in the Mediterranean. Ecological Modeling 155:127-147.

Mayr, S., Kartusch, B., Kikuta, S. 2014. Evidence for Air-Seedling: watching the formation of embolism in conifer xylem. The Journal of Plant Hydraulics 1:e0004.

McDowell, N.G., Fisher, R.A., Xu, C., Domec, J.-C., Höltaä, T., Mackay, D.S., Sperry, J.S….Pockman, W.T. 2013. Evaluating theories of drought-induced vegetation mortality using a multimodel-experiment framework. New Phytologist 200:304-321.

Mellerowicz, E.J., Baucher, M., Sundberg, B., Boerjan, W. 2001. Unravelling cell wall formation in the woody dicot stem. Plant Molecular Biology 47:239-274.

Nadeau, J.A., Sack, F.D. 2002. Stomatal Development in Arabidopsis. In: The Arabidopsis Book. The American Society of Plant Biologists doi: http://dx.doi.org/10.1199/tab.0066

Noves, E., Kirst, M., Chiang, V., Winter-Sederoff, H., Sederoff, R. 2010. Lignin and biomass: a negative correlation for wood formation and lignin content in trees. Plant Physiology 154(2):555-561.

Ogasa, M., Miki, N.H., Murakami, Y., Yoshikawa, K. 2013. Recovery performance in xylem hydraulic conductivity is correlated with cavitation resistance for temperate deciduous tree species. Tree Physiology 33(4):335-344.

Pallardy, S.G. 2008. Physiology of Woody Plants. 3rd Ed. Elsevier, San Diego.

Pittermann, J., Choat, B., Jansen, S., Stuart, S.A., Lynn, L., Dawson, T.E. 2010. The relationships between xylem safety and hydraulic efficiency in the Cupressaceae: the evolution of pit membrane form and function.

Pittermann J., Sperry, J.S., Wheeler, J.K., Hacke, U.G., Sikkema, E.H. 2006a. Mechanical reinforcement against tracheid implosion compromises the hydraulic efficiency of conifer xylem. Plant, Cell and Environment 29:1618–1628.

Pittermann J., Sperry J.S., Wheeler, J.K., Hacke, U.G., Sikkema, E.H. 2006b. Inter-tracheid pitting and the hydraulic efficiency of conifer wood: the role of tracheid allometry and cavitation protection. American Journal of Botany 93:1265–1273.

Preibisch, S., Saalfeld, S., Tomancak, P. 2009. Globally optimal stitching of tiled 3D microscopic image acquisitions. Bioinformatics 25(11):1463-1465.

Preston, R.D. 1964. Interdisciplinary Approaches to Wood Structure in Cellular Ultrastructure of Woody Plants. In: Cote, W.A (ed.). Proceedings for the Advanced Science Seminar. Upper Saranac Lake, New York. Syracuse University Press, Syracuse, New York.

Real, L.A., Brown, J.H. (eds.). 1991. Foundations of Ecology: classic papers with commentaries. The University of Chicago Press, Chicago.

RStudio Team (2015). RStudio: Integrated Development for R. RStudio, Inc., Boston, MA URL http://www.rstudio.com/.

Ruzin, S.E. 1999. Plant Microtechnique and Microscopy. Oxford University Press, Inc, New York.

Sant'Anna, C., Costa, L.T., Abud, Y., Biancatto, L., Miguens, F.C., de Souza, W. 2013. Sugarcane Cell Wall Structure and Lignin Distribution Investigated by Confocal and Electron Microscopy. Microscopy research and technique 76:829-834.

Santiago, L.S., Goldstein, G., Meinzer, F.C., Fisher, J.B., Machado, K., Woodruff, D., Jones, T. 2004. Leaf photosynthetic traits scale with hydraulic conductivity and wood density in Panamanian forest canopy trees. Oecologia 140:543-550.

Schindelin, J., Arganda-Carreras, I., Frise, E. 2012. Fiji: an open source platform for biological-image analysis. Nature methods 9(7):676-682.

Schulte, P.J., Hacke, U.G., Schoonmaker, A.L. 2015. Pit membrane structure is highly variable and accounts for a major resistance to water flow through tracheid pits in stems and roots of two boreal conifer species. New Phytologist 208:102-113.

Schweingruber, F.H. 2007. Wood Structure and Environment. Springer, New York.

Sperry, J.S., Nichols, K.L., Sullivan, J.E.M., Eastlack, S.E. 1994. Xylem embolism in ring-porous, diffuse-porus, and coniferous trees of Northern Utah and Interior Alaska. Ecology 75(6):1736-1752.

Sperry, J.S., Hacke, U.G., Pitterman, J. 2006. Size and function in conifer tracheids and angiosperm vessels. American Journal of Botany 93(10):1490-1500.

Sterck, F.J., Martinez-Vilalta, J., Menucuuini, M., Cochard, H., Gerrits, P., Zweifel, R., Herrero, A….Sass-Klaassen, U. 2012. Understanding trait interactions and their

impacts on growth in Scots pine branches across Europe. Functional Ecology 26:541-549.

Tyree, M.T., Ewers, F.W. 1991. The hydraulic architecture of trees and other woody plants. New Phytologist 119(3):345-360.

Tyree, M.T., Zimmermann, M.H. 2002. Xylem Structure and the Ascent of Sap. 2nd Ed. Springer, Verlag, Berlin.

Venables, W. N., Ripley, B. D. 2002. Modern Applied Statistics with S. 4th Ed. Springer, New York.

Woodruff, D.R. 2014. The impacts of water stress on phloem transport in Douglas-fir trees. Tree Physiology 34:5-14.

Zelinka, S.L., Bourne, K.J., Hermanson, J.C., Glass, S.V., Costa, A., Wiedenhoeft, A.C. 2015. Force-displacement measurements of earlywood bordered pits using a mesomechanical tester. Plant, Cell and Environment 38:2088-2097.

Zhang, J., Elo, A., Helariutta, Y. 2011. *Arabidopsis* as a model for wood formation. ScienceDirect 22:293-299.

Zimmermann, M.H. 1983. Xylem Structure and the Ascent of Sap. Springer, New York.

Zuur, A.F., Ieno, E.N., Walker, N.J., Savelieve, A.A., Smith, G.M. 2009. Mixed Effects Models and Extensions in Ecology with R. Springer, New York.

Chapter 2

A comparison of P_{50} estimates, anatomical characteristics, and functional traits to *in planta* embolism in very young conifer stems using X-ray computed microtomography

INTRODUCTION

Conifers are dominant in many forested ecosystems across our globe (Biswas and Johri 1997; Farjon 2008; Lin et al. 2010). These forests provide vast amounts of terrestrial ecosystems services and functions including oxygen production, carbon sequestration, water filtration, erosion control and wildlife habitat not to mention numerous anthropogenic services such as recreation and aesthetics (Allen et al. 2010; also see Adams et al. 2013 and references therein). Unfortunately, unpredictable large scale mortality events are already changing forest composition, structure, species abundance (Martinez-Vilalta and Piñol 2002; Bigler et al. 2007; Carnicer et al. 2011; Hereş et al. 2012; Barbeta et al. 2013; Breshears et al. 2015; Clark et al. 2016) and decimating plantation and monoculture ecosystems, (e.g. Millar et al. 2012; Michaelian et al. 2010; Garcia de la Seranna et al. 2015; Slezak 2016). Fortunately, the geographical distributions of these forests are surprisingly versatile within the temporal context of planet Earth history; latitudinal migrations of Pinaceae are evident in fossil records (see references in Brodribb et al. 2012) and current species migrations are already under observation (Allen and Breshears 1998; Gworek et al. 2007; Rapacciuolo et al. 2014), yet the IPCC predicts that, on average, tree migration rates (km yr^{-1}) will be unable to track with climate change velocity (°C yr^{-1}) for even the lowest rates of climate change model estimates (Settele 2014; see also Loarie et al. 2009).

Successful migration for forest species necessarily and fundamentally depends upon seedling establishment beyond current borders (Johnson et al. 2011), yet seedlings are the most susceptible to drought- and temperature-induced mortality (e.g. Moyes et al. 2013), with highest rates of mortality documented during the first year (Haig et al. 1941; Burns and Honkala 1990; Cui and Smith 1990; Mori et al. 2004). This may indicate that seedling recruitment is a bottleneck to forest natural regeneration and migration (Clark et al. 2016), especially if adult mortality rates exceed seedling recruitment rates.

Surprisingly, research to date is sparse in regards to first-year seedling hydraulic properties and drought-induced dysfunction (Kolb and Robberecht 1996, Cui and Smith 1990; Reinhardt et al. 2015; MLR in prep; Brix 1979; Zavitkovski and Ferrell 1968; Maherali et al. 2002), with very little from the 21st century. The little information available demonstrates that seedling vulnerability cannot be extrapolated from their adult counterparts. Based on hydraulic conductivity measurements, resistance to hydraulic dysfunction in seedlings – seedlings in this context is used loosely and does not necessarily refer to first-year seedlings – can be greater than, less or equal to their respective adult counterparts depending on the species (Cui and Smith 1990; Urli et al. 2013; DMJ unpublished) and intra-species variations in first-year seedlings across geographical ranges is virtually unknown, although Kavanagh et al. (1999) found that there were differences in xylem resistance to cavitation and conductivity between four populations of three-year-old *P. menziesii* seedlings and Reinhardt et al. (2011) found differences in stomatal conductance and photosynthesis between two different populations of *Pinus flexilis* seedlings. Additionally, several hydraulic properties in mature species, such as capacitance and xylem specific conductivity, have been shown to vary by geographical regions for a number of different species (Corcuera et al. 2012; Maherali et al. 2002; Barnard et al. 2011); it seems reasonable, therefore, to assume that first-year seedling functional traits and characteristic would be different between populations or provenances.

This suggests a regionalized approach may be necessary, with research necessarily focused on local species and seed sources. An understanding of native conifer seedling responses to drought is critical in order to better predict changing species distributions, especially in places like the Pacific Northwest USA, which is characterized by summer seasonal drought. Very young seedlings must be able to tolerate drought as early as within the first month of above ground life (Haig et al. 1941). However, with the unprecedented speed of our changing climate (Allen and Breshears 1998), seedlings may face increasing water-related stress very early in their life cycle, which is attributed to longer growing seasons (Settele et al. 2014), smaller snow packs (Mote et al. 2005), potential for higher transpiration rates (further exacerbated by increases in temperatures), and decreased summer and fall precipitation (Abatzoglou et al. 2014).

If we wish to understand seedling hydraulic dysfunction and potentially predict mortality in the context of a changing climate, we must first understand how *in vitro*

measurements of hydraulic conductivity during desiccation and subsequent P_{50} estimates coincide with *in planta* hydraulic dysfunction and actual mortality. Even though P_{50} is often used as a proxy for plant resistance to embolism, these *in vitro* measurements do not necessarily reflect plant natural distributions nor do they enable accurate drought-induced mortality predictions. For instance, multiple studies have illustrated that *P. ponderosa* wood is more inherently vulnerable to embolism (i.e. less negative P_{50}) as compared to *P. menziesii* (Martinez-Vilalta et al. 2004, Domec et al. 2009, and Barnard et al. 2011), yet *P. ponderosa* typically inhabits more xeric habitats (Burns and Honkala 1990). This pattern is illustrated across multiple species, where species from more xeric habitats are not necessarily more resistant to embolism (see Bouche et al. 2014 and references therein). In terms of predicting mortality, Schwantes et al. (2016) has unequivocally shown that *Juniperus ashei* experienced the highest mortality rates in Texas after several years of severe drought, even though it had been considered the most drought tolerant tree species within that ecosystem (i.e. most negative P_{50}) (McElrone et al. 2004). Conversely, *Quercus fusiformis*, one of the species with the least negative P_{50}, exhibited very little drought-induced mortality. We do not, as of yet, fully comprehend how *in vitro* hydraulic properties relate to functional capacities to survive dry and drought conditions.

To further complicate the issue with young seedlings, there is very little research detailing species-specific xylem anatomical characteristics, development, and hydraulic properties. As discussed by MLR (Chapter 1), little is known about the mechanisms for mitigating hydraulic dysfunction in seedlings and the little available research indicates that seedling hydraulic characteristics cannot be extrapolated from adult counterparts. The lack of species-specific anatomical information is also critical as many aspects of xylem anatomy, including tracheid and pit characteristics, are associated with plant hydraulic properties and embolism resistance (Tyree and Zimmermann 2002).

In a previous study (MLR in prep), we analyzed and compared xylem anatomical characteristics and functional traits at five different time periods during early development in *Pseudotsuga menziesii* var. *glauca*, *Pinus ponderosa* var. *ponderosa* and *Larix occidentalis* to infer theoretical embolism resistance and hydraulic capacities. Here, we combined a subset of those data with *in vivo* embolism imaging using high resolution x-ray computed microtomography (microCT) during desiccation as well as traditional stem hydraulic

vulnerability curves to elucidate *in vitro* versus *in vivo* hydraulic dysfunction in 6-week-old *P. menziesii* var. *glauca*, 6-week-old *L. occidentalis*, and 4-week-old *P. ponderosa* var. *ponderosa*. High resolution x-ray computed microtomography is a relatively new technological tool in the plant physiologist's toolkit, which allows for *in planta*, real time, 3-dimensional imaging of internal plant structures (Stuppy et al. 2003; Brodersen et al. 2012), stem and leaf hydraulic dysfunction during drought (Brodersen et al. 2013; Choat et al. 2015) and embolism repair (Brodersen et al. 2010). Based on the results from our previous study (MLR Chapter 1), we developed the following objectives and hypotheses:

Hypotheses and Objectives

(1) Objective 1: Compare measured hydraulic traits with calculated theoretical functional traits.

(2) Objective 2: Visualize actual embolized tracheids during desiccation with microCT imaging and compare to hypothesized embolism resistance based on measured anatomical characteristics, with special focus given to the differences between primary and secondary xylem.

(3) Objective 3: Compare overall visualized seedling embolism among species and compare to hypothesized embolism resistance based on anatomical measurements and estimated P_{50} values.

(4) Hypothesis: Protoxylem, metaxylem and secondary xylem will be the least to most embolism resistant, respectively.

(5) Hypothesis: *P. ponderosa*, *L. occidentalis*, and *P. menziesii* represent least to most embolism resistant respectively.

MATERIALS AND METHODS

Plant Materials and Growing Conditions

Seeds from all species were initially germinated at the University of Idaho's Franklin H. Pitkin Forest Nursery located in Moscow, ID, USA (46°43'N, 116°59'W) and subsequently transported to the University of Idaho's Sixth Street Greenhouse. All seeds were sourced from locally collected seeds to minimize geographical differences in intra-species characteristics. Seedlings used for the anatomical analysis were grown as described by ML Riley (see methodologies Chapter 1).

On May 20, 2015, approximately two weeks after germination for *P. menziesii* and *L. occidentalis,* seedlings were transplanted from styro-growing blocks into 9.1 x 9.1 x 10.8 cm Anderson Pots (AB45; Stuewe & Sons, Tangent, OR, USA); *P. ponderosa* was sown directly from seed on the same date. All species were grown in a commercial potting mix (Metro-Mix Custom Blend, Sun Gro Horticulture, Agawam, MA, USA) consisting of 40-50% Canadian Sphagnum peat moss, vermiculite, and bark.

One month after planting/transplanting, seedlings from each species were randomly selected for one of three watering treatments: well-watered, mid-watered, and low-watered, resulting in 16-18 seedlings per treatment per species. Watering treatments were determined by counting the number of passes with the watering hose required to saturate the well-watered seedlings; mid-watered seedlings received half as many passes and the low-watered treatment received only one pass. Seedlings were shipped overnight from Moscow, ID to Berkeley, CA one day prior to the commencement of microCT imaging.

Confocal Laser Scanning Microscopy (CLSM)

CLSM was used for shallow 3D optical imaging of seedling anatomy and vascular development. Stem preparation and imaging protocols were thoroughly described by MLR (in prep). Briefly, seedlings were collected from the greenhouse and stored in FAA (95% ethanol: acetic acid: 37% formaldehyde: water; 50:5:10:35 v/v) (Ruzin 1999). Prior to imaging, seedling stems were stained with Safranin O, dehydrated and rehydrated in stepped acetone concentrations, cleared with glycerol, hand sectioned and mounted in glycerol. Images were optically scanned with an Olympus FV1000 Confocal Microscope (Olympus Corp, Center Valley, PA, USA) using three laser lines 405, 488, and 559 nm at three different magnifications (10x, 20x, and 60x); composite images were used for anatomical analyses. See MLR Chapter 1 for more details on CLSM.

X-ray computed microtomography (microCT)

Actual hydraulic dysfunction during desiccation was visualized *in vivo* using high resolution computed microtomography (microCT) (Beamline 8.3.2; Advanced Light Source, Berkeley, CA), with concurrently measured hydraulic conductivity and water potential measurements to generate vulnerability curves (see next section) at the 4-week age class for *P. ponderosa* and 6-week age classes for and *P. menziesii* and *L. occidentalis*. Different age classes were necessitated for *P. ponderosa* due to plant and container size restrictions for

microCT imaging. Eighty total seedlings were scanned between the root collar and the crown base: 16, 19, and 15 intact stems for *P. ponderosa*, *P. menziesii* and *L. occidentalis* respectively and 10 excised stems per species (see next section).

All seedlings were imaged using the procedure described in-depth by McElrone et al. (2013). Seedlings were mounted into a custom holder, covered by an acrylic cylinder to reduce vibrations, and imaged using continuous tomography at 24 keV while the seedling was rotated from 0-180°. Images were captured by a camera (PCO EDGE; Cooke Corp., Romulus, MI, USA) with a 5x magnification Mitutoyo long working distance lens. Scanned volumes were larger for intact seedlings with an effective volume height of 2.2mm, resulting in 1025 raw 2-dimensional images per stem while excised stem volume heights were 21.4µm resulting in 513 raw 2D images. Raw images were then reconstructed using Octopus Software ImageJ plugin (Institute for Nuclear Sciences, University of Ghent, Belgium), resulting in 1636 .tif image slices and 16 .tif image files respectively with a voxel size of 1.338µm x 1.338µm x 1.338µm (x, y, z pixel dimensions). After imaging, seedlings were processed for vulnerability curves.

Vulnerability Curves

Vulnerability curves (VCs) express the relationship between hydraulic conductivity and increasing xylem tension (Sperry and Saliendra 1994; Kolb et al. 1996). Procedures for constructing vulnerability curves have been well established with numerous variants (Sperry and Saliendra 1994; Melcher et al. 2010; Barnard et al. 2011; McCulloh et al. 2012; Barigah et al. 2013), but few of these variants have been used for very delicate, small diameter tissues, where standard conductivity measurements and water potential measurements (pressure bomb) are likely to cause severe mechanical damage.

We therefore combined standard bench dehydration methods with a modified Sperry apparatus (Sperry et al. 1988). Stem hydraulic conductance (K_h) was measured using a Sensirion SLI-0430 low flow meter (Stafa, Switzerland) after microCT imaging. One end of the stem segment was connected through the low flow meter to a reservoir containing filtered, degassed 20mM KCl aqueous solution. The other tip of the stem segment was placed directly in a shallow water resevoir to prevent flow variability due to water bubble buildup and release. This required only one side of the stem to undergo physical manipulation, which reduced possible mechanical damage from handing as well as leaks at the stem-to-tube

connection point. K_h was calculated as the output of the flowmeter (volume/time) divided by the pressure gradient, which was then normalized by the length and stem diameter of the sample for an estimate of stem specific conductivity (K_s) (Zimmermann et al. 1983; Sperry et al. 1988). In our case, soft tissues were not removed from the stem prior to conductivity measurements due to the excessively small (0.94 ± 0.04 mm) and delicate nature of the xylem.

Native K_s was measured on an average of 10 ± 1 (SD) intact seedlings per species across all watering treatments. Due to the water retention properties of the soil combined with the volume of the pots, the low-watering treatment seedlings were not dehydrated enough to construct a full vulnerability curve (VC). Thus, to supplement the VC, ten individuals per species were randomly selected from the well-watered group and stems between the root collar and crown base were excised. These excised stems were placed in degassed, filtered, 20mM KCl water under a partial vacuum overnight. Two stems per species were immediately imaged and subsequently measured for K_s max; the remainder of the excised stems were bench dehydrated, imaged in pairs, and then measured for K_s and water potential.

Thermocouple psychrometers (Merrill Specialty Equipment, Logan, UT) were used to measure water potential on equilibrated leaf tissue in the case of intact plants or small stem segments in the case of excised stems. Prior to stem measurements, the psychrometers were calibrated on-site with four different salt solutions from which a calibration factor was derived (Brown and Bartos 1982). Samples were enclosed in stainless steel psychrometer chambers, triple-bagged, submerged in a 25^{o}C water bath, and equilibrated for at least four hours or until sequential measurements were stable. Psychrometers were measured by an AM16/32B multiplexer interfaced to a CR6 data logger (Campbell Scientific, Logan, UT). Full vulnerability curves for each species were constructed with K_s as a function of water potential using both intact and excised stem measurements.

Anatomical and Trait Characteristic Comparisons

Mean anatomical measurements including stem cross-sectional diameters (D_s), xylem cross-sectional diameters (A_s), actual functional xylem area (A_{tfx}), tracheid diameters (D_t), tracheid area distributions, tracheid cell wall thickness (Tw), torus and margo diameters (D_{tor}, D_m), torus widths (W_t), pit aperture diameters (D_{pa}), tracheid densities (T_{den}) and leaf areas (A_L) as well as functional traits including theoretical $K_{s(t)}$ and $K_{h(t)}$, functional tracheid lumen

fraction (A_{tfx}:A_x), thickness-to-span ratios (Tw Dt^{-1}), and torus-to-pit aperture overlap (TPO), were measured or calculated and subsequently analyzed for inter- and intraspecies comparisons as described by MLR (Chapter 1). Here, we also calculated two additional pit functional characteristics: margo flexibility [$F_m = (D_m-D_{tor})/D_{tor}$)] and valve effect [$V_{ef} = F_m$ * TPO], both of which are hypothesized to relate to seal capillary air seeding resistance.

We also compared theoretical $K_{s(t)}$ for each species at their respective ages (week 4 for *P. ponderosa* and week 6 for *P. menziesii* and *L. occidentalis*) to hydraulically measured values. Actual embolized tracheids as visualized by microCT imaging were compared between species for each xylem type (i.e. proto-, primary or secondary xylem) to determine if *in vivo* embolism was consistent with hypothetical embolism resistance as posited by MLR in Chapter 1, where *P. ponderosa*, *L. occidentalis* and *P. menziesii* represent the spectrum from least to most embolism resistant respectively at these specific ages.

Statistical Analysis

All anatomical measurement analyses, including F_m and V_{ef} were conducted in R Studio (RStudio Team 2015) as described by MLR (Chapter 1). Here, pairwise post-hoc analyses were conducted to compare *P. ponderosa* at week 4 to *P. menziesii* and *L. occidentalis* at week 6. All fixed-effects models were analyzed using ANOVA type III for an unbalanced design. Liner mixed modeling was performed using "lmer" from the "lmerTest" package and Post-hoc Tukey's pairwise tests were performed for both model types using "lsmean" package for significant differences at $P < 0.05$. Vulnerability curve fits were conducted in Sigma Plot 12.5 (Systat Software, San Jose, CA).

RESULTS

Anatomical and Trait Comparisons

Table 2.1 Anatomical and Functional Traits of Interest.

Trait	***P. menziesii*** (week 6)	***L. occidentalis*** (week 6)	***P. ponderosa*** (week 4)
A_s (mm^2)	0.637±0.042[a]	0.370±0.027[b]	1.824±0.099[c]
A_x (mm^2)	0.118±0.008[a]	0.061±0.006[b]	0.335±0.025[c]
A_{tfx} (mm^2)	0.069±0.005[a]	0.039±0.002[a]	0.148±0.010[b]
D_t (μm)	6.89±0.22[a]	8.23±0.22[a]	10.93±0.29[b]
$K_{s(t)}$ (kg m^{-1} s^{-1} MPa^{-1})	1.01±0.14[a]	1.40±0.09[a]	2.58±0.020[b]
$K_{h(t)}$ (kg m s^{-1} MPa^{-1})	7.11E-5±1.17E-5[a]	5.38E-5±5.36E-6[a]	3.89E-4±5.11E-5[b]
Tw Dt^{-1}	0.73±0.04[a]	0.57±0.02[ab]	0.40±0.01[b]
W_t (μm)	0.63±0.026[a]	0.83±0.019[b]	0.68±0.016[ab]
TPO	0.56±0.017[a]	0.48±0.014[b]	0.45±0.014[b]
F_m	0.84±0.03[a]	0.91±0.03[a]	1.05±0.03[a]
V_{ef}	0.46±0.02[a]	0.41±0.01[a]	0.42±0.01[a]

Mean +/- SE. Reproduced from MLR (in prep). Different letters per trait indicate significance at $P < 0.05$. Traits in bold were used to determine hypothesized species' resistance to embolism. Statistical analyses were performed on transformed variables; means are reported are on original scale.

Table 2.1 was partially reproduced from MLR (in prep) illustrating reported differences among 6-week old *P. menziesii*, 6-week old *L. occidentalis*, and 4-week old *P. ponderosa*. The only exception is TPO, in which the values reported were averaged over measurements from 5 different time periods. The largest TPO and Tw Dt^{-1} in *P. menziesii* indicate a better overall resistance to hydraulic dysfunction during drought though it exhibits the lowest theoretical specific conductivity ($K_{s(t)}$). *P. ponderosa* exhibits the lowest values for both TPO and Tw Dt^{-1}, indicating that at this age, it may be the least resistant to embolism compared to the other two species. Even though *P. ponderosa* is several weeks younger, it is significantly larger and more hydraulically conductive.

For both margo flexibility (F_m) and valve effect (V_{ef}), results indicated no statistically significant differences between the species at this age. This is likely due to complex interactive effects between xylem type, species and age. However, when comparing all factors and interaction effects, there are significant differences of both F_m and V_{ef} between *P.*

ponderosa and *L. occidentalis* primary xylem (P = 0.047, P = 0.045 respectively) and near significant differences for both traits between *P. ponderosa* and *P. menziesii* (P = 0.057, P = 0.071 respectively). There are no statistical differences for these traits within the secondary xylem, though it is worth noting that both traits in the primary xylem are significantly larger compared to the secondary xylem across all species.

Vulnerability Curves

P. menziesii was fitted with a 4-parameter sigmoid function [R^2 = 0.52, Adjusted R^2 = 0.39, P = 0.03] and *P. ponderosa* and *L. occidentalis* were fitted with a 3-parameter exponential growth function [R^2 = 0.34, Adj. R^2 = 0.25, P = 0.04; R^2 = 0.65, Adj R^2 = 0.59, P = 0.002 respectively] (Fig. 2.1 A-C). P_{50} values were estimated by calculating the water potential at 50% of max K_s for each fitted curve where the maximum value was estimated using the maximum values of the fitted curve (i.e. P_0). Estimated P_{50} values are -1.56 MPa, -0.39 MPa and -1.04 MPa respectively.

Based on plotted vulnerability curves, K_s max was estimated to be 0.92, 0.52, and 1.55 kg m^{-1} s^{-1} MPa^{-1} for *P. menziesii*, *L. occidentalis*, and *P. ponderosa* respectively. Actual maximum measured values were 1.27, 0.77, and 1.90 kg m^{-1} s^{-1} MPa^{-1} respectively. Theoretical maximum K_s values calculated from anatomical measurements were 1.01, 1.40 and 2.58 kg m^{-1} s^{-1} MPa^{-1} respectively. Theoretical values indicated that *L. occidentalis* would have a greater capacity for water transport, but actual values did not reflect this.

MicroCT Imaging

Magnification of the xylem bundle shows gas-filled intercellular spaces and pith (dark grey) clearly distinct from live cells and water-filled functional xylem (Fig. 2.2). However, it appears that live cell contents and dead, water-filled xylem are not distinguishable in the microCT images. This demonstrates the necessity of having corresponding CLSM or light microscopy images for determining actual functional xylem (Fig. 2.3).

MicroCT imaging during desiccation shows similar patterns of embolism for all three species (Fig. 2.4 A-R). Embolism occurs first (at the least negative water potentials) in intercellular spaces within the cortex, then the pith, followed by the protoxylem clusters in *P. ponderosa* and *P. menziesii* (Fig. 2.4 A-D, G-J). In *L. occidentalis*, the order of embolism between the pith and the primary xylem clusters are reversed where embolism occurs first in the proto xylem then extends into the lignified pith cells (Fig. 2.4 M-P). The difference in the

embolism pattern of *L. occidentalis* is likely due to the lignification of parenchyma within the pith, which is not seen in the other two species (MLR in prep). Sustained desiccation resulted in embolism of the remaining primary xylem and severe tissue damage to the cortex, epidermal tissues, and resin canals (*P. ponderosa* only) (Fig. 2.4 E, K, Q). Secondary xylem tracheids embolized only at the most severe levels of water stress (Fig. 2.4 F, L, R). Even though stems were severely warped and dehydrated, *L. occidentalis* was the only species to undergo significant secondary xylem embolism (Fig. 2.4 R).

DISCUSSION

MicroCT imaging illustrates clear differences in cavitation resistance between proto-, primary and secondary xylem with protoxylem being the least resistant to embolism, followed by primary xylem then secondary xylem. However, species comparisons of embolism resistance are not as straight forward. We hypothesized that, based on anatomical and functional characteristics reported by MLR (Chapter 1), *P. ponderosa, L. occidentalis* and *P. menziesii* would represent the least, intermediate, and most resistant to hydraulic dysfunction respectively, and the results from vulnerability curve-estimated P_{50} values corroborate this hypothesis. Yet, given the same dry down time periods and treatments for both intact and excised seedlings, *L. occidentalis* experienced extensive amounts of secondary xylem embolism compared to the other two species, which provides strong evidence that *in planta*, *L. occidentalis* is the least resistant to embolism. This is surprising from an anatomical perspective, as *L. occidentalis* exhibited intermediate traits normally correlated with resistance to embolism at this age (i.e. TPO and Tw Dt^{-1}).

Interestingly, MLR (Chapter 1) suggested that torus width (W_t) may play a critical role in resistance to air seeding, whereby a larger width decreased flexibility and reduced ability of the torus to adequately seal the associated bordered pit aperture. Our results here are the first reported in support of this hypothesis; this is the only trait for L. occidentalis that indicated a possible increased vulnerability to xylem embolism compared to the other two species. Though, it is worth noting that any conclusions based on anatomical or functional traits here are predicated on the assumption that anatomical characteristics and inter-species relationships are the same between the seedlings used for anatomical analysis and those used for microCT image analysis and vulnerability curves.

In terms F_m and V_{ef}, some studies have found increased V_{ef} confers better resistance to embolism by increasing the ability for the torus-margo to seal against the pit aperture (Delzon et al. 2010; Bouch et al. 2014). Conversely, F_m has been hypothesized to both positively and negatively correlate to reduced air seeding (Hacke et al. 2004; Delzon et al. 2010). Bouche et al. (2014) found the V_{ef} variability to be mostly attributed to the TPO component as opposed to F_m, for which they found varied weakly among all studied species. Torres-Ruiz et al. (2016) found little difference in TPO, F_m and V_{ef} between inner and outer parts of the xylem within branches of *Pinus sylvestris*, so the actual correlation of V_{ef} and F_m to embolism resistance across multiple species and tissue types remains inconclusive.

We hypothesized that *P. ponderosa* would be the least resistant to hydraulic dysfunction and *P. menziesii* would be the most; however, we were unable, even in the most desiccated stems, to induce complete secondary embolism in either of the two species as visualized by microCT imaging. The lack of secondary xylem embolism is interesting considering *P. ponderosa* reached ca. 95% percent loss conductivity (PLC) and *P. menziesii* reached ca. 85% PLC as estimated from maximum and minimum K_s values on our vulnerability curves. This implies that (1) a portion of the initial decline in hydraulic conductance can be attributed to conductance through extra-xylary tissue (including intercellular spaces and the pith) and (2) primary xylem contribute a very large proportion of hydraulic conductance in these very young stems. Cuneo et al. (2016) also reported a decrease in K_s with extra-xylary embolism in grape roots. In our case, further results may be gleaned by modeling total embolized area within different tissues of the stems to the numerous measured traits to in order to quantify correlations and statistical significance.

Interestingly, from an anatomical perspective, the seedlings at this age most resemble roots as opposed to mature tree boles and our results indicate they also hydraulically, most resemble mature roots based on published root P_{50} values. For *P. menziesii*, root P_{50} values ranged from -1.0 to -1.4 MPa (Domec et al. 2006) and *P. ponderosa* roots ranged from -0.07 to -1.98 MPa (Domec et al. 2004; Koepke and Kolb 2013). Our estimated P_{50} for *P. menzieii* is just slightly outside this range (-1.56 MPa) and our estimate for *P. ponderosa* falls within this range (-0.39 MPa). To our knowledge, there are no reported P_{50} estimates for *L. occidentalis* roots. If hydraulic measurements had been performed without microCT visualization of embolism, we would have concluded that the seedlings had reached

maximum PLC when we stopped seeing a decrease of K_s with more negative water potentials. Interestingly, Domec et al. (2004) also reported a maximum native PLC (%) of 87 (±7) and 70 (±6) for young *P. ponderosa* and *P. menziesii* roots respectively, which is similar to what we observed as estimated by our fitted vulnerability curves, though about 10% lower. To date and to the authors' knowledge, there are no other published vulnerability curves or P_{50} values reported for first-year conifer seedlings. The closest analog was reported by Vance and Zaerr (1991), who found mortality in *P. ponderosa* var. *ponderosa* occurred when xylem pressures fell below -4.0MPa (~54% relative water content) in 15-week old seedlings.

Regardless of *P. ponderosa*'s estimated vulnerability to embolism, it typically inhabits more xeric habitats as compared to the other two species, though *P. ponderosa* and *P. menziesii* can co-exist in transition zones (Burns and Honkala 1990). One possible attribute that may facilitate *P. ponderosa*'s increased survivability in more xeric habitats, among others discussed in MLR (Chapter 1), is that *P. ponderosa* seedlings have a much larger distribution of tracheid sizes with numerous tracheids that are much larger than the other two species and thus contribute much more to hydraulic conductivity. Previous anatomical analyses (MLR in prep) show that these very large tracheids primarily occur within the primary xylem. If these very large tracheids embolized first, we would expect to see *P. ponderosa* seedlings reach their respective P_{50} quickly, which is, in fact, what we do see. However, P_{50} values do not represent or describe what remains of in terms of functional xylem; *P. ponderosa* still may be as competitive or more competitive in terms of hydraulic conductivity as compared to the other two species. Indeed, we see that, based off of our fitted curves, *P. ponderosa* K_s at P_{50} is 0.78 (kg m^{-1} s^{-1} MPa^{-1}), compared to a K_s max of 0.92 and 0.52 for *P. menziesii* and *L. occidentalis* respectively, indicating *P. ponderosa* may still be just as competitive after 50% loss of conductivity.

Based on the theoretical xylem specific conductivities ($K_{s(t)}$), we hypothesized that *P. ponderosa* should exhibit the highest K_s values, which was confirmed by the *in vitro* hydraulic measurements. However, our predicted theoretical values indicated that *L. occidentalis* should have greater K_s compared to *P. menziesii*, but our measured values indicated the opposite. This may be attributed to the different methods used for calculating K_s between the measured and theoretical values. We used functional xylem area (A_{tfx}) for

theoretical values whereas we used the entire stem area (A_s) for the measured K_s values. Theoretical $K_{s(t)}$ was calculated as follows (MLR in prep):

$$K_s = \frac{\pi\rho}{128\eta A_{tfx}} \sum_{i=1}^{n} D_{t\,i}^4$$

where

$$\sum_{i=1}^{n} D_{t\,i}^4 = \text{sampled} \sum_{i=1}^{n} D_{t\,i}^4 \left(\frac{A_{tfx}}{A_{fx}}\right)$$

K_s is the xylem specific conductivity (kg m^{-1} MPa^{-1} s^{-1}), ρ is the density of water (kg m^{-1}) and η is the dynamic viscosity of water (MPa) at 20°C, and other symbols as described previously. Actual functional xylem area (A_{tfx}), which was calculated as a subset of total xylem area (only a portion of lignified tissue within the total xylem area were mature xylem). By contrast, total stem area (A_s) was used for actual K_s values; as that was the most practical measurement at the time of the study. By using a smaller estimate of functional xylem area, we would expect that our actual K_s values would increase, though the magnitude of that increase for each species is unknown. MLR has shown that in small seedlings, there is a poor allometric relationship between stem area and total functional xylem area, and so functional xylem area cannot be estimated from stem measurements alone.

Generally, when using mature plant organs for conductivity measurements, such as branches, roots, and stems, anything outside the xylem is not considered. The extra-xylary "soft" tissues including bark, phloem and vascular cambium are peeled away from the segment ends and the pith is sealed, leaving only the woody xylem associated with the conductivity measurement as well as the segment diameter measurements utilized in K_s calculations. In our case, we could not peel away excess tissue as the xylem alone was too small and delicate for independent measurements and thus the entire stem was used for conductivity measurements. As it stands, our measured K_s values are more representative of entire stem conductivities and may not reflect xylem specific conductivities and thus actual maximum K_s and P_{50} values should be viewed as estimates.

However, we posit that altering the area used for K_s calculations (i.e. decreasing area) would only shift the fitted curves upward towards greater values of K_s, and so their overall shape and associated water potentials would not change. The only exception may be *L*.

occidentalis, which experienced close to 100% embolism as corroborated by both microCT and associated hydraulic conductivity measurements of near 0 K_s at the most negative water potentials. Decreasing the area used in calculating K_s for *L. occidentalis* would move the K_s values associated with less negative water potentials upward toward greater K_s while K_s values that are closer to zero at more negative water potentials would remain the same, effectively increasing the slope of the fitted curve and shifting the associated P_{50} estimate towards less negative water potentials. This is what we would expect based on anatomical and functional traits of *L. occidentalis* pits and torus-margo membranes, where the capacity to limit air seedling from tracheid to tracheid seems more limited compared to the other two species and should result in a steep loss of conductivity slope (MLR Thesis Chapter 1).

In order to better estimate xylem specific conductivity, it would have been prudent to utilize image-derived measurements of xylem area as opposed to stem area in the K_s calculations. However, this approach inherently produces its own set of complications. Typically, the xylem diameter at each end of the stem segment is measured and the xylem area averaged over the length of the stem segment is used in calculating K_s. In our case, if we used one 2D image for xylem area estimates, there would be only one single measurement per stem representing a stem length of 2-3μm. Furthermore, the relationship between where the optical imaging occurred in relationship to stem segment used for conductivity measurements was only estimated as approximately the mid-stem, but likely varied during imaging. This remains one of the major drawbacks to using microCT and relating back to anatomical measurements. Even when the location of the microCT imaging is marked, subsequent anatomical measurements using light microscopy/CLSM images are time consuming to match, if even possible. However, this does not preclude the necessity of concurrent light or confocal microscopy imaging. As we have discussed, not all lignified cells within the xylem area are mature xylem. Therefore, any vulnerability to embolism curves constructed based on imaged embolized area (as described by Choat et al. 2015) would overestimate total functional xylem area and thus underestimate vulnerability.

It is worth noting that the same pattern of embolism during desiccation was observed for both intact and excised stems, which indicates that (1) through initial stages of embolism, bench dehydrating is appropriate for seedlings and (2) capacitance plays a role in these very young seedlings. Embolism of cortex tissue, pith and intercellular spaces indicated that these

serve as sources of capacitance during drought to reduce tension in the xylem and lessen tracheid embolization. If soft tissues (i.e. not xylem) desiccate in order to keep xylem functional, this begs the question: what is the desiccation threshold from which seedlings cannot recover? This also suggests that embolism refilling could potentially present a real advantage for survival in these very young seedlings, especially in places with variable early seasonal water availability.

CONCLUSION

This study demonstrates some of the unique challenges associated with measuring water potential and hydraulic conductivity very young seedlings. Due to the delicate nature of young seedlings, many techniques for measuring vulnerability to hydraulic dysfunction (e.g., pressure sleeve, centrifuge) simply do not work or they damage the seedling and necessitate utilizing the entire stem as opposed to isolating the xylem. Additionally, flows in in small seedlings are so low that only very sensitive flow meters or balances are able to accurately detect flows through young seedling stems. This illustrates the necessity for methodological research and analyses to establish protocols for accurately measuring xylem specific conductivities and water potentials for very delicate tissue subject to mechanical damage where the xylem cannot be separated from the remainder of the stem tissue.

Despite some inherent drawbacks, this experiment successfully combined state-of-the art technologies with traditional hydraulic measurements to report the first vulnerability curves and P_{50} values on seedlings at this age and compared these results to *in vivo* hydraulic dysfunction. Based on *in vivo* microCT imaging, *L. occidentalis* appears to be the least embolism resistant, which is not surprising based on known drought deciduosity. However, the vulnerability curve estimated P_{50} values do not corroborate with embolism visualized by microCT nor do they accurately reflect known species' habitats, which adds to the growing body of evidence that P_{50} values should not be used to predict *in planta* hydraulic dysfunction. Our P_{50} estimates support the conclusion that *P. ponderosa* is more inherently vulnerable to embolism, which is corroborated by the anatomical measurements and is already well established for mature specimens.

Although we were unable to induce complete secondary xylem embolism in both *P. ponderosa* and *P. menziesii*, and thus unable to determine which of these two species may be

more embolism resistant from a functional perspective, we have provided some plausible explanations for *P. ponderosa*'s ability to thrive in xeric conditions even though it seems to be more inherently vulnerable to embolism. This is particularly critical to seedling-stage individuals, as they likely lack external mitigating factors present in mature trees, including rooting depth, stomatal control, thick leaf cuticle, and large water and carbohydrate stores.

REFERENCES

Abatzoglou, J.T., Rupp, D.E., Mote, P.W. 2014. Season climate variability and change in the Pacific Northwest of the United States. American Meteorological Society. DOI: 10.1175/JCLI-D-13-00218.1

Adams, H.D., Germino, M.J., Breshears, D.D., Barron-Gafford, G.A., Guardiola-Claramonte, M., Zou, C.B., Huxman, T.E. 2013. Nonstructural leaf carbohydrate dynamics of *Pinus edulis* during drought-induced tree mortality reveal role for carbon metabolism in mortality mechanism. New Phytologist 197:1142-1151.

Allen, C.D., Breshears, D.D. 1998. Drought-induced shift of a forest-woodland ecotone: rapid landscape response to climate variation. PNAS 95:14839-14842.

Allen, C.D., Macalady, A.K., Chenchouni, H., Bachelet, D., McDowell, N., Vennetier, M., Kitzberger, T….Cobb, N. 2010. A global overview of drought and heat-induced tree mortality reveals emerging climate risks for forests. Forest Ecology and Management 259:660-684.

Barbeta, A., Ogaya, R., Peñuelas, J. 2013. Dampening effects of long-term experimental drought on growth and mortality rates of a Holm oak forest. Global Change Biology 19:3133-3144.

Barigah, T.S., Charrier, O., Douris, M., Bonhomme, M., Herbette, S., Améglio, T., Fichot, R., Brignolas, F., Cochard, H. 2013. Water stress-induced xylem hydraulic failure is a causal factor of tree mortality in beech and poplar. Annals of Botany 1-7, doi:10.1093/aob/mct204.

Barnard, D.M., Meinzer, F.C., Lachenbruch, B., McCulloh, K.A., Johnson, D.M., Woodruff, D.A. 2011. Climate-related trends in sapwood biophysical properties in two conifers: avoidance of hydraulic dysfunction through coordinated adjustments in xylem efficiency, safety and capacitance. Plant, cell and environment 34(4):643-654.

Bigler, C., Gavin, D.G., Cunning, C., Veblen, T. 2007. Drought induces lagged tree mortality in a subalpine forest in the Rocky Mountains. Oikos 116:1983-1994.

Biswas, C., Johri, B.M. 1997. The Gymnosperms. Narosa Publishing House, New Delhi, India.

Bouche, P.S., Larter, M., Domec, J.-C., Burlett, R., Gasson, P., Jansen, S., Delzon, S. 2014. A broad survey of hydraulic and mechanical safety in the xylem of conifers. Journal of Experimental Botany 65(15):4419-4431.

Breshears, D.D., Myers, O.B., Meyer, C.W., Barnes, F.J., Zou, C.B., Allen, C.D., McDowell, N.G., Pockman, W.T. 2015. Tree die-off in response to global change-type drought: mortality insights from a decade of water potential measurements. Frontiers in Ecology and the Environment 7(4):185-189.

Brix, H. 1979. Effects of plant water stress on photosynthesis and survival of four conifers. Canadian Journal of Forest Research 9:160-165.

Brodersen, C.R., McElrone, A.J. 2013. Maintenance of xylem network transport capacity: a review of embolism repair in vascular plants. Frontiers in Plant Science doi: 10.3389/fpls.2013.00108

Brodersen, C.R., McElrone, A.J., Choat, B., Lee, E.F., Shackel, K.A., Matthews, M.A. 2013. In vivo visualizations of drought-induced embolism spread in *Vitis vinifera*. Plant Phytology 161:1820-1829.

Brodersen, C.R., McElrone, A.J., Choat, B., Matthews, M.A., Shackel. 2010. The dynamics of embolism repair in xylem: in vivo visualizations using high-resolution computed tomography. Plant Physiology 154:1088-1095.

Brodribb, T.J., Pittermann, J., Coomes, D.A. 2012. Elegance versus speed: examining the competitions between conifer and angiosperm trees. International Journal of Plant Sciences 173(6):673-694.

Brown, R.W., Bartos, D.L. 1982. A Calibration Model for Screen-caged Peltier Thermocouple Psychrometers. Research Paper INT-293 USDA Forest Service Intermountain Forest and Range Experiment Station.

Burns, R.M., Honkala, B.H. (tech. coords.) 1990. Silvics of North America: 1. Conifers; 2. Hardwoods. Agriculture Handbook 654. U.S. Department of Agriculture, Forest Service, Washington, DC.

Carnicer, J., Coll, M., Ninyerola, M., Pons, X., Sánchez, G., Peñuelas, J. 2011. Widespread crown condition decline, food web disruption and amplified tree mortality with increased climate change-type drought. PNAS 108(4):1474-1478.

Choat, B., Brodersen, C.R., McElrone, A.J. 2015. Synchrotron X-ray microtomography of xylem embolism in *Sequoia sempervirens* saplings during cycles of drought and recovery. New Phytologist 205:1095-1105.

Clark, J.S., Iverson, L., Woodall, C.W., Allen, C.D., Bell, D.M., Bragg, D.C…Zimmerman, N.E. 2016. The impacts of increasing drought on forest dynamics, structure and biodiversity in the United States. Global Change Biology 22:2329-2352.

Corcuera, L., Gil-Pelegrin, E., Notivol, E. 2012. Differences in hydraulic architecture between mesic and xeric *Pinus pinaster* populations at the seedling stage. Tree Physiology 32:1442-1457.

Cui, M., Smith, W.K. 1990. Photosynthesis, water relations and mortality in Abies lasiocarpa seedlings during natural establishment. Tree Physiology 8:37-46.

Cuneo, I.F., Knipfer, T., Brodersen, C.R., McElrone, A.J. 2016. Mechanical failure of fine root cortical cells initiates plant hydraulic decline during drought. Plant Physiology 172:1669-1678.

Delzon, S., Douthe, C., Sala, A., Cochard, H. 2010. Mechanism of water-stress induced cavitation in conifers: bordered pit structure and function support the hypothesis of seal capillary-seedling. Plant, Cell and Environment 33:2101-2111.

Domec, J.-C., Lackenbruch, B., Meinzer, F. 2006. Bordered pit structure and function determine spatial patterns of air-seeding thresholds in xylem of Douglas-fir (Pseudotsuga menzeisii; Pinaceae) trees. American Journal of Botany 93(11):1588-1600.

Domec, J.-C., Warren, J.M., Meinzer, F.C., Lachenbruch, B. 2009. Safety factors for xylem failure by implosion and air-seeding within roots, trunks and branches of young and old conifer trees. IAWA Journal 30(2):100-120.

Domec, J.-C., Warren, J.M., Meinzer, F.C., Brooks, J.R., Coulombe, R. 2004. Native root xylem embolism and stomatal closure in stand of Douglas-fir and ponderosa pine: mitigation by hydraulic redistribution. Oecologia 141(1):7-16.

Farjon, A. 2008. A Natural History of Conifers. Timber Press, Inc, Portland, OR.

Garcia de la Serrana, R., Vilagrosa, A., Alloza, J.A. 2015. Pine mortality in southeast Spain after an extreme dry and warm year: interactions among drought stress, carbohydrates and bark beetle attack. Trees 29:1791-1804.

Gworek, J.R., Vander Wall, S.B., Brussard, P.F. 2007. Changes in biotic interactions and climate determine recruitment of Jeffrey pine along an elevation gradient. Forest Ecology and Management 239:57-68.

Hacke, U.G., Sperry, J.S., Pittermann, J. 2004. Analysis of circular bordered pit function II. Gymnosperm tracheids with torus-margo pit membranes. American Journal of Botany 9(3):386-400.

Haig, I.T., Davis, K.P., Weidman, R.H. Natural Regeneration in the Western White Pine type. 1941. United States Department of Agriculture. Northern Idaho Forest Genetics Center Technical Bulletin No. 767.

Hereş, A.-M., Martinez-Vilalta, J., López, B.C. 2012. Growth patterns in relation to drought-induced mortality at two Scots pine (*Pinus sylvestris* L.) sites in NE Iberian Peninsula. Trees 26:621-630.

Johnson, D.M., McCulloh, K.A., Reinhardt, K. 2011. The earliest stages of tree growth: development, physiology and impacts of microclimate. In: Meinzer, F.C., Lackenbruch, B., Dawson, T.E., (eds.): 65-87. Size- and Age-Related Changes in Tree Structure and Function. Springer, Netherlands.

Kavanagh, K.L, Bond, B.J., Aitken, S.N., Gartner, B.L., Knowe, S. 1999. Shoot and root vulnerability to xylem cavitation in four populations of Douglas-fir seedlings. Tree Physiology 19:31-37.

Koepke, D.F., Kolb, T.E. 2013. Species variation in water relations and xylem vulnerability to caviation at a forest-woodland ecotone. Forest Science 59(5), http://dx.doi.org/10.5849/forsci.12-053 .

Kolb, P.F., Robberecht, R. 1996. Higher temperatures and drought stress effects on survival of *Pinus ponderosa* seedlings. Tree Physiology 16:665-672.

Kolb, K.J., Sperry, J.S., Lamont, B.B. 1996. A method for measuring xylem hydraulic conductance and embolism in entire root and shoot systems. Journal of Experimental Botany 47 (304):1805-1810.

Lin, C.-P., Huang, J.-P., Wu, C.-S., Hsu, C.-Y., Chaw, S.-M. 2010. Comparative chloroplast genomics reveals the evolution of Pinaceae genera and subfamilies. Genome Biology and Evolution 2:504-517.

Loarie, S.R., Duffy, P.B., Hamilton, H., Asner, G.P., Field, C.B., Acherly, D.D. 2009. The velocity of climate change. Nature 462:1052-1057.

Maherali, H., Williams, B.L., Paige, K.N., DeLucia, E.H. 2002. Hydraulic differentiation of ponderosa pine populations along a climate gradient is not associated with ecotypic divergence. Functional Ecology 16:510-521.

Martinez-Vilalta, J., Piñol, J. 2002. Drought-induced mortality and hydraulic architecture in pine populations of the NE Iberian Peninsula. Forest Ecology and Management 161:247-256.

Martinez-Vilalta, J., Sala, A., Piñol, J. 2004. The hydraulic architecture of Pinaceae – a review. Plant Ecology 171:3-13.

McCulloh, K. A., Johnson, D.M., Meinzer, F.C., Voelker, S.L., Lachenbruch, B., Domec, J.-C. 2012. Hydraulic architecture of two species differing in wood density: opposing strategies in co-occurring tropical pioneer trees. Plant, cell & environment 35(1):116-125.

McElrone, A.J., Choat, B., Parkinson, D.Y., MacDowell, A.A., Brodersen, C.R. 2013. Using high resolution computed tomography to visualize the three dimensional structure and function of plant vasculature. Journal of Visualized Experiments 74:e50162.

McElrone, A.J., Pockman, W.T., Martínez-Vilalta, J. and Jackson, R.B., 2004. Variation in xylem structure and function in stems and roots of trees to 20 m depth. New Phytologist, 163(3):507-517.

Melcher, P.J., Holbrook, N.M., Burns, M.J., Zwieniecki, M.A., Cobb, A.R., Brodribb, T.J., Choat, B., Sack, L. 2012. Measurements of stem xylem hydraulic conductivity in the laboratory and field. Methods in Ecology and Evolution 3:685-694.

Michaelian, M., Hogg, E.H., Hall, R.J., Arsenault, E. 2011. Massive mortality of apsen following severe drought along the southern edge of the Canadian boreal forest. Global Change Biology 17:2084-2094.

Millar, C.I., Westfall, R.D., Delany, D.L., Bokach, M.J., Flint, A.L., Flint, L.E. 2012. Forest mortality in high-elevation whitebark pine (*Pinus albicaulic*) forests of eastern California, USA; influence of environmental context, bark beetle, climate water deficit, and warming. Canadian Journal of Forest Research 42:749-765.

Mori, A., Mizumachi, E., Osono, T., Doi, Y. 2004. Substrate-associated seedling recruitment and establishment of major conifer species in an old-growth subalpine forest in central Japan. Forest Ecology and Management 196:287-297.

Mote, P.W., Hamlet, A.F., Clark, M.P., Lettenmaier, D.P. January 2005. Declining mountain snowpack in Western North America. American Meteorological Society. DOI: 10.1175/BAMS-86-1-39

Moyes, A.B., Castanha, C., Germino, M.J., Kueppers, L.M. 2013. Warming and the dependence of limber pine (*Pinus flexilis*) establishment on summer soil moisture within and above its current elevation range. Oecologia 171(1):271-282.

Rapacciuolo, G., Maher, S.P., Schneider, A.C., Hammond, T.T., Jabis, M.D., Walsh, R.E., Iknayan, K.J., Walden, G.K., Oldfather, M.F., Ackerly, D.D., Beissinger, S.R. 2014. Beyond a warming fingerprint: individualistic biogeographic responses to heterogeneous climate change in California. Global Change Biology 20:2841-2855.

Reinhardt, K., Castanha, C., Germino, M.J., Kueppers, L.M. 2011. Ecophysiological variation in two provenances of *Pinus flexilis* seedlings across an elevation gradient from forest to alpine. Tree Physiology 31:615-625l.

Reinhardt, K., Germino, M.J., Kueppers, L., Domec, J.-C., Mitton, J. 2015. Linking Carbon and water relations to drought-induced mortality in *Pinus flexilis* seedlings. Tree Physiology 35:771-782.

RStudio Team (2015). RStudio: Integrated Development for R. RStudio, Inc., Boston, MA URL http://www.rstudio.com/.

Ruzin, S.E. 1999. Plant Microtechnique and Microscopy. Oxford University Press, Inc, New York.

Schwantes, A., Swenson, J.J., Jackson, R.B. 2016. Quantifying drought-induced tree mortality in the open canopy woodlands of central Texas. Remove Sensing of Environment 181:54-64.

Settele, J., Scholes, R., Betts, R., Bunn, S., Leadley, P., Nepstad, D., Overpeck, J.T., Taboada, M.A. 2014. Terrestrial and inland water systems. In: Climate Change 2014: Impacts, Adaptation, and Vulnerability. Contribution of Working Group II to the Fifth Assessment Report of the Intergovernmental Panel on Climate Change [Field, C.B., Barros, V.R., Dokken, D.J., Mach, K.J., Mastrandrea, M.D., Bilir, T.E., Chatterjee, M….White, L.L. (eds.). Cambridge University Press, Cambridge, UK.

Slezak, M. 2016. Massive mangrove die-off on Gulf of Carpentaria worst in the world, says expert [online]. The Guardian. Website: https://www.theguardian.com/environment/2016/jul/11/massive-mangrove-die-off-on-gulf-of-carpentaria-worst-in-the-world-says-expert [accessed 31 October 2016].

Sperry, J.S., Donnelly, J.R., Tyree, M.T. 1988. A method for measuring hydraulic conductivity and embolism in xylem. Plant, Cell and Environment 11:35-50.

Sperry, J.S., Saliendra, N.Z. 1994. Intra- and inter- plant variation in xylem cavitation in *Betula occidentalis*. Plant, Cell and Environment 17:1233-1241.

Stuppy, W.H., Maisano, J.A., Colbert, M.W., Rudall, P.J., Rowe, T.B. 2003. Three-dimensional analysis of plant structure using high-resolution X-ray computed tomography. Trends in Plant Science 8(1):2-6.

Torres-Ruiz, J.M., Cochard, H., Mencuccini, M., Delzon, S., Badel, E. 2016. Plant Cell and Environment doi: 10.1111/pce.12840.

Tyree, M.T., Zimmermann, M.H. 2002. Xylem Structure and the Ascent of Sap. 2nd Ed. Springer, Verlag, Berlin.

Urli, M., Porte, A.J., Cochard, H., Guengant, Y., Burlett, R. 2013. Xylem embolism threshold for catastrophic hydraulic failure in angiosperm trees. Tree Physiology 33(7):672-683.

Vance, N.C., Zaerr, J.B. 1991. Influence of drought stress and low irradiance on plant water relations and structural constituents in needles of *Pinus ponderosa* seedlings. Tree Physiology 8:175-184.

Zavitkovski, J., Ferrell, W.K. 1968. Effect of drought upon rates of photosynthesis, respiration, and transpiration of seedlings of two ecotypes of Douglas-fir. Botanical Gazette 129(4): 346-350.

Zimmermann, M.H. 1983. Xylem Structure and the Ascent of Sap. Springer,Verlag, Berlin.

Figures

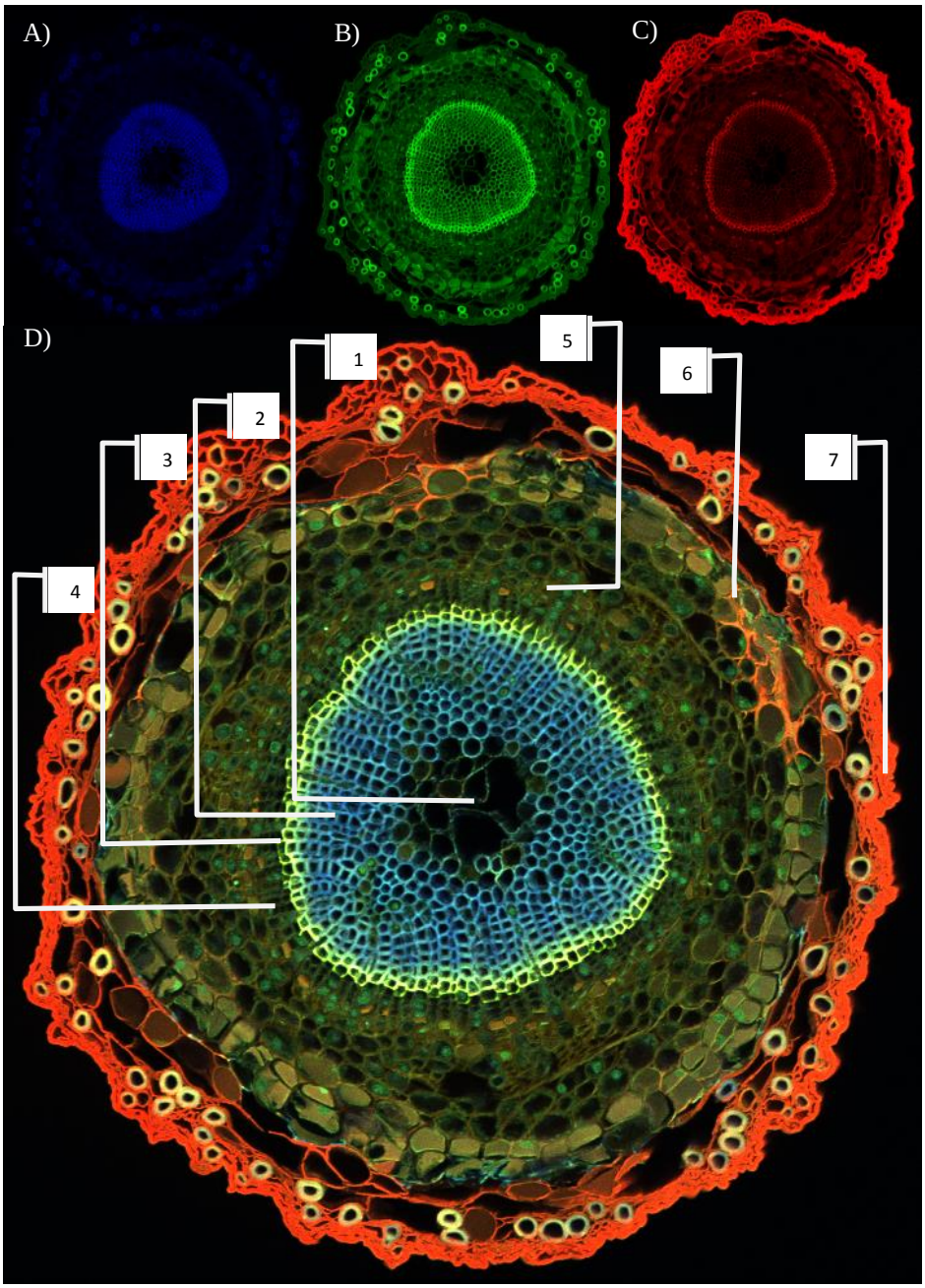

Figure 1.1 Composite confocal microscopy image of *P. menziesii*. The three confocal laser wavebands (A) 405nm, (B) 488nm, and (C) 559nm excite overlapping and individual anatomical and cellular components based on cellular and chemical properties. The composite image (D) illustrates how the three wavelengths can produce images very clearly delimiting stem anatomy: 1. pith, 2. mature xylem, 3. differentiating xylem, 4. vascular cambium, 5. phloem, 6. cork cambium, and 7. epidermis. The differences in color of the cell walls between differentiating xylem and mature xylem are likely due to differences in lignin/cellulose content.

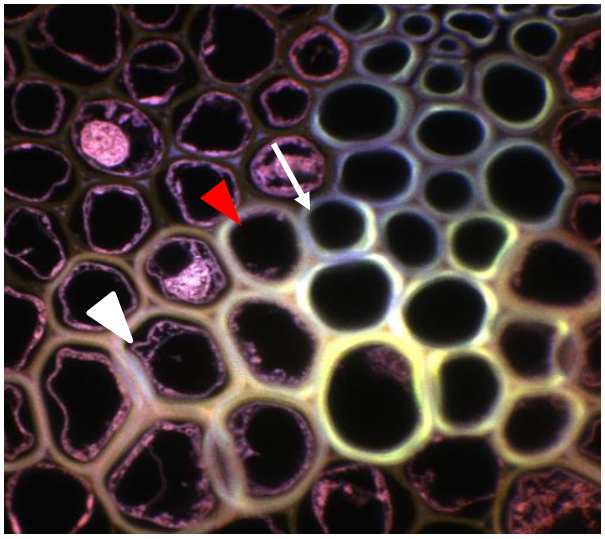

Figure 1.2 Differentiating xylem. Live cell membranes and nuclei (pink) are visible with safranin O staining, enabling identification of live xylem undergoing differentiating (white arrowhead), tracheids undergoing programmed cell death with remanent cell wall contents (red arrowhead) and a mature functional tracheid (white arrow). Note the differences in cell wall color between older, mature xylem (blue) and live xylem (orange/yellow).

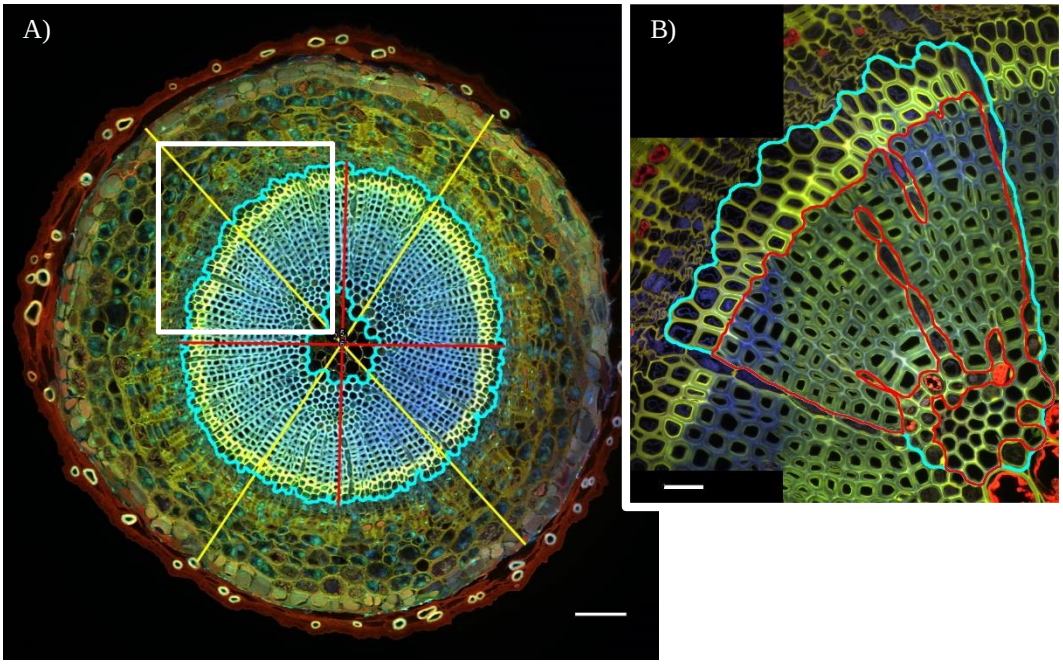

Figure 1.3 Example of stem and xylem area measurements. (A) 10x magnification; yellow lines are used for calculating A_s; red lines used for calculating A_x; cyan outlines area area used for A_{tx}; Bar = 100 µm; Inset = white box. (B) 60x magnification; cyan outline is area used for A_{sx} and red outline is A_{sfx}, where A_{sx}, A_{sfx} and A_{tx} are used to calculated total functional xylem (A_{tfx}). Bar = 25 µm. A_s = cross-sectional stem area, A_x = cross-sectional xylem area, A_{tx} = actual measured xylem area, A_{sx} = sampled xylem area, A_{sfx} = functional xylem within the sampled xylem area.

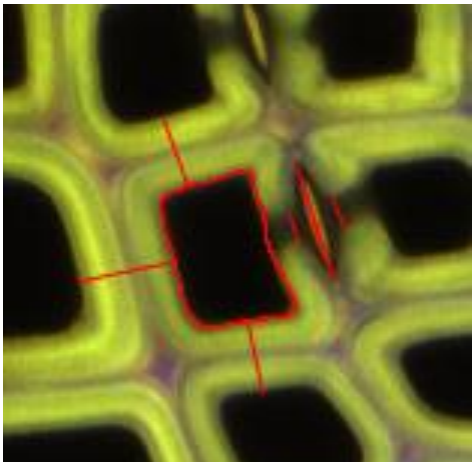

Figure 1.4 Tracheid and pit measurements. Examples of (1) tracheid area (A_t), (2) wall thickness (Tw), and (3) pit anatomical measurements in *P. ponderosa* secondary xylem.

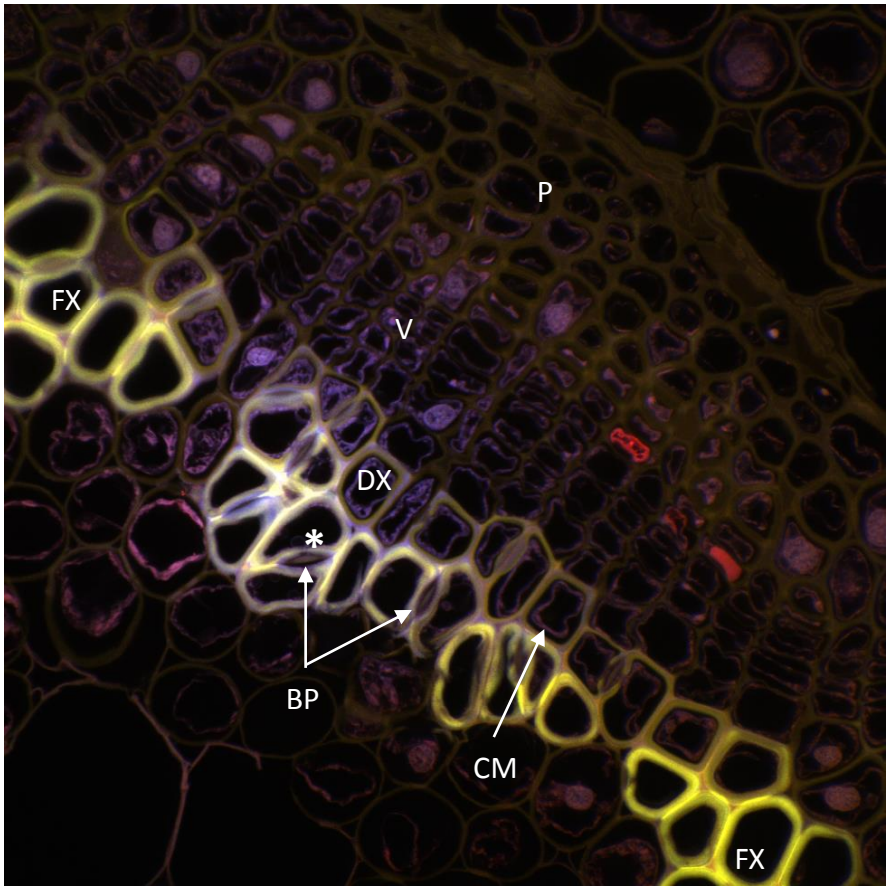

Figure 1.5 Vascular tissue of 3-week-old *P. menziesii*. Functional xylem (FX), differentiating xylem (DX), tracheid undergoing programmed cell death, (*), vascular cambium (VC), plasmolyzed cell membrane (CM), bordered pits with visible torus (BP), phloem and cell wall S1 to S3 cell layers (not shown).

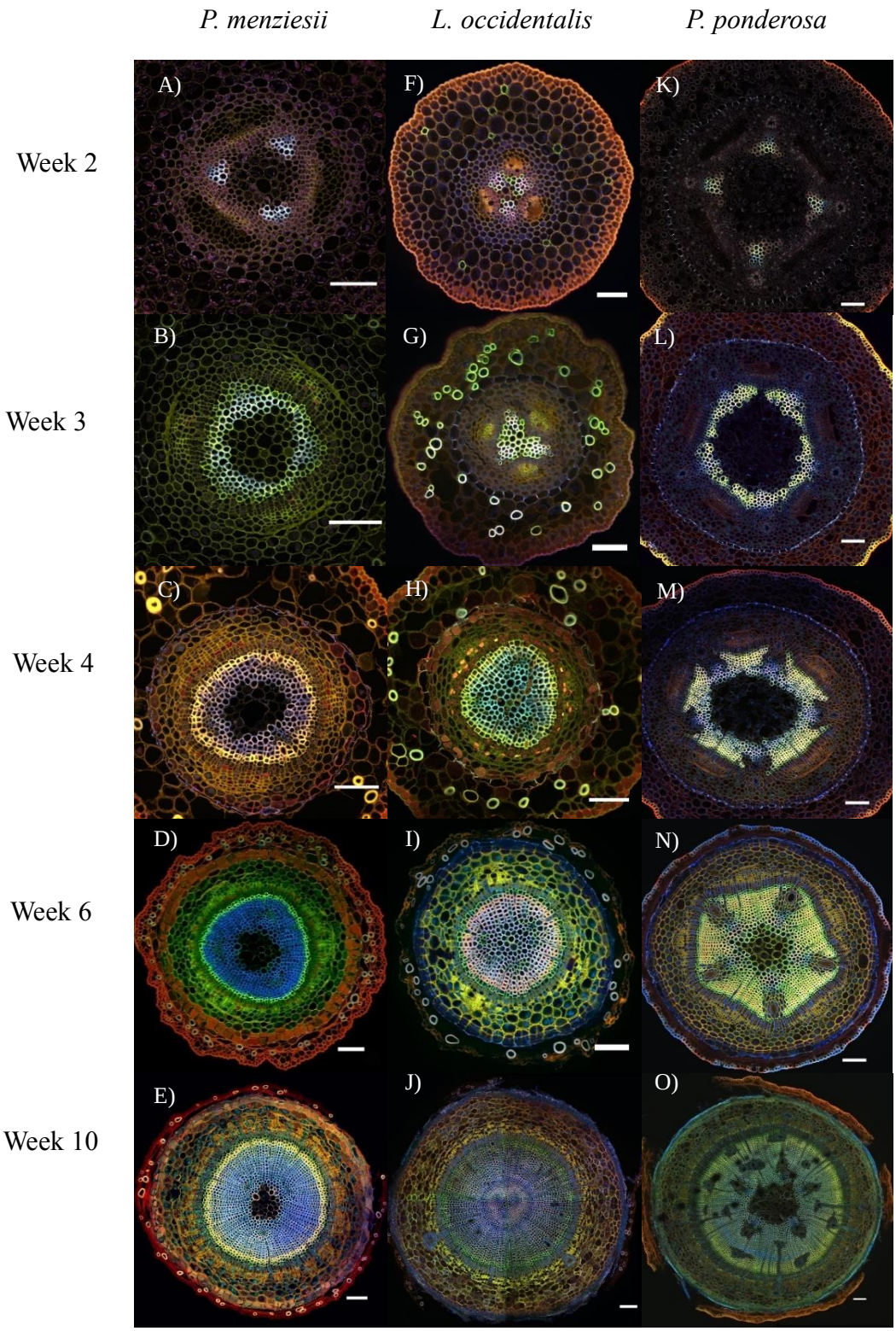

Figure 1.6 Vascular development over 10 weeks. Xylem development in *P. menziesii* (A-E), *L. occidentalis* (F-J), and *P. ponderosa* (K-O) imaged with confocal laser scanning microscopy (CLSM) at 2 (A, F, K), 3 (B, G, L), 4 (C, H, M), 6 (D, I, N) and 10 (E, J, O) weeks after planting (AP). Bars = 100µm.

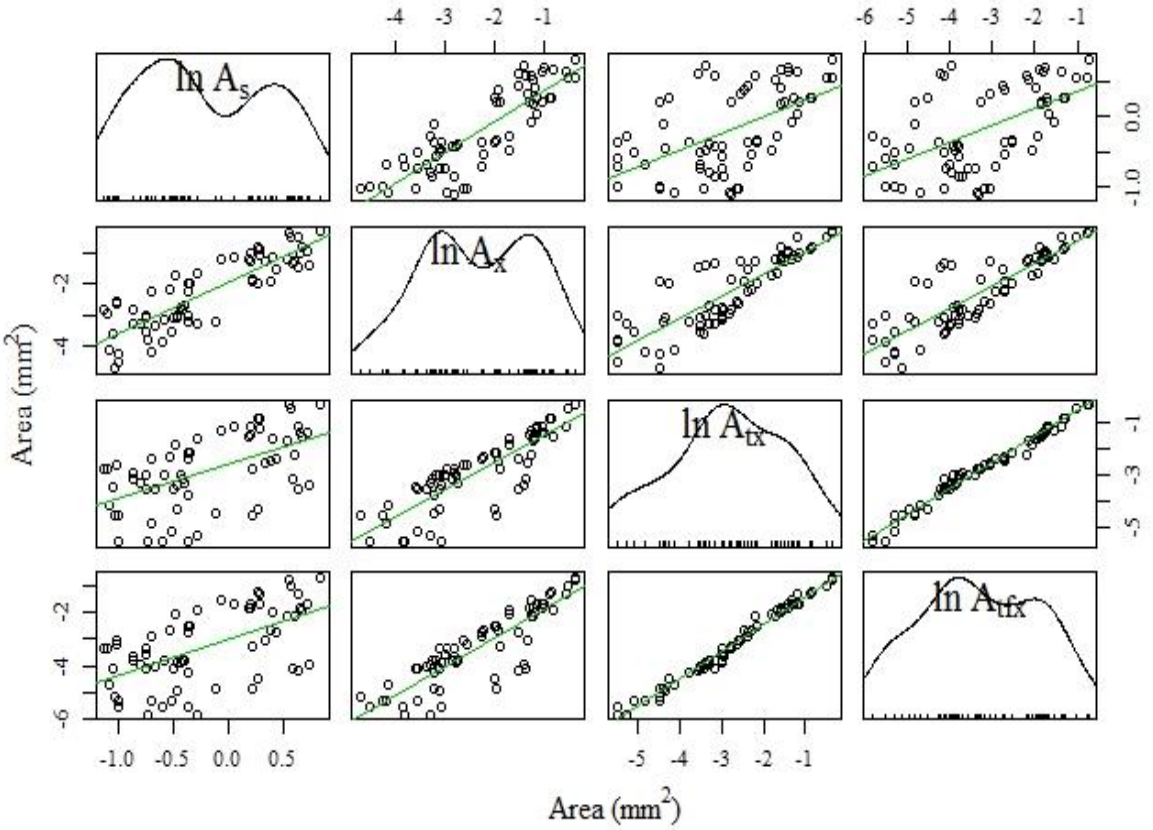

Figure 1.7 Correlation between seedling area measurements. Scatterplot on a natural log scale for all area measurements showing the correlation between the four main area variables across all three species. Each point per graph is a single tree. Green lines are best fit lines. A_s = stem cross-sectional area, A_x = cross-sectional xylem area, A_{tx} = total xylem area as directly measured with ImageJ to exclude the pith, A_{tfx} = calculated total functional xylem area, ln = natural log.

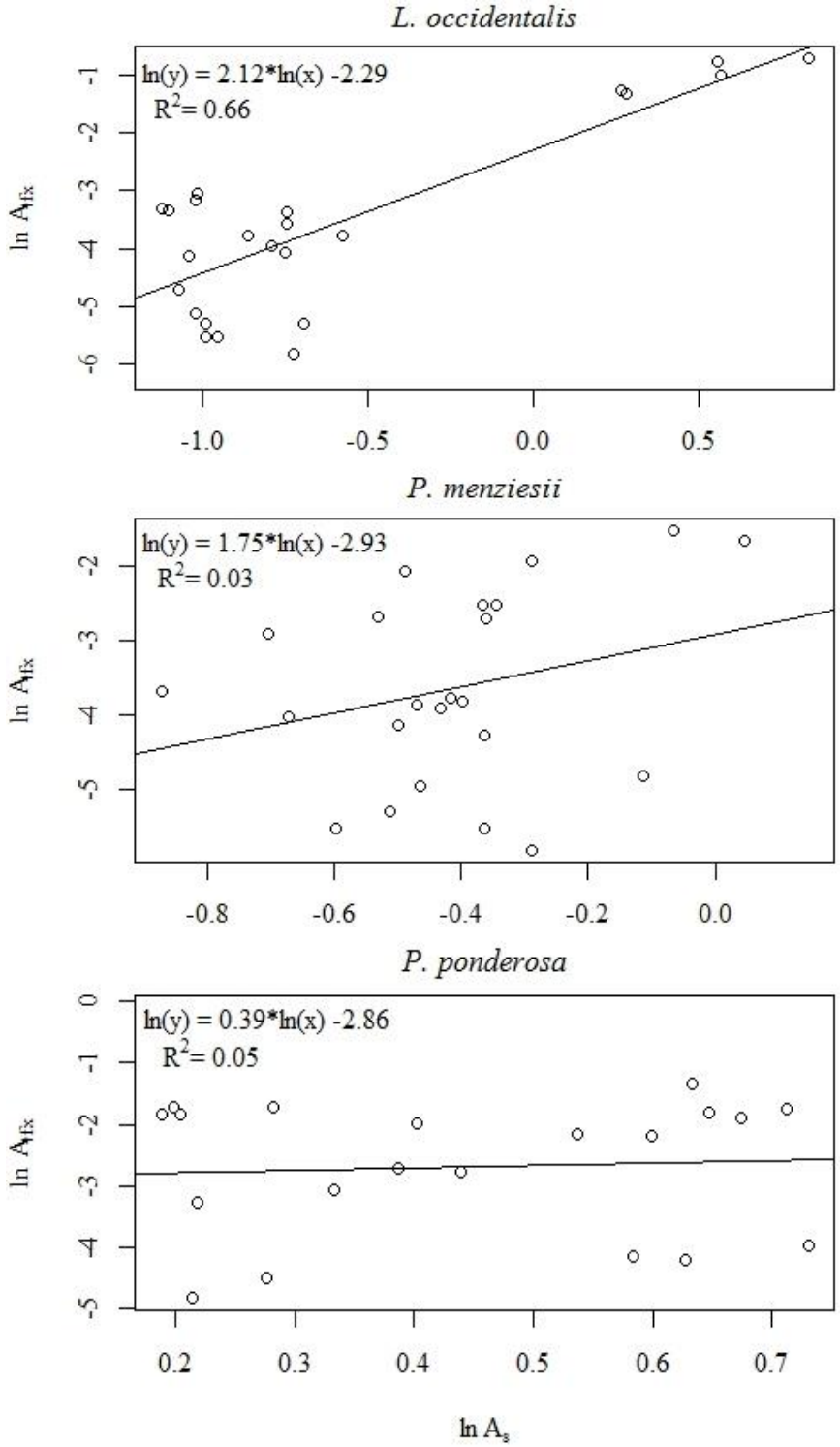

Figure 1.8 Relationships between stem cross-sectional area and calculated total functional xylem area per species. Each point per graph is a single seedling. (A) *L. occidentalis*, (B) *P. menziesii* and (C) *P. ponderosa*. Graphs (B) and (C) illustrate that stem cross-sectional area cannot be used to accurately predict actual functional xylem area in very young seedlings. A_s = stem cross-sectional area, A_{tfx} = calculated total functional xylem area, ln = natural log.

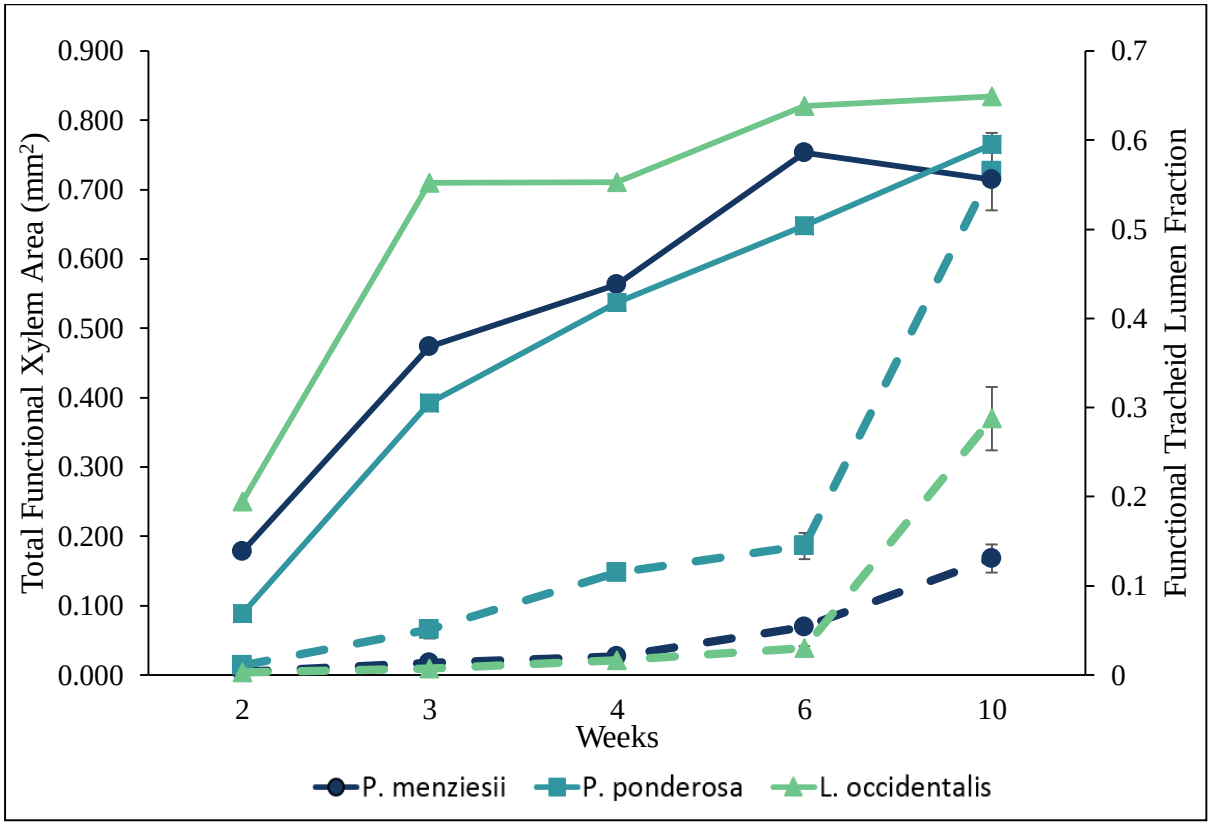

Figure 1.9 Total functional xylem area and functional tracheid lumen fraction. Dotted lines illustrate the increase in total functional xylem area over time per species. The tracheid lumen fraction (solid lines) are the ratio of total functional xylem area (A_{tfx}) and xylem cross-sectional area (A_x). Each point per line corresponds to the average per species at time period.

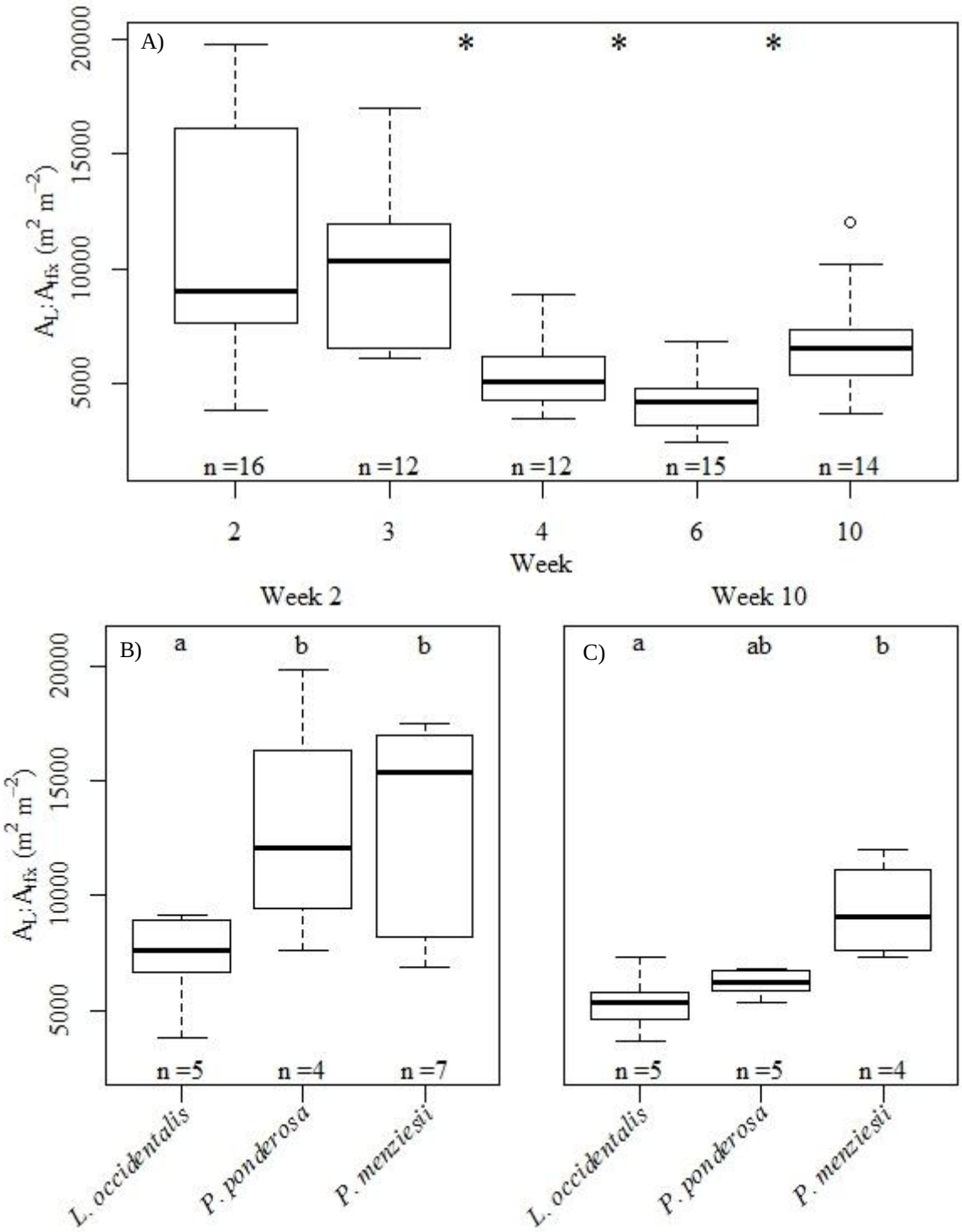

Figure 1.10 Leaf area to functional xylem area ratio comparisons. (A) changes in A_L:A_{tfx} over time averaged for all species. Asterisks mark difference between adjacent time periods. Week 2 and week 10 are not significantly different. (B) *L. occidentalis* is significantly lower than the other two species at week 2; no difference between *P. menziesii* and *P. ponderosa*, though the mean for *P. menziesii* appears to trend higher. (C) At week 10, all intraspecies variability is much smaller; *L. occidentalis* still remains low while *P. menziesii* trends higher than the other two with much smaller variances within species. Lack of statistical significant differences between *P. menziesii* and *P. ponderosa* may be attributed to smaller sample sizes. A_L = leaf area, A_{tfx} = total functional xylem area.

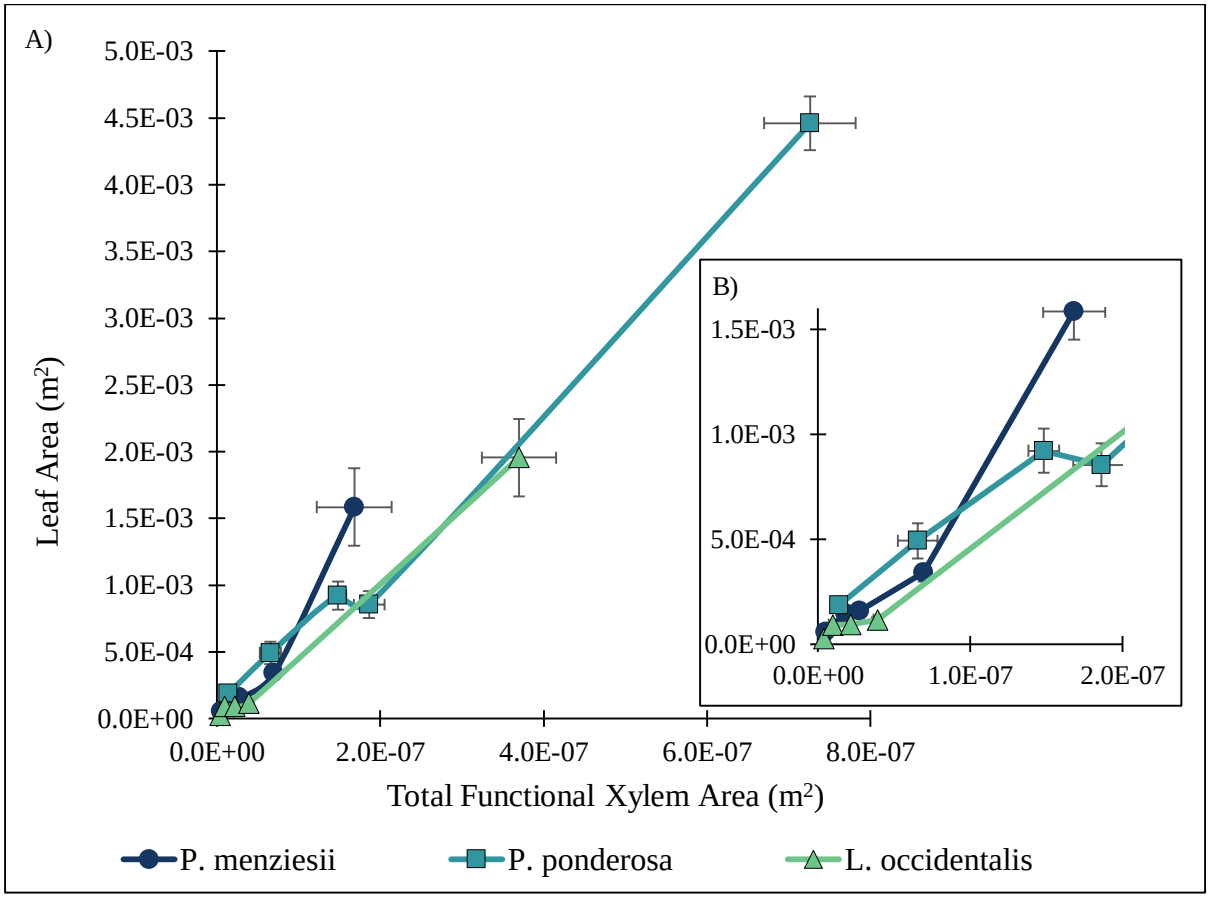

Figure 1.11 Leaf area to total functional xylem area. Each point per line represents the averages of each species with SE error bars per time period of 2, 3, 4, 6 and 10 weeks respectively. Slope of the line between adjacent points is the leaf area to sapwood area ratio, which is an oft reported functional trait. (A) The steep slope between weeks 6 and 10 for *P. menziesii* indicates that there is a smaller area of functional xylem supporting water to a given crown area. This also implies that for a given transpiration rate, *P. menziesii* will have the most negative xylem water potential. (B) Short spacing of the first 4 points for *P. menziesii* and *L. occidentalis* indicate minimal functional xylem and leaf area expansion during this time. Growth for *P. ponderosa* is greater for all time periods compared to the other two species, but also expands greatly for both crown area and functional xylem area between weeks 6 and 10.

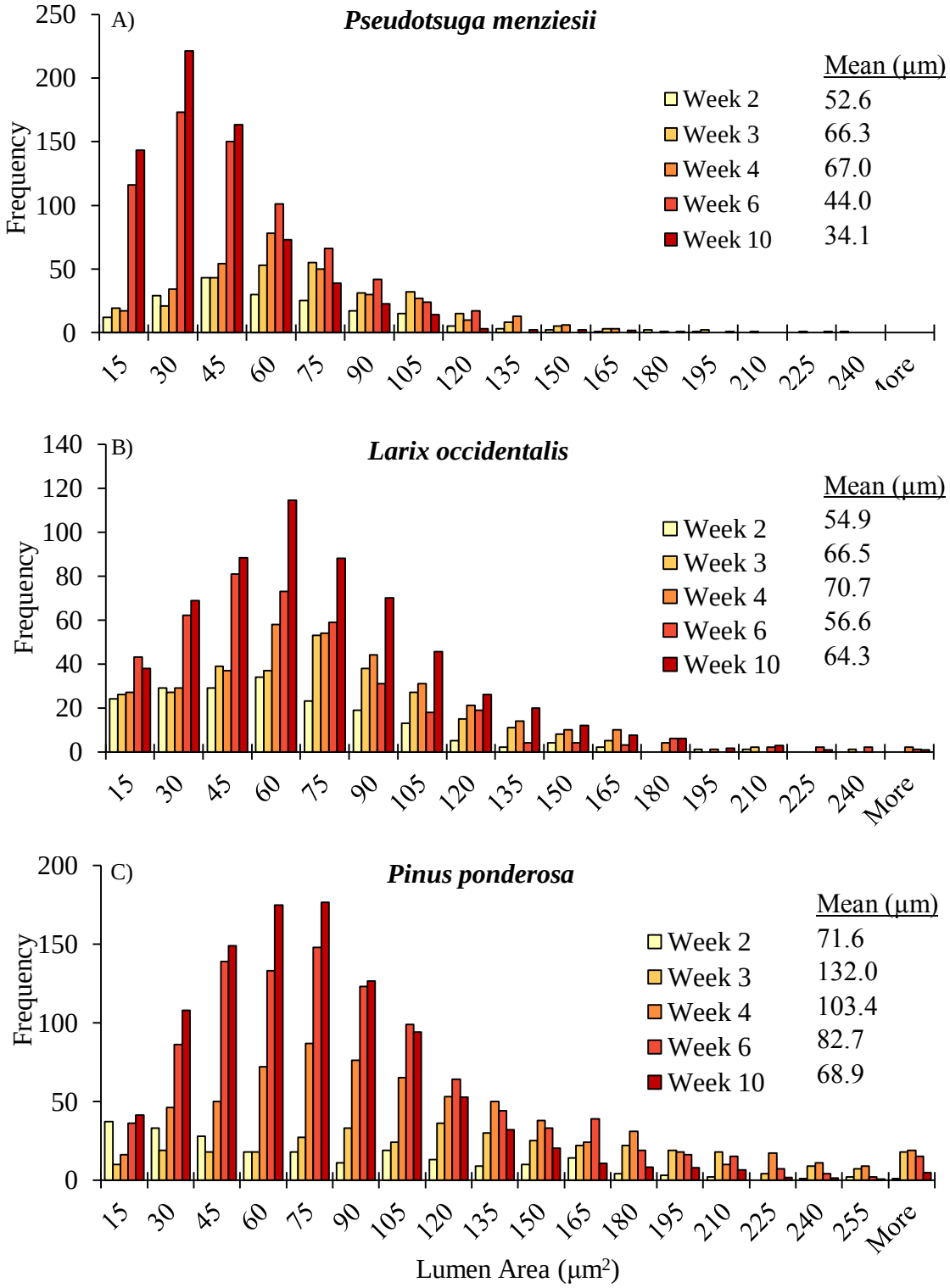

Figure 1.12 Lumen area distributions. For all species, distributions shift right then left over time, indicating a slight increase in average tracheid diameter followed by decreasing diameters. (A) distribution for *P. menziesii*, (B) distribution for *L. occidentalis*, and (C) distribution for *P. ponderosa*. Frequencies have been adjusted for weeks 6 and 10 due to higher numbers of tracheids measured when compared to the other weeks.

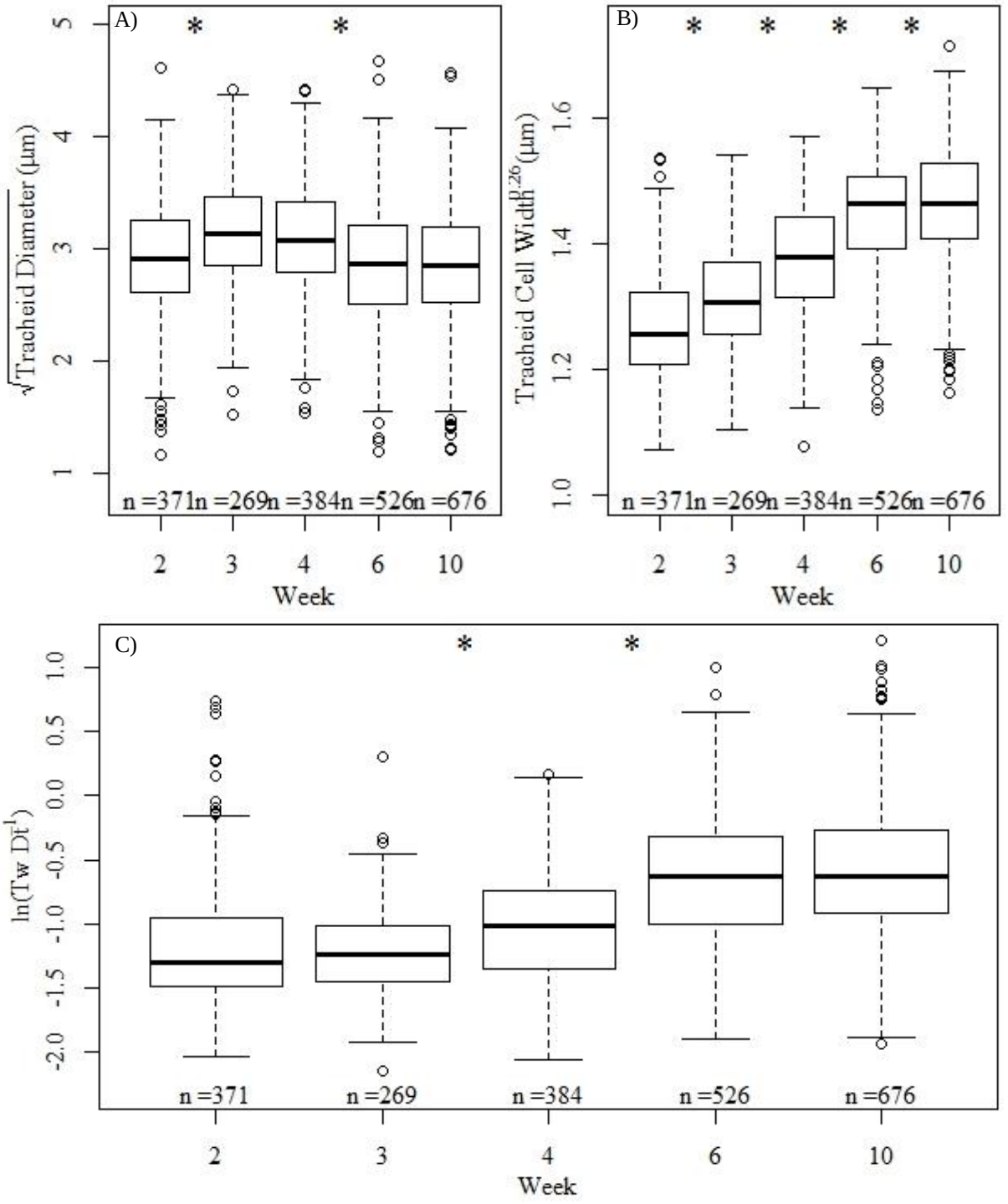

Figure 1.13 Tracheid characteristics: tracheid diameter (D_t), cell wall thickness (Tw) and thickness-to-span ratios ($Tw\ Dt^{-1}$). (A) Tracheid diameter on a square root scale for each week averaged across all species. Large boxplot whiskers and outliers indicate a very wide range of values skewed heavily right (see histogram figures 1.12). (B) Cell wall thickness as measured by the double cell wall thickness for each week averaged over all species show a statistically significant increase between all weeks. (C) $Tw\ Dt^{-1}$ on a log scale illustrates that Tw governs $Tw\ Dt^{-1}$. Asterisks indicate significance between adjacent weeks at $P < 0.05$.

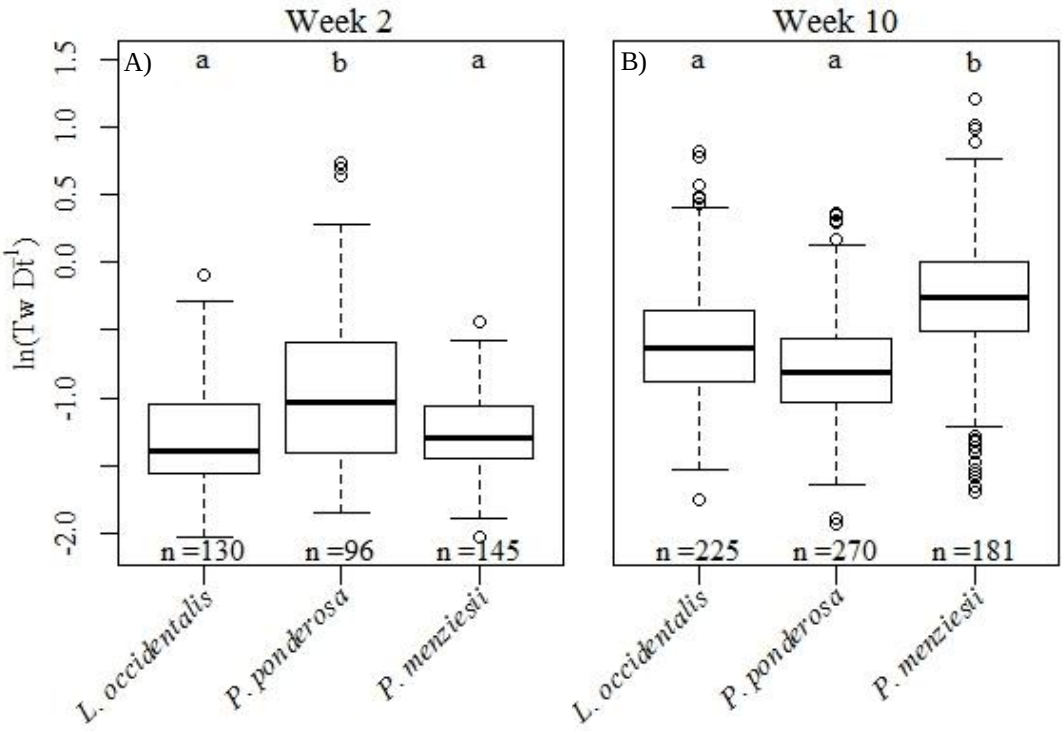

Figure 1.14 Thickness-to-span ratios at weeks 2 and 10. (A) Natural log of thickness-to-span ratios (Tw Dt^{-1}) for each species at week 2. (B) Natural log of thickness-to-span ratios for each species at week 10. Different letters per panel indicate significant differences at $P < 0.05$. Graphical representations do not take into account repeat measurements performed on multiple tracheids within the same tree.

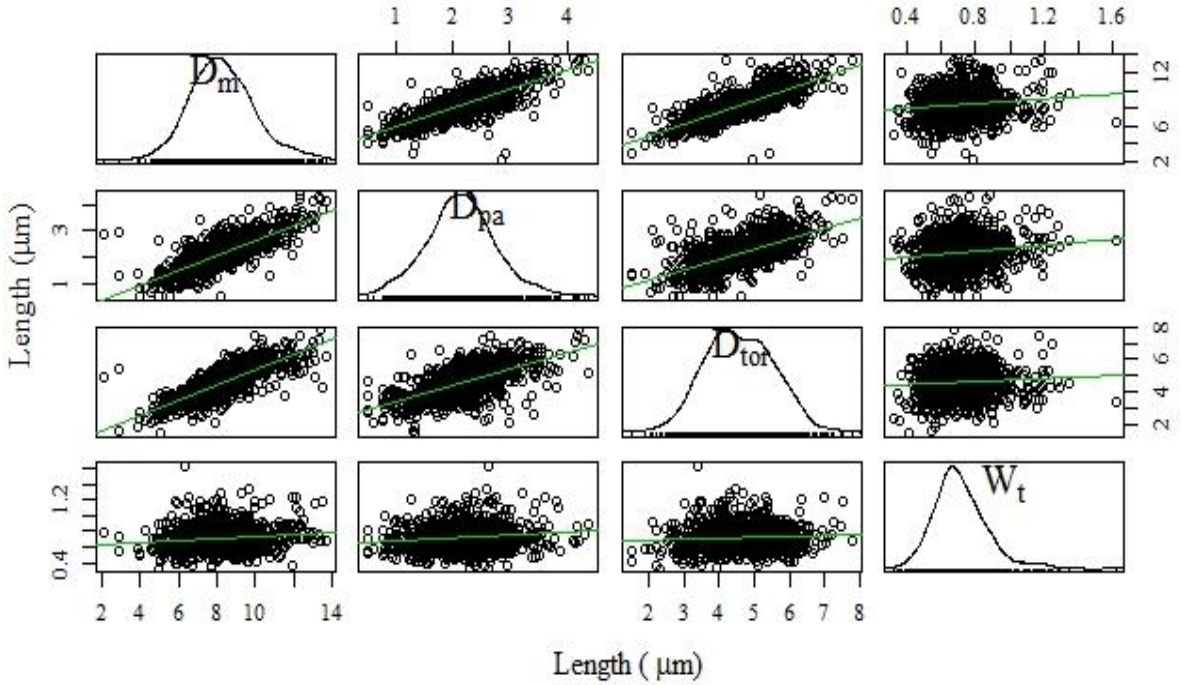

Figure 1.15 Correlation of the four measured pit features. Plots show that torus width is not strongly associated with any other pit characteristics while there are significant correlations between the other three characteristics. Green lines are best fit lines. D_m = margo diameter, D_{pa} = pit aperture diameter, D_{tor} = torus diameter, W_t = torus width.

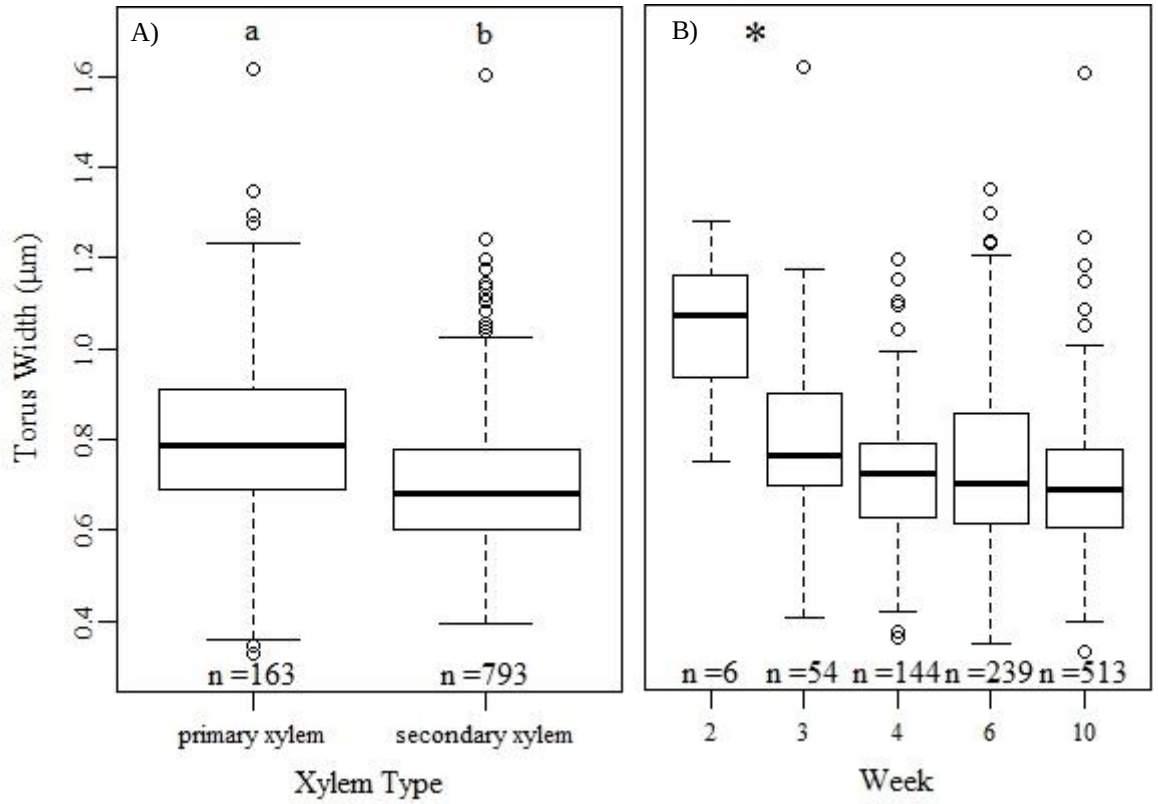

Figure 1.16 Torus width comparisons. (A) Torus width as a function of xylem type averaged over all species. Different letters indicate significant difference at $P < 0.05$. (B) Decreases in torus width over time indicate a transition from primary to secondary xylem. Asterisks indicate significance between adjacent weeks at $P < 0.05$.

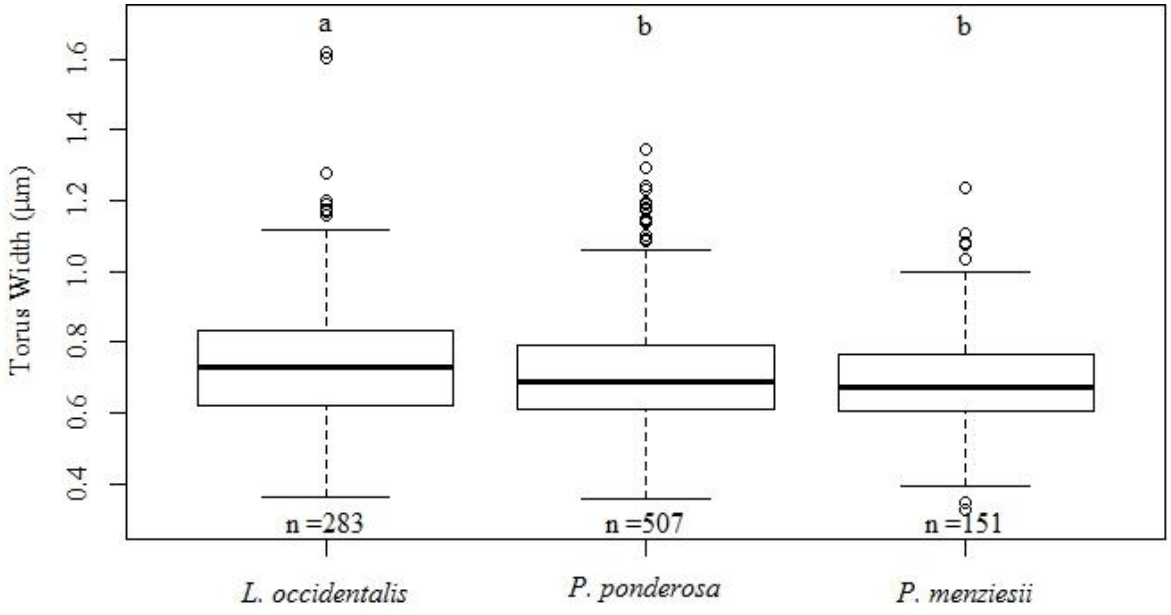

Figure 1.17 Torus widths per species averaged over time and xylem type. Different letters indicate significant difference at $P < 0.05$.

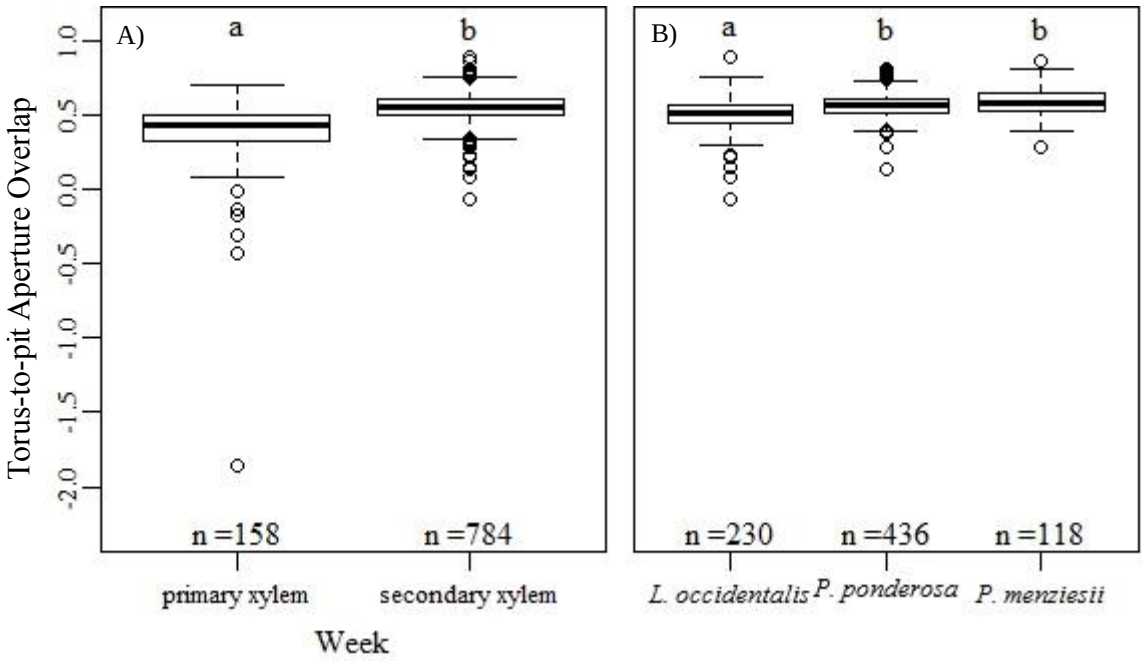

Figure 1.18 Torus-to-pit aperture overlap (TPO) comparisons. (A) Torus to pit overlap between primary and secondary xylem averaged over all species. Values below zero are due to a smaller torus diameter as compared to the pit aperture. (B) Differences in TPO within secondary xylem between all species averaged over all time periods in which secondary xylem was identified. Different letters per panel indicate significance at $P < 0.05$.

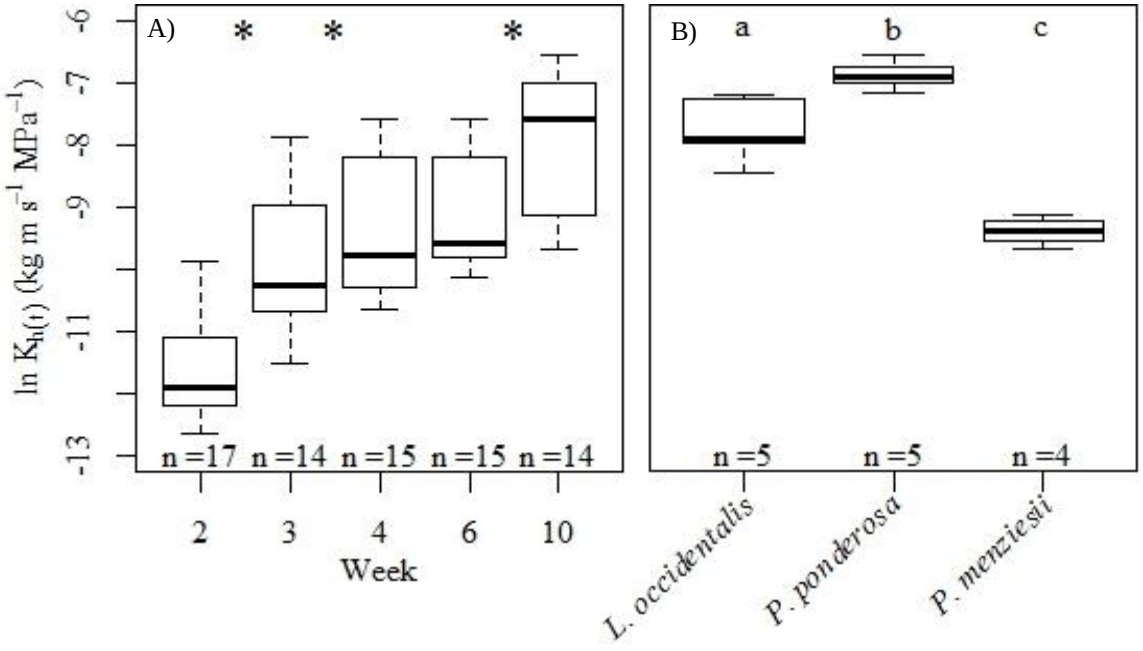

Figure 1.19 Stem conductance. (A) Stem conductance each week averaged over all species and (B) stem conductance at week 10 for each species. Asterisks (A) or different numbers (B) per panel indicate statistical significance at $P < 0.05$.

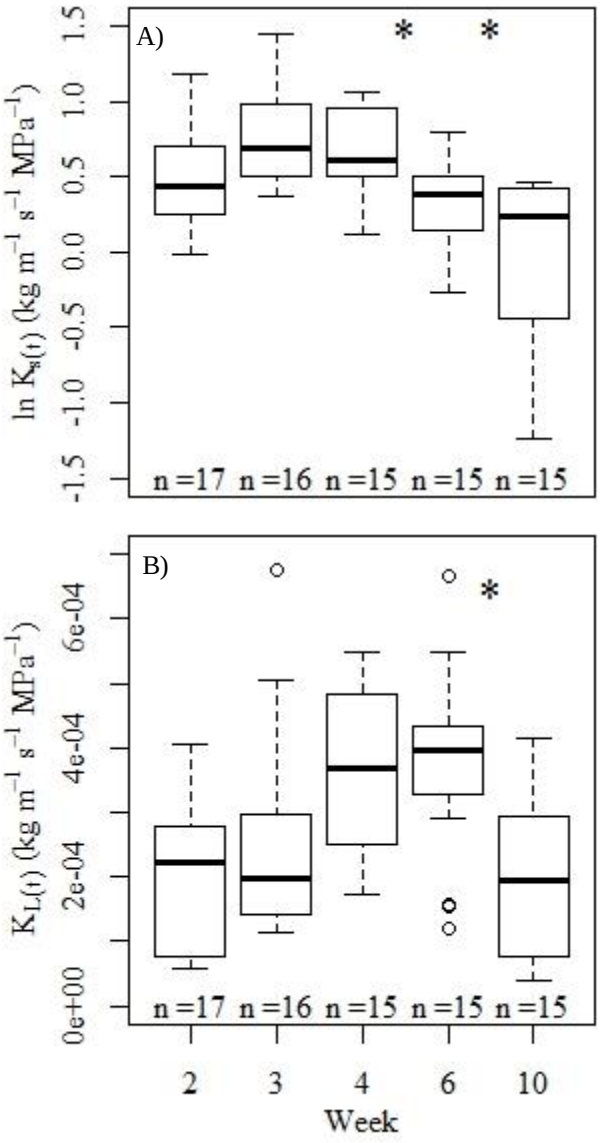

Figure 1.20 $K_{s(t)}$ and $K_{L(t)}$ for each week. (A) Theoretical xylem specific conductivity for each week averaged over all three species. (B) Theoretical leaf specific conductivity ($K_{L(t)}$) at each week for all species. The trend illustrates an increase over time until a statistically significant drop between weeks 6 and 10 for all species. Asterisks indicate significant differences between adjacent time periods at $P < 0.05$.

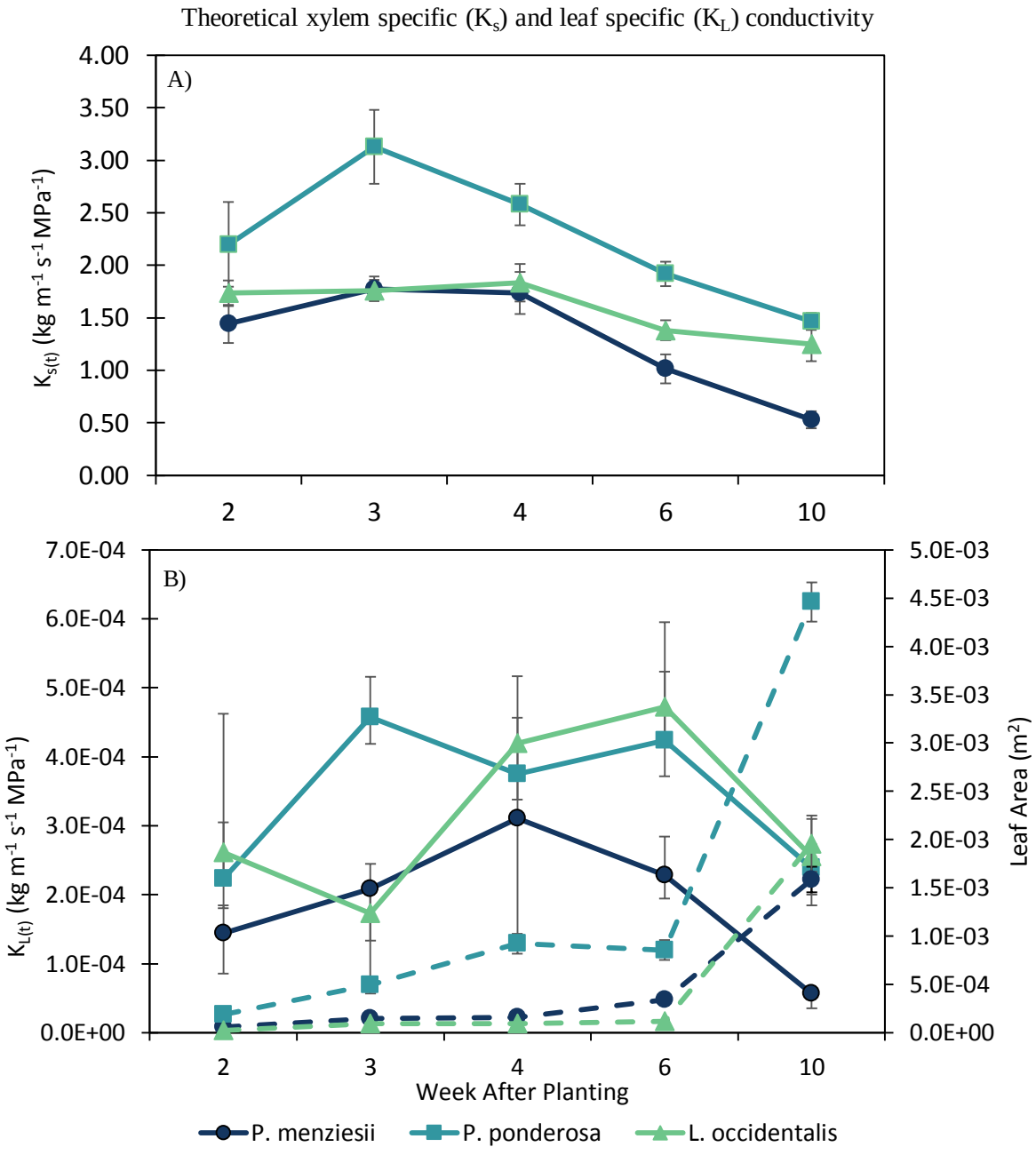

Figure 1.21 $K_{s(t)}$, $K_{L(t)}$ and A_L over time for all species. (A) Theoretical xylem specific conductivity ($K_{s(t)}$; dashed line) and theoretical leaf specific conductivity ($K_{L(t)}$; solid line) as a function of time after planting. (B) Theoretical leaf specific conductivity ($K_{L(t)}$; solid lines) and absolute crown leaf area (A_L; dashed lines) averaged per species per time period with error bars (SE). Drop in $K_{L(t)}$ for *L. occidentalis* is likely due to a low sample size. Error bars (SE) are included for both measurements, but the scale of $K_{L(t)}$ prevents visualization in this graph.

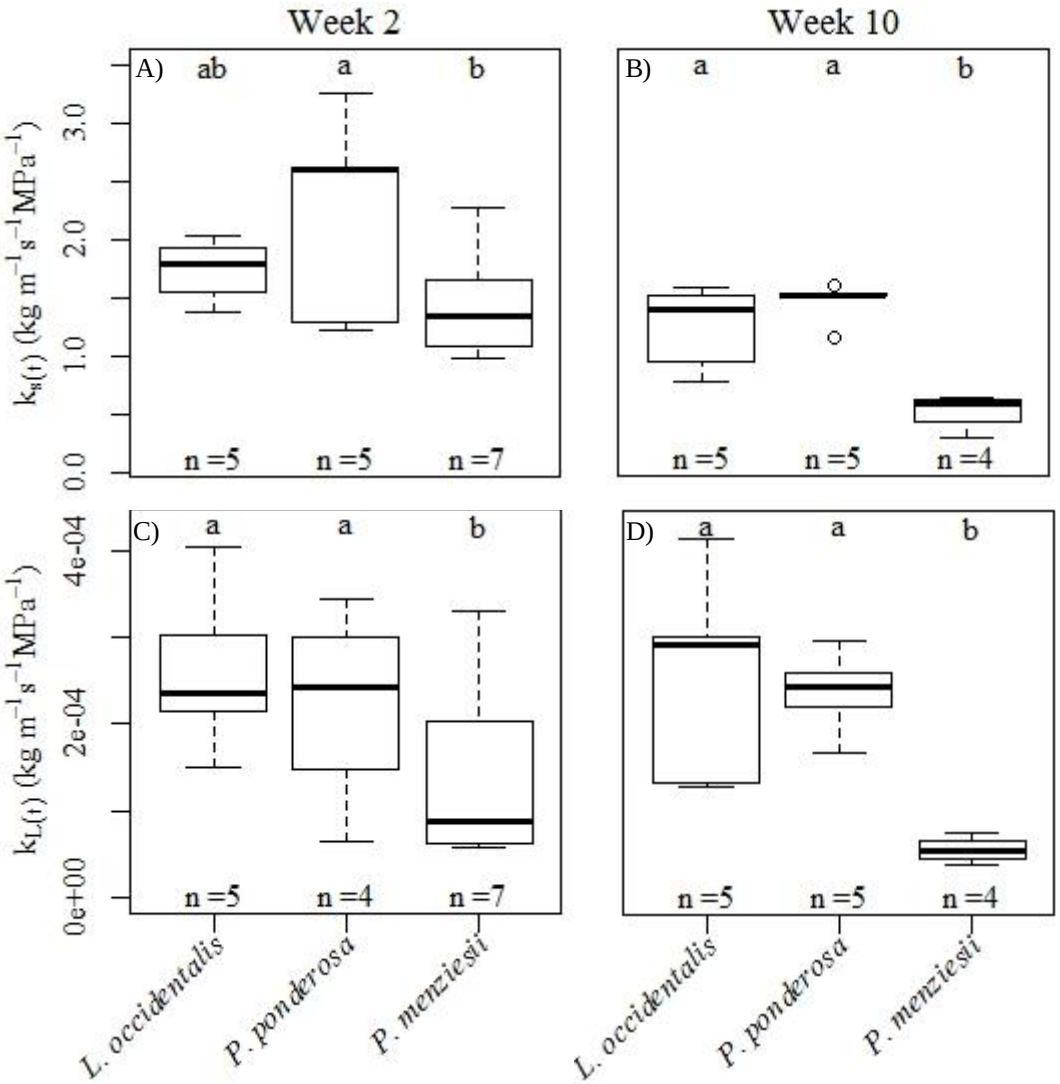

Figure 1.22 Comparison of $K_{s(t)}$ and $K_{L(t)}$ at weeks 2 (A, C) and 10 (B, D) per species. Differences in $K_{s(t)}$ between week 2 (A) and week 10 (B) illustrate a decline for all species. *P. menziesii* is significantly less by week 10, indicating there may be a trade-off between safety and hydraulic conductivity. Differences in $K_{L(t)}$ between week 2 (C) and week 10 (D) show no overall difference between the two, although *P. menziesii* exhibits the lowest theoretical value. Different numbers within a panel indicate statistically significant differences at $P < 0.05$. $K_{s(t)}$ = theoretical xylem specific conductivity; $K_{L(t)}$ = theoretical leaf specific conductivity.

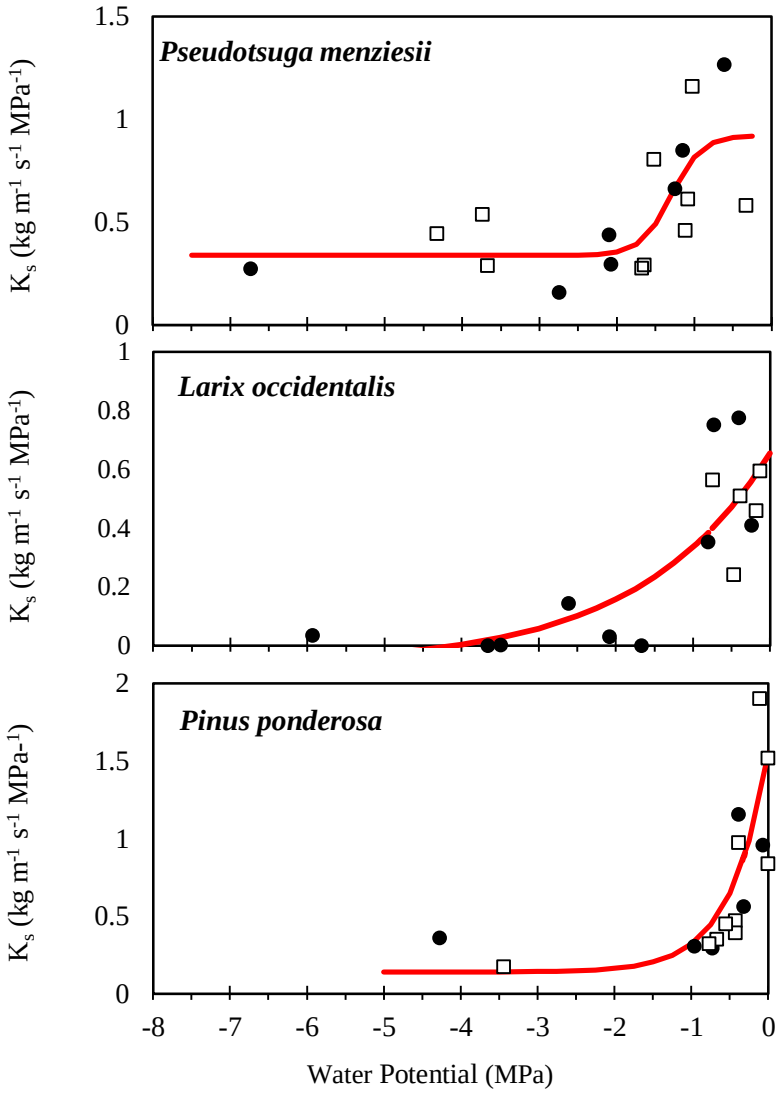

Figure 2.1 Hydraulic vulnerability curves constructed for *P. menziesii*, *P. ponderosa* and *L. occidentalis* based on excised and intact stem conductivity and water potential measurements. A 4-parameter sigmoid function [y0+a/(1+exp(-(x-x0)/b))] was used for *P. menziesii* and a 3-parameter exponential growth function [y0+a*exp(b*x)] was fitted to *P. ponderosa* and *L. occidentalis* to estimate P50 stem water potentials. Black circles (●) are excised stems and boxes (□) are intact stems. Estimated P_{50} values: *P. menziesii*: -1.56 MPa; *L. occidentalis*: -1.04; *P. ponderosa*: -0.39 MPa.

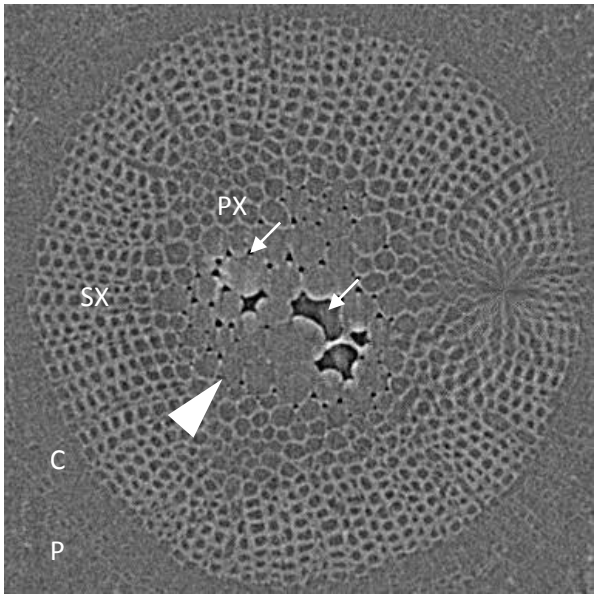

Figure 2.2 MicroCT image of vascular tissue illustrating the visual differences between the medium grey water-filled or cytoplasm filled cells (white arrow head) versus the dark grey embolized pith and intercellular spaces (white arrows). Lignified cell walls are visible as light grey outlines. Star-like artefact on the right mid-center side is a consequence of the image reconstruction parameters. P = phloem, C = cambial zone, PX = primary xylem, SX = secondary xylem.

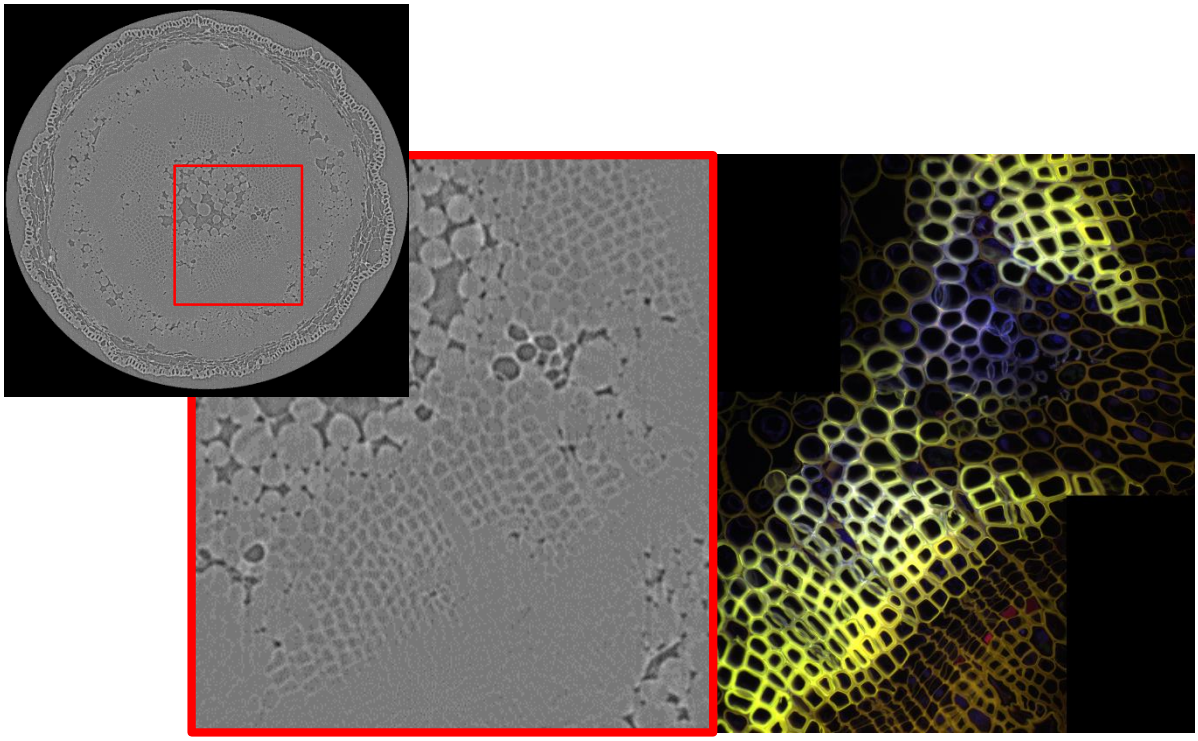

Figure 2.3 *P. ponderosa* microCT image. Inset is a magnification of the microCT image compared to an analagous confocal laser scanning microscopy image. Using the CLSM image as a reference helps distinguish primary xylem, especially adjacent to the pith, secondary xylem, lignified axial parenchyma, and rays.

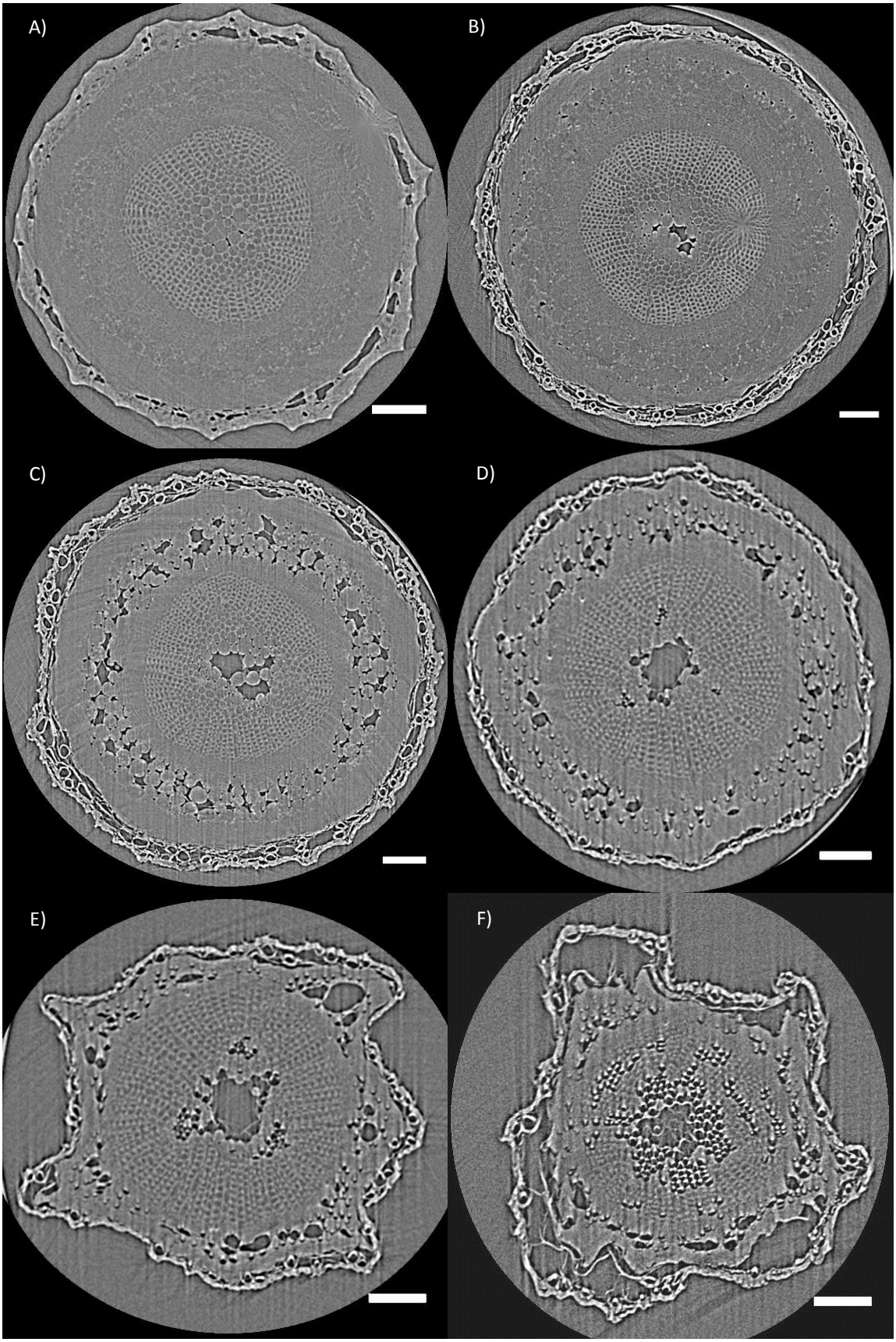
A)
B)
C)
D)
E)
F)

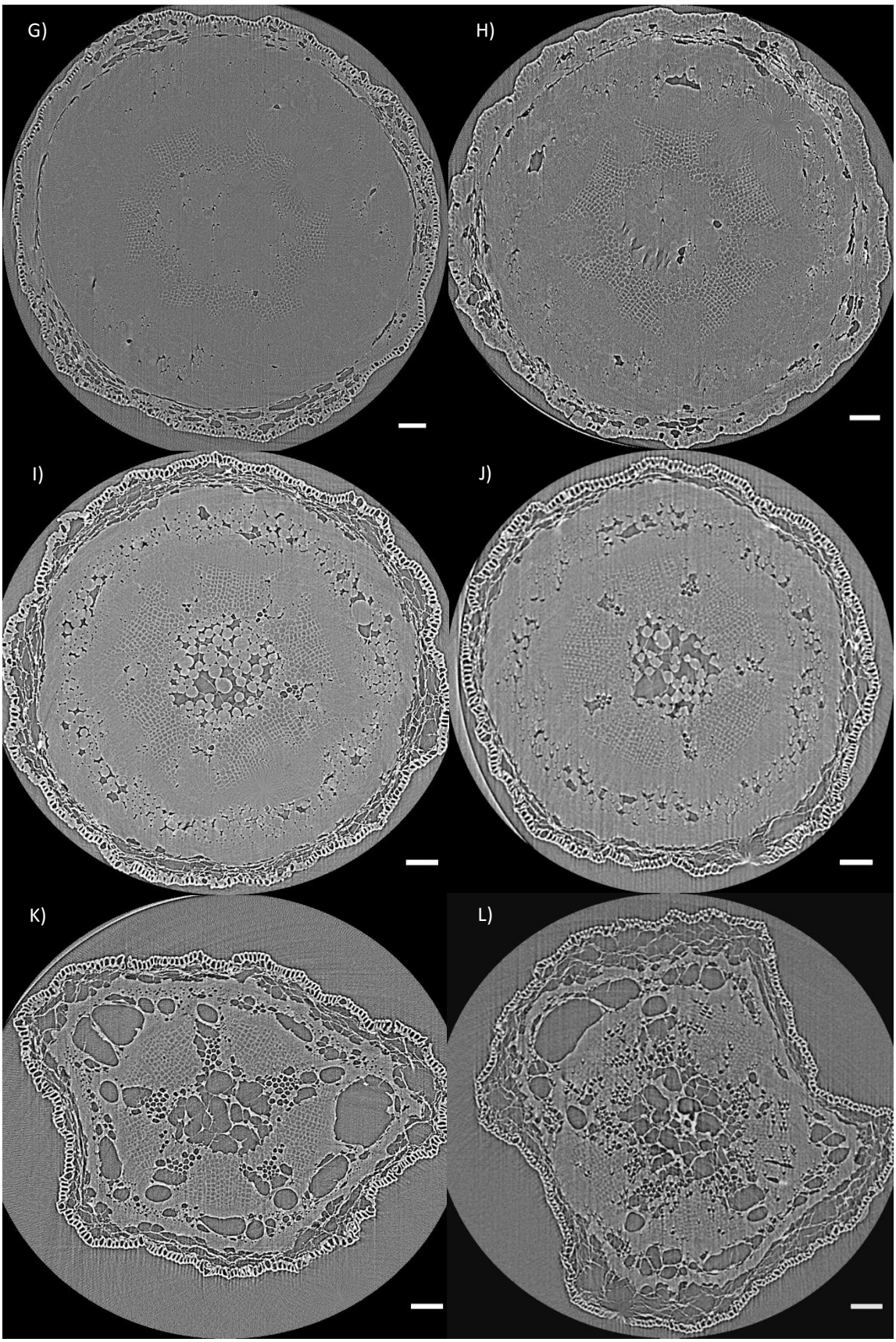
G)
H)
I)
J)
K)
L)

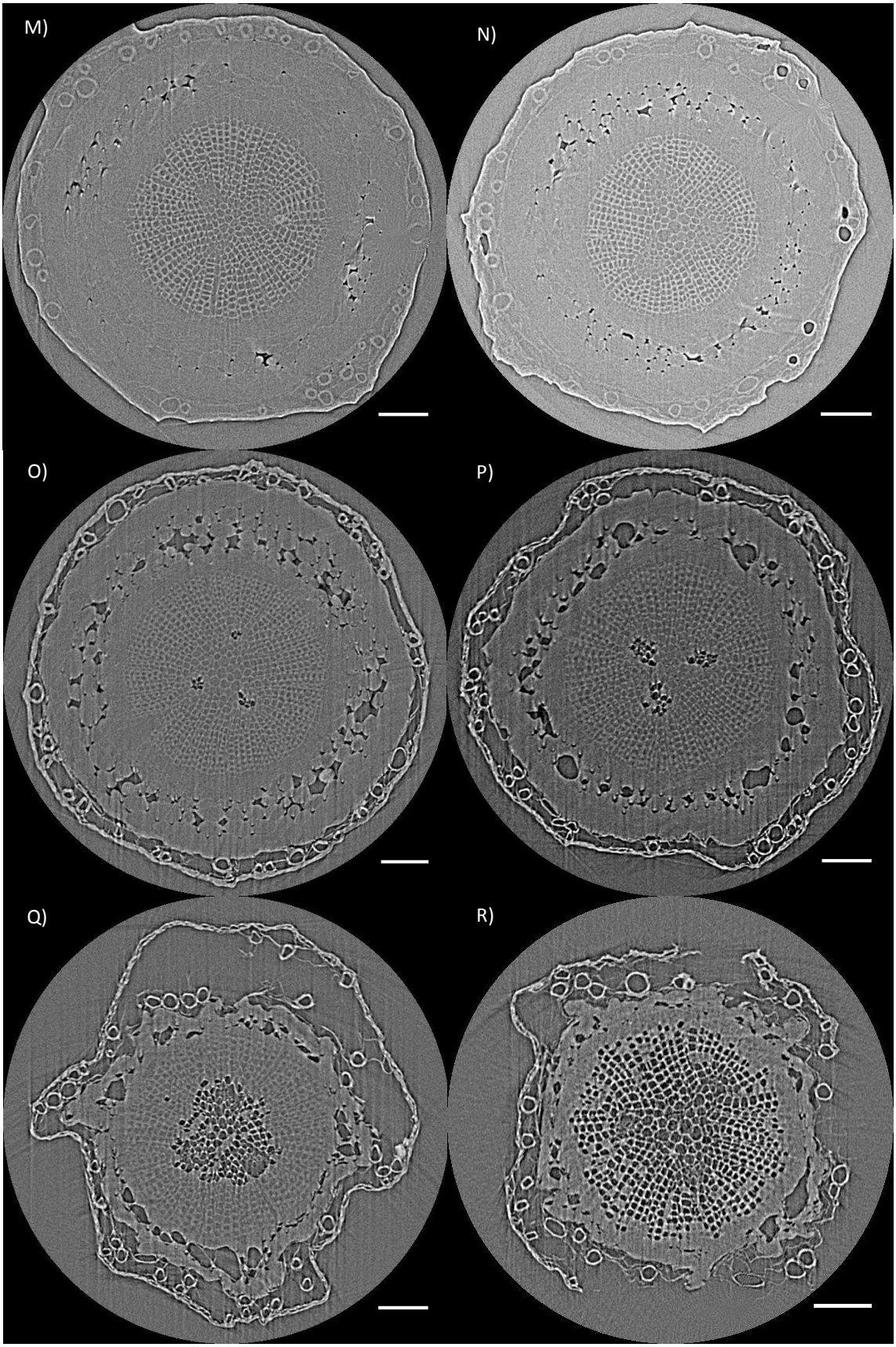
M)
N)
O)
P)
Q)
R)

Figure 2.4 MicroCT imaging of *P. menziesii* (A-F), *P. ponderosa* (G-L), and *L. occidentalis* (M-R) excised during desiccation. Images B & C, D & E, H & I, and J & K are the same stems respectively, but only the latter image in each set was measured for a water potential. All images are from excised stems. *L. occidentalis* was the only species to exhibit extensive secondary embolism (R). Water potentials (in MPa) are: A = -1.3, C= -0.6, E= -2.1, F= -6.7, G= -0.10, I= -0.96, K= -0.73, L= -4.27, M= -0.2, N= -0.8, O= -2.6, P= -3.3, R= -2.1. Bars = 100um.

Table A.1 Stem, Xylem and Leaf Area Measurements.

Species	Week	A_s (mm^2)	SE	A_x (mm^2)	SE	A_{tfx} (mm^2)	SE	A_L (m^2)	SE	A_L: A_{tfx}	SE
P. menziesii	2	0.686	0.050	0.037	0.004	0.005	0.001	5.6E-05	3.6E-06	12877	1829
	3	0.639	0.031	0.049	0.005	0.018	0.001	1.5E-04	2.1E-05	9380	1251
	4	0.576	0.079	0.062	0.002	0.027	0.003	1.6E-04	1.5E-05	6066	827
	6	0.637	0.042	0.118	0.008	0.069	0.005	3.4E-04	4.1E-05	4922	558
	10	0.901	0.099	0.302	0.064	0.168	0.020	1.6E-03	1.3E-04	9368	1072
P. ponderosa	2	1.660	0.163	0.202	0.026	0.014	0.002	1.9E-04	1.6E-05	12880	2550
	3	1.497	0.095	0.214	0.028	0.065	0.013	4.9E-04	8.4E-05	8847	2577
	4	1.824	0.099	0.355	0.025	0.148	0.010	9.2E-04	1.0E-04	6960	1920
	6	1.373	0.130	0.369	0.056	0.186	0.019	8.5E-04	1.0E-04	4570	243
	10	4.939	N/A	1.219	0.097	0.726	0.056	4.5E-03	2.0E-04	6214	273
L. occidentalis	2	0.434	0.033	0.019	0.002	0.004	0.000	2.5E-05	3.7E-06	7244	967
	3	0.386	0.029	0.017	0.004	0.009	0.003	9.1E-05	7.3E-06	11413	2114
	4	0.452	0.034	0.039	0.003	0.021	0.002	9.3E-05	7.9E-06	4430	318
	6	0.370	0.027	0.061	0.006	0.039	0.002	1.2E-04	1.1E-05	2964	131
	10	1.687	0.181	0.569	0.063	0.370	0.046	2.0E-03	2.9E-04	5354	611

Table A.2 Anatomical Measurements.

Species	Week	D_m (µm)	SE	D_{pa} (µm)	SE	D_{tor} (µm)	SE	W_t (µm)	SE	D_t (µm)	SE	Tw (µm)	SE
P. menziesii	2	6.25	0.275	2.60	0.109	3.85	0.259	1.02	0.050	8.59	0.194	2.37	0.039
	3	7.21	0.128	2.10	0.041	3.34	0.101	0.88	0.103	9.63	0.361	2.51	0.075
	4	7.35	0.203	2.13	0.073	3.88	0.123	0.70	0.031	8.68	0.278	3.31	0.106
	6	7.23	0.140	1.77	0.074	4.00	0.100	0.63	0.026	6.89	0.224	4.09	0.078
	10	6.93	0.132	1.58	0.051	3.88	0.066	0.68	0.013	6.61	0.178	4.79	0.088
P. ponderosa	2	7.61	0.302	2.75	0.125	6.11	0.909	--	--	9.44	0.415	3.31	0.066
	3	9.19	0.276	2.59	0.073	4.85	0.169	1.07	0.204	12.06	0.332	3.53	0.083
	4	9.18	0.174	2.48	0.057	4.73	0.105	0.68	0.016	10.93	0.290	3.86	0.060
	6	8.38	0.153	2.17	0.052	4.75	0.082	0.72	0.016	9.46	0.198	4.38	0.057
	10	8.49	0.085	2.23	0.028	4.99	0.053	0.70	0.008	9.01	0.173	4.01	0.049
L. occidentalis	2	7.25	0.356	2.74	0.176	3.00	0.254	1.06	0.161	8.35	0.247	2.20	0.033
	3	7.12	0.368	2.52	0.247	3.80	0.333	0.94	0.102	8.82	0.227	2.64	0.044
	4	7.51	0.170	2.27	0.071	4.10	0.128	0.75	0.020	9.16	0.231	3.14	0.063
	6	7.31	0.129	2.01	0.056	3.92	0.090	0.83	0.019	8.24	0.221	4.08	0.075
	10	7.79	0.094	2.19	0.041	4.05	0.058	0.68	0.011	8.75	0.187	4.66	0.067

Table A.3 Functional Traits

Species	Week	$K_{L(t)}$	SE	$K_{s(t)}$	SE	$K_{h(t)}$	SE	TPO	SE	Tw Dt^{-1}	SE
P. menziesii	2	1.44E-04	4.05E-05	1.44	0.18	7.63E-06	1.99E-06	0.31	0.211	0.29	0.007
	3	2.08E-04	3.61E-05	1.78	0.12	3.2E-05	3.51E-06	0.32	0.047	0.28	0.013
	4	3.11E-04	5.95E-05	1.73	0.20	4.83E-05	9.49E-06	0.48	0.017	0.42	0.023
	6	2.28E-04	5.63E-05	1.01	0.14	7.11E-05	1.17E-05	0.56	0.017	0.73	0.037
	10	5.64E-05	7.44E-06	0.53	0.08	8.48E-05	9.57E-06	0.59	0.014	0.87	0.037
P. ponderosa	2	2.24E-04	5.83E-05	2.20	0.4	3.32E-05	8.88E-06	0.50	0.082	0.47	0.038
	3	4.58E-04	1.42E-04	3.13	0.35	2.14E-04	5.36E-05	0.44	0.015	0.31	0.010
	4	3.75E-04	1.72E-04	2.58	0.20	3.89E-04	5.11E-05	0.45	0.014	0.40	0.014
	6	4.23E-04	3.34E-05	1.92	0.12	3.58E-04	4.41E-05	0.53	0.017	0.52	0.014
	10	2.39E-04	2.14E-05	1.47	0.08	1.07E-03	1.19E-04	0.55	0.004	0.50	0.014
L. occidentalis	2	5.83E-05	4.73E-05	1.7	0.12	6.44E-06	1.19E-06	0.02	0.151	0.30	0.013
	3	1.42E-04	7.23E-05	1.8	0.09	1.69E-05	5.39E-06	0.44	0.047	0.33	0.013
	4	1.72E-04	8.95E-05	1.8	0.81	4E-05	6.3E-06	0.43	0.024	0.39	0.015
	6	3.34E-05	4.71E-05	1.4	0.09	5.38E-05	5.36E-06	0.48	0.014	0.57	0.022
	10	2.14E-05	2.78E-05	1.2	0.16	4.79E-04	1.08E-04	0.46	0.012	0.61	0.021